Atmospheric Physics

Adrian Tompkins

These course notes and presentations have benefitted enormously from material taken (with permission!) from the following people:
Dr. Stephan de Roode (Thermodynamics and convection),
Prof. Keith Shine (Thermodynamics, Cloud Physics and Radiation)
Prof. John Chiang (Introduction and Radiation),
Profs Vince Larson and Bill Cotton (cloud physics).
Dr Francesca Di Giuseppe (Radiation)
Introductory material also taken from IPCC AR4 report and Wikipedia used for a number of additional graphics. Apologies to authors of graphic material that have not been properly attributed (sources referenced as "unknown" presently). Please contact me for citation corrections, mistakes, and other suggestions at tompkins@ictp.it

1 Introduction

Course overview

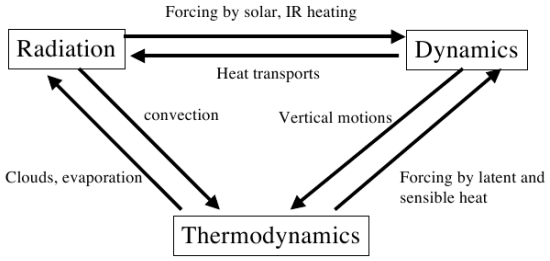

This course will concern itself with

- Thermodynamics
- Cloud Physics
- Radiation

This course on *atmospheric physics* concerns itself with the areas of thermodynamics, cloud physics and radiation. The topic of atmospheric dynamics is handled in a separate course *Atmospheric dynamics*.

Net Radiation Budget

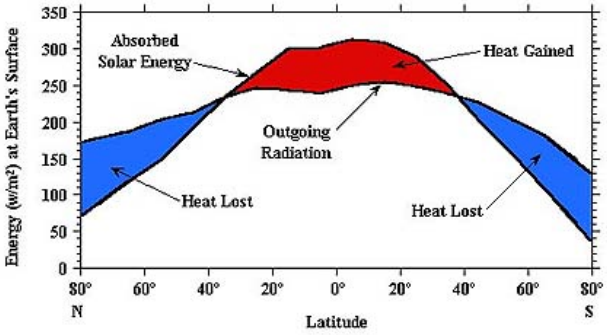

Solar radiation absorbed by earth-atmosphere system balanced by outgoing thermal radiation on average globally, but not locally.

Q: How is a local energy equilibrium maintained? The earth-atmosphere system receives incident radiation from the sun at wavelengths of 0.2 to 4 μm. Some of this radiation is absorbed or reflected back to space by the atmosphere, while the rest is absorbed or reflected back to space by the earth's surface. The net solar radiation absorbed by the earth-atmosphere system must be

balanced by the outgoing thermal infra-red radiation that this system emits at longer wavelengths of 4 to 500 μm.

The solar radiation is not equally distributed over the global, with the tropics receiving more incoming solar energy than the poles. The energy lost to space through infra-red emission does not locally balance the solar radiation (i.e. there is not a local radiative equilibrium). Instead the energy is redistributed by large-scale dynamical motions. These will be discussed in the *atmospheric dynamics* course.

Atmospheric vertical structure

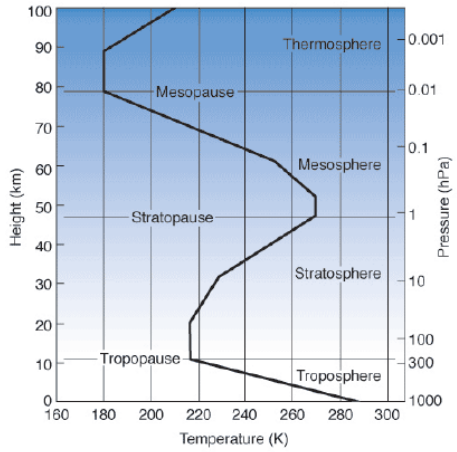

Atmosphere is divided into distinct vertical layers according to temperature lapse-rate:

- Lower (troposphere)
- middle (stratosphere and mesosphere)
- upper (thermosphere)

This course is concerned with tropospheric processes

The atmospheric gases

Constituent	Mol. Wt.	Conc. by vol.	
Nitrogen (N_2)	28.013	0.7808	Major constituents
Oxygen (O_2	32.000	0.2095	
Argon (Ar)	39.95	0.0093	Minor constituents
Water vapor (H_2O)	18.02	variable	
Carbon dioxide (CO_2)	44.01	380 ppmv	
Neon (Ne)	20.18	18	
Helium (He)	4.00	5	
Methane (CH_4)	16.	1.75 "	
Hydrogen (H_2)	2.02	0.5 "	
Nitrous oxide (N_2O)	56.03	0.3 "	
Ozone (O_3)	48.00	0-0.1 "	

Q: Are these gases well-mixed in the atmosphere? The atmosphere consists of a number of gases, for which the molecular weight and concentration by volume are given in the table. For most of these gases it can be assumed that they are well-mixed up to a height of approximately 100km. However for water vapour the situation is different and the concentration varies strongly with latitude, longitude and altitude. This is shown on the following diagram.

Atmospheric Water Vapour Distribution

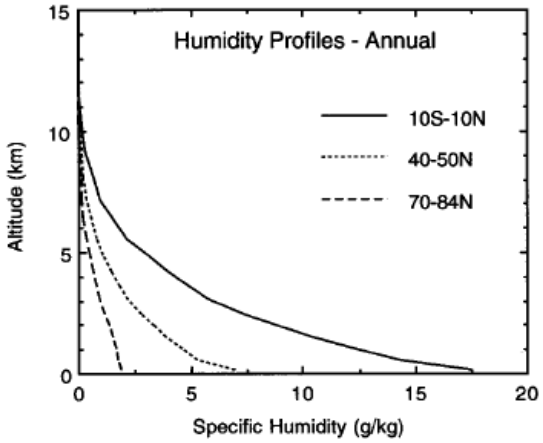

It is seen that the concentration of water vapour in the atmosphere falls rapidly with height, and is much higher in the tropics relative to the subtropics and midlatitudes.

Q: Do you know why this might be? The thermodynamics part of this course will show how the saturation vapour pressure is a function of temperature, increasing with increasing temperature. If the water vapour content of the atmosphere exceeds this threshold the excess condenses rapidly into numerous droplets to form clouds. At least, this description is reasonable for liquid clouds, although it will be seen that the situation is more complicated for mixed phase and ice clouds.

Clouds

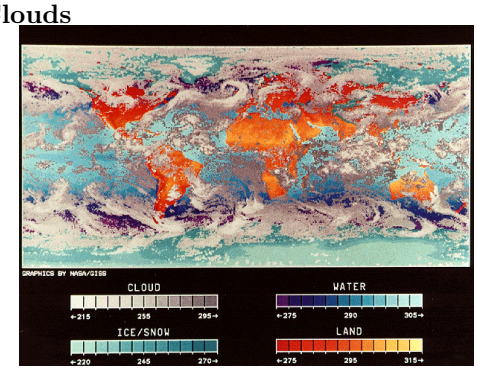

Clouds are a common feature *Q: What is the global mean annual cloud cover?*

They have a major impact on both the hydrological cycle and radiation budget (refer to earlier processes schematics)

Atmospheric Processes

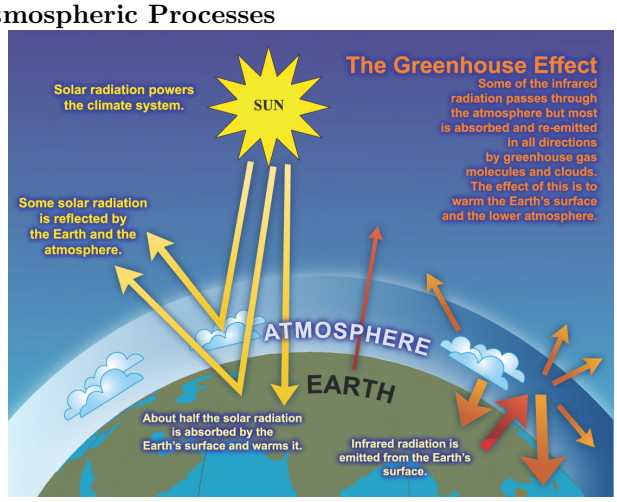

Q: What would be the global mean annual surface temperature

- today?

- in the absence of the atmosphere?
- with an atmosphere but without clouds or aerosols?

In the absence of the greenhouse effect and an atmosphere, the Earth's average surface temperature of 15^{o}C could be as low as -18^{o}C, the black body temperature of the Earth. We will derive these figures approximately later in this course. On the other hand the green-house effect of the atmosphere without the cooling effect of clouds and aerosols in the short-wave would result in a mean temperature of around 30^{o}C. Note that the atmosphere is a thin layer O(100km) compared to the radius of the Earth at O(6400km).

Atmospheric Energy partition

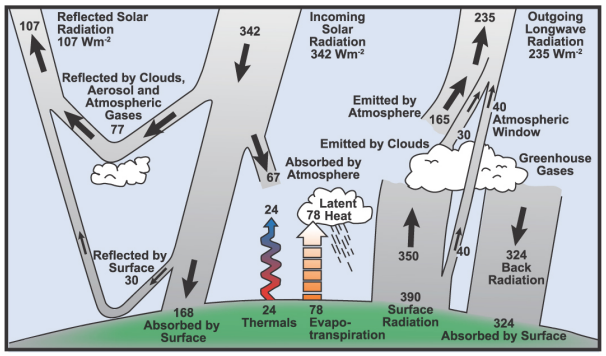

This figure gives more details of the balance, showing how the radiative budgets is affected by clouds for example. Note also that the earth's surface loses energy via latent and sensible heat fluxes in addition to infra-red emission. These warm the atmosphere above which itself emits long-wave radiation to space.

Atmospheric Processes

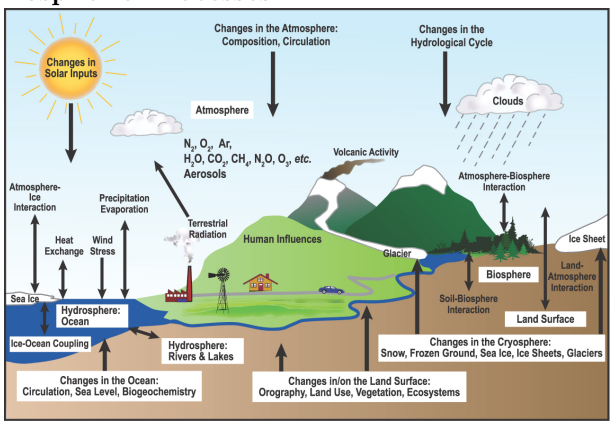

The climate system is in fact complicated, depending on a huge array of interacting processes. This course will only tackle the basic aspects of cloud microphysics, radiative interaction with the earth-atmosphere system.

2 Dry Thermodynamics

The ideal gas law and the first and second law of thermodynamics will be discussed briefly. The Clausius-Clapeyron equation is derived to obtain the dependency of the water vapor saturation pressure on the temperature.

2.1 Equation of state: The ideal gas law

Ideal Gas

The ideal gas model is a model of matter in which the molecules are treated as non-interacting point particles which are engaged in a random motion that obeys conservation of energy.

The model tends to fail at lower temperatures or higher pressures, when the molecules come close enough that they start interacting with each other, and not just with their surroundings. This is usually associated with a phase transition.

The *equation of state for an ideal gas* relates its pressure p, volume V and temperature T by

$$pV = NkT = \nu R^* T, \tag{1}$$

where

- N is the number of identical molecules
- ν is the number of moles of gas
- $k = 1.3806 \times 10^{-23}$ J K $^{-1}$ is Boltzmann's constant,
- $R^* \equiv N_a k = 8.341$ J mol^{-1} K^{-1} is the universal gas constant,
- with $N_a = 6.022 \times 10^{23}$ mol $^{-1}$ Avogadro's number.

As pointed out in the introduction, the Earth's atmosphere is a mixture of gases, mostly nitrogen, oxygen and argon, trace gases like carbon dioxide, ozone and methane, and variable amounts of water in its three physical phases (see Table 1).

Neglecting water vapour for the moment, the dry atmosphere can be taken to a very good approximation as an ideal gas.

In general, it is useful to formulate the thermodynamic relations in terms of *intensive* variables. An intensive variable is one whose value does not depend on the amount of matter in the system, like the temperature of pressure. In contrast, an *extensive* variable, depends on the size of the system. For instance, the internal energy of a gas is an extensive variable since if we double its size, all else being kept equal, its internal energy will double.

Given a system whose volume V contains an amount of mass M,

$$v = \frac{V}{M} \tag{2}$$

denotes the *specific volume* of the system. In principle, every extensive variable can be converted to its corresponding intensive form by normalizing it by the amount of matter it describes.

We will (generally, but not always!) use lower case letters to denote specific intensive quantities, as opposed to their non-intensive counterpart for which we will use capital letters, e.g. the specific volume v and the volume V.

We would like to write the gas law in terms of kilograms rather than moles and use the molecular weight of a species i, m_i (g/mol), which is the mass of 1 mole of identical molecules in grams.

If the total mass of the gas is M_i, we can express the gas law as,

$$pV = \frac{M_i}{m_i} R^* T. \tag{3}$$

The molecular weight can be substituted out by using the *specific gas constant* R_i for a species i, which is defined as

$$R_i \equiv R^*/m_i. \tag{4}$$

Partial Pressure

For a mixture of ideal gases the partial pressure p_i of the i^{th} gas is defined as the pressure p_i that it would have if the same mass (M_i) existed alone at the same temperature T and occupying the same volume V.

By (3) and (4) the partial pressure for an ideal gas can thus be expressed as

$$p_i = \frac{T}{V} M_i R_i. \tag{5}$$

Dalton's Law

According to *Dalton's law of partial pressures*, the total pressure p of a mixture of (ideal) gases is the sum of the pressures $\sum p_i$ of each species i as if it alone occupied a volume V,

$$p = \frac{T}{V}\sum_i (M_i R_i) = \rho R_m T. \tag{6}$$

If $M_{tot} = \sum_i M_i$ is the total mass, then $R_m = 1/M_{tot}\sum_i M_i R_i$ the specific gas constant for the mixture, and $\rho = M_{tot}/V$ is the density.

Equation. (6) is the form of the gas law generally used in meteorology.

Table 1 shows the value of the gas constant for dry air, $R_d = 287.05$ J kg^{-1} K^{-1}.

Gas	Molecular weight m_i [g mol^{-1}]	Molar fraction	Mass fraction M_i/M_{tot}	Specific gas constant R_i [J kg^{-1} K^{-1}]	$(M_i/M_{tot})R_i$ [J kg^{-1} K^{-1}]
NO_2	28.013	0.7809	0.7552	296.80	224.15
O_2	31.999	0.2095	0.2315	259.83	60.15
Ar	39.948	0.0093	0.0128	208.13	2.66
CO_2	44.010	0.0003	0.0005	188.92	0.09
total		1.0000	1.0000		287.05

Table 1: Main components of dry atmospheric air (source Smithsonian Meteorological Tables).

Reminders

1. What is the definition of a Ideal Gas?
2. Can dry air be considered an ideal gas?
3. What is Dalton's law?

2.2 The first law of thermodynamics

first law of thermodynamics

The *first law of thermodynamics* is a statement of two empirical facts:

1. Heat is a form of energy
2. Energy is conserved

Thus, the internal energy of a closed system (U) can change only if heat (Q) is added or if work (W) is done *on*[1] the system by its surroundings:

$$dU = dQ + dW \tag{7}$$

and for a unit mass of gas:

$$du = dq + dw \tag{8}$$

The rate of work is given by

$$dW = -pdV, \tag{9}$$

such that (7) can be expressed as

$$dU = dQ - pdV. \tag{10}$$

[1]Attention! Sometimes defined as work done *by* the gas thus changing the sign convention for dW

2.3 Rules for differentiating

If the equation of state is governed by three variables (p, v, T) then we can write

$$p = f_1(v, T) \quad , \quad v = f_2(p, T) \quad \text{or} \quad T = f_3(p, v). \tag{11}$$

In other words, there are only two independent state variables,

$$dp = \frac{\partial f_1}{\partial v} dv + \frac{\partial f_1}{\partial T} dT \ , \ dv = \frac{\partial f_2}{\partial p} dp + \frac{\partial f_1}{\partial T} dT \ , \ dT = \frac{\partial f_3}{\partial p} dp + \frac{\partial f_1}{\partial v} dv. \tag{12}$$

If we differentiate state variables other than p, v, or T, for instance, the specific internal energy u, we must specify which set of thermodynamics parameters we use. Otherwise $(\partial u/\partial p)$ is ambiguous and depends on the choice of thermodynamic coordinates, for example whether u is defined as a function of p and v or as a function of p and T.

Notation for differentiating
To express the rate of change of u as a result of an isothermal process, i.e. a change in the pressure p, we write

$$\frac{\partial u(p, T)}{\partial p} \equiv \left(\frac{\partial u}{\partial p} \right)_T \tag{13}$$

meaning that p and T are chosen as thermodynamical coordinates and that the the temperature is held constant for this process.

2.4 Enthalpy and specific heat

A measure of the quantity of heat needed to raise the temperature of one gram of a substance by 1 °C is called the heat capacity C, and is defined as:

$$C = dQ/dT. \tag{14}$$

But this definition is incomplete. There are many ways to add heat to a system. One could add heat to a system at *constant volume* or at *constant pressure*, or one could add heat as both the volume and pressure change.

Q: One can even add heat to a system even at constant temperature - how?

We now define the specific heat capacity at constant pressure, c_p and the specific heat capacity at constant volume, c_v. These are very different.

$$c_v = \left(\frac{\partial q}{\partial T} \right)_v . \tag{15}$$

$$c_p = \left(\frac{\partial q}{\partial T} \right)_p . \tag{16}$$

For dry air, $c_p = 1005$ J kg^{-1} K^{-1} and $c_v = 718$ J kg^{-1} K^{-1}

If one chooses the specific volume v and the temperature T as thermodynamic coordinates, then the specific internal energy u can be expressed as,

$$du = \left(\frac{\partial u}{\partial v} \right)_T dv + \left(\frac{\partial u}{\partial T} \right)_v dT = \left(\frac{\partial u}{\partial T} \right)_v dT. \tag{17}$$

where the last equality follows from the fact that the internal energy of an ideal gas does not depend on its volume,

$$\left(\frac{\partial u}{\partial v} \right)_T = 0. \tag{18}$$

(18) implicitly assumes that the intermolecular forces are negligibly small, and therefore is applicable only to an ideal gas. The density in the gas law (6) can be replaced by the specific volume, giving $pv = RT$. Substituting this form into (10) and using (17) gives

$$dq = \left(\frac{\partial u}{\partial T} \right)_v dT + p dv, \tag{19}$$

where dq indicates the differential amount of heat added. For an *isometric* process $dv = 0$, and thus from our definition of c_v:

$$dq = c_v dT + pdv, \tag{20}$$

Eqn. 20 is still not in a form useful in meteorology due to the difficulty of measuring volume of an air mass. We therefore use the first law again to write

$$dq = c_v dT + RdT - vdp, \tag{21}$$

$$dq = (c_v + R)dT - vdp, \tag{22}$$

For an isobaric process $dp = 0$, it is clear that

$$c_p = c_v + R. \tag{23}$$

which leads to the form of the first law commonly used in meteorology since it is formed in measurable quantities:

$$dq = c_p dT - vdp, \tag{24}$$

We now introduce another state variable that is often used in atmospheric thermodynamics is the *enthalpy* h

$$h = u + pv. \tag{25}$$

Given this definition, the first law can be expressed as

$$dq = du + pdv = dh - d(pv) + pdv = dh - vdp. \tag{26}$$

The enthalpy gives a measure of total potential energy of the atmosphere.

2.5 Adiabatic Processes

A parcel of air can be subject to input of heat and changes in pressure. *Q: Name some common atmospheric diabatic processes* First we shall consider the case where no heat is input.

Adiabatic Process
An *adiabatic process* is one where there is no heat exchange, $dq = 0$, thus

$$c_p dT = vdp, \tag{27}$$

Adiabatic processes have special significance as many atmospheric motions can be approximated as adiabatic. Assuming that the atmosphere is in a hydrostatic balance[2], $dp/dz = -\rho g$, then (27) can be written

$$c_p dT = -v\rho g dz = -g dz, \tag{28}$$

This gives the adiabatic lapse rate as

$$\frac{dT}{dz} = -\frac{g}{c_p} \tag{29}$$

Thus if we lift a dry air parcel without heat exchange its temperature will fall by by 9.8 K km^{-1}

Figure 1 shows the measured lapse rate on one particular day measured in Holland. The lapse rate is seen to be close to adiabatic.

Q: Can you think as to why this may be? Hint: Stability Using the equation of state we get

$$c_p dT = vdp = \frac{RT}{p} dp \tag{30}$$

$$\frac{dT}{T} = \frac{R}{c_p p} dp \tag{31}$$

Poisson's Equation

[2]you have already come across the notion of hydrostatic balance in an earlier course, but as a reminder hydrostatic equilibrium exists if the force due to gravity is balanced by the vertical pressure gradient force, leading to this relationship. Hydrostatic equilibrium is widely satisfied over horizontal scales exceeding 10km, and thus the assumption is used to simplify the governing equations of numerical models of the atmosphere that use a grid-cell size exceeding this threshold

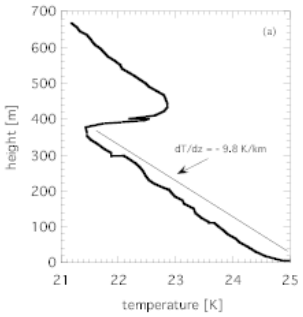

Figure 1: Vertical profile of the temperature T for a clear convective boundary layer as observed by a tethered balloon at Cabauw, Netherlands, around 10:00 h (local time), 23 Aug 2001.

Eqn. 31 can be integrated to give *Poisson's Equation*:

$$\frac{T}{T_0} = \left(\frac{p}{p_0}\right)^{\frac{R_d}{c_p}} \tag{32}$$

where T_0 and p_0 are constants of integration. *see Exercise: Derive this equation.*

Note that we have reintroduced the subscript d on the gas constant to emphasize that this considers dry air.

2.6 Potential Temperature

Potential Temperature
If we set the reference pressure p_0 to 1000 hPa then T_0 is defined as the *potential temperature* (for dry air) which is commonly denoted θ:

$$\theta = T\left(\frac{p_0}{p}\right)^{\frac{R_d}{c_p}}. \tag{33}$$

The potential temperature θ can be interpreted as the temperature a parcel would have if it were displaced adiabatically to a reference height where the pressure is p_0, which is usually taken $p_0 =$ 1000 hPa. In other words, a parcel with temperature T at pressure level p will have a potential temperature θ, which value is equal to the temperature T_0 at the pressure level p_0.

The *lapse rate* of the potential temperature can be obtained by differentiating (33) with respect to height

$$\frac{d\theta}{dz} = \frac{\theta}{T}\left(\frac{dT}{dz} - \frac{R_d T}{pc_p}\frac{dp}{dz}\right) \tag{34}$$

Assuming that the atmosphere is in a hydrostatic balance, $dp/dz = -\rho g$, then with aid of the gas law (34) can be written as

$$\frac{d\theta}{dz} = \frac{\theta}{T}\left(\frac{dT}{dz} + \frac{g}{c_p}\right). \tag{35}$$

Since $-\frac{g}{c_p} = \Gamma_d$ is the *dry adiabatic lapse rate*, we conclude that if the temperature profile follows the dry adiabatic lapse rate, the potential temperature is constant with height.

2.7 Entropy

A *reversible* process is defined as

$$\oint \frac{\delta Q}{T} = 0. \tag{36}$$

This integral is independent of the path. The specific entropy ϕ is defined as

$$d\phi = \frac{dq}{T}. \tag{37}$$

Unlike heat and work, the entropy is a state variable, thus we can speak of the entropy in state A or B. Note that, with the temperature in the denominator of (36), heat and entropy are not linearly related.

An isentropic process (iso = "equal" (Greek); entropy = "disorder") is one during which the entropy of the system remains constant; a reversible, adiabatic process is isentropic.

The second law of thermodynamics states that a process will tend to increase the entropy of a system, thus $Td\phi = du + pdv \geq 0$. The relevance of entropy to meteorologists is clear if we define the potential temperature in terms of the entropy:

$$d\phi = c_p d \ln \theta. \tag{38}$$

Exercise: Derive eqn. 38. Hint: Take logs of eqn. 33 and differentiate

2.8 Thermodynamic charts

The heat added in a cyclic process is[3]

$$\oint dq = \oint T d\phi = c_p \oint T d(ln\theta), \tag{39}$$

where the last equality follows from using (38). Thus it is clear that a chart that has perpendicular coordinates of temperature T and entropy ϕ, or equivalently T versus $ln\theta$ will have the properties of *equal areas=equal energy* ; useful properties of a thermodynamic diagram.

tephigrams

Such a chart is known as a *tephigram*. Using (33) one can plot p as a function of the two ordinates. Note that the lines of constant pressure, (isobars), are not exactly straight lines.

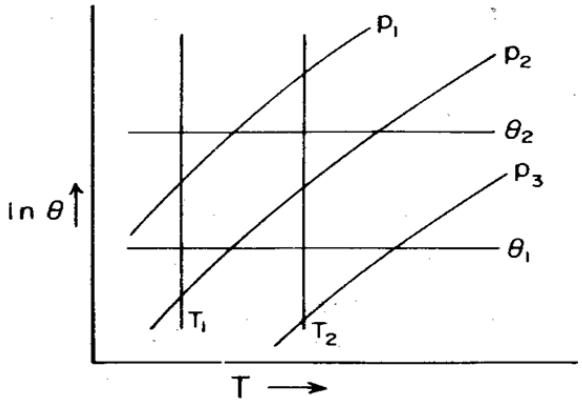

Figure 2: The tephigram basic structure

Meteorologists are used to using pressure as a vertical height coordinate and thus rotate the chart to make the curved pressure lines almost horizontal, as shown in Figure 3.

2.9 Buoyancy force on a parcel

To calculate the buoyancy force on a parcel of air we will assume that the atmosphere is in hydrostatic balance and that pressure field is not perturbed by the presence of the air parcel. The parcel of (dry) air has a with volume V, temperature T and density ρ. It displaces an equal volume of ambient environmental (noted by subscript env) air having properties T_{env}, ρ_{env}. The downward force on the parcel is $\rho g V$ and on the air it displaces $\rho_{env} g V$. The upward force $-V\frac{\delta p}{\delta z}$ is identical for both. Hence the net upward force is $Vg(\rho_{env} - \rho)$ and the buoyancy force per unit mass

$$F_B = g\left(\frac{\rho_{env} - \rho}{\rho}\right) \tag{40}$$

[3]This can also be derived directly from the first law and the hydrostatic relation.

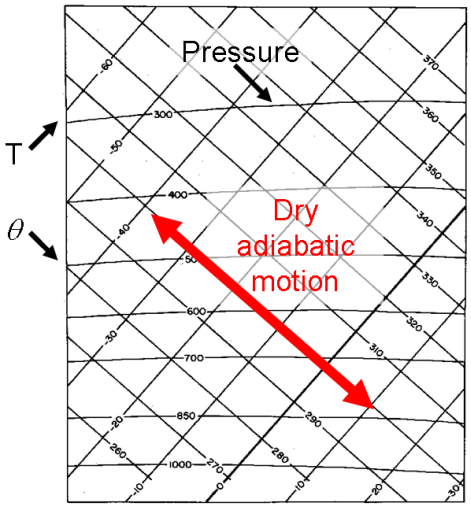

FIG. 1.7. Skeleton of a tephigram. Isobars are approximately horizontal, labeled in mb. Isotherms in deg C go upwards and to the right. Dry adiabats are normal to the isotherms and are labeled according to potential temperature (deg K).

Figure 3: A tephigram as they are usually used, with the chart rotated to make the pressure lines horizontal. Note that the lines of θ are not equally spaced - **Q: Why?**.

Now using Poisson's eqn, (40) can written

$$F_B = g\left(\frac{\theta - \theta_{env}}{\theta_{env}}\right) \tag{41}$$

If a parcel of air is warmer(cooler) than its environment it will be subject to a net upwards (downwards) buoyancy force and will accelerate upwards (downwards), and is usually referred to as *positively (negatively) buoyant*. Equal temperatures are referred to as *neutral buoyancy*.

A parcel of air that is neutrally buoyant and subjected to a small vertical displacement may become positively or negatively buoyant, depending on whether the parcel's temperature changes changes more or less rapidly than the environmental lapse rate.

The environmental θ lapse rate is $\frac{d\theta_{env}}{dz}$ and we will assume the lifted parcel cool adiabatically (reminder: what does this mean?) and thus θ of the parcel is invariant.

We can thus define three situations:
$\frac{d\theta_{env}}{dz} < 0$: **Unstable**
$\frac{d\theta_{env}}{dz} = 0$: **Neutral**
$\frac{d\theta_{env}}{dz} > 0$: **Stable**

With the example stable and unstable profiles shown in Fig. 4 We will now return to the Cabauw profiles (Fig. 1). *Q: Why do you think the profile is near neutral?* Figure 5 shows observations made in a clear convective boundary layer (CBL). Because of solar radiative heating turbulent eddies are driven from ground surface. The thermals can penetrate into the thermal inversion, which for this case is located at about 380 m, above which they are damped by the stable stratification. The turbulent eddies warm the upper boundary layer thus bringing an unstable stratification profile back towards neutrality. The fact that the profile of temperature is "well-mixed", with the temperature following approximately the dry-adiabatic lapse rate, implies that the warming timescale associated with the turbulent eddy mixing is fast compared to the processes that destabilize the profile (such as radiative cooling of the boundary layer). Were this not the case, super-adiabatic unstable layers could form, such as in the surface layer when strongly heated by the sun.

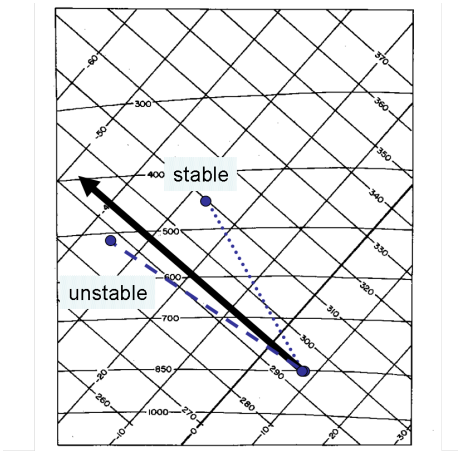

Figure 4: Two idealized profiles showing (dotted/dashed) stable/unstable environmental temperature profiles

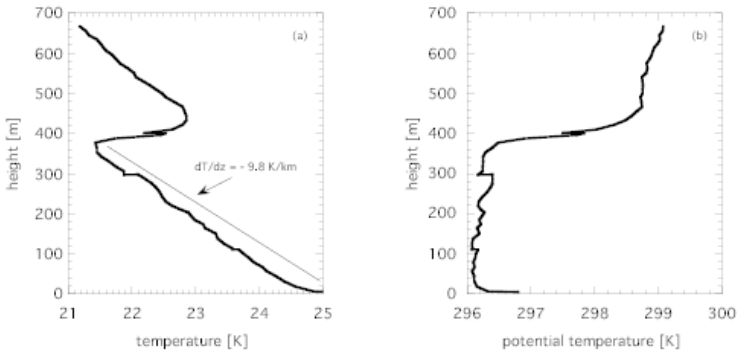

Figure 5: Vertical profile of the potential temperature θ for the Cabauw profile in Fig. 1.

Without instrumentation to measure the profile of temperature one can not say whether a boundary layer is well mixed, however one clue is the presence of a gusty intermittent wind associated with the turbulent eddies, while if the layer is deep enough such that the top of the boundary layer becomes saturated and forms "fair weather cumulus" cloud (see next section) then this is a sure sign that the boundary layer is well mixed and close to neutral stability.

Thus *unstable* layers are quite uncommon except in the lowest few metres of the atmosphere, *neutral* layers are quite common and result from the convective/turbulent reaction to processes that produce instability, and *stable* layers are also common. In this case displaced parcels of air will undergo simple harmonic motion.

Lenticular or lee-wave cloud indicating atmospheric stable layer. Courtesy UCAR

Reminders:

- If we express the gas law in terms of mass instead of moles, we switch from using the universal gas constants to a specific gas constant whose value depends on the molecular weight.
- The dry atmosphere and water vapor can be taken to a good approximation as an ideal gas.
- The state of the atmosphere can be expressed by three state variables, p, v and T, of which two are independent.
- The first law of thermodynamics dictates that energy is conserved.

2.10 Exercises

1. Assume that a parcel of air undergoes net diabatic radiative cooling of 10^{-5} Ks^{-1}. The parcel is also undergoing vertical motion at the same time at a velocity of w. We will assume that we can neglect the impact of radiation if the heating/cooling associated with the vertical motion is at least ten times greater. What would be the minimum vertical velocity of the parcel for this to be the case? What are typical rates of ascent in cumulus clouds in comparison?
2. In the subtropical free (above the boundary layer) troposphere there is an approximate balance between radiative cooling and dry adiabatic descent of the air. Assuming a net radiative cooling of 10^{-5} Ks^{-1}, what rate must the air descend at to maintain equilibrium?

3 Moist thermodynamics

Moist Thermodynamics
In the previous section we restricted our analysis to dry air, *we now extend this to include water*, which unlike other atmospheric constituents, can appear in all its three phases: solid, liquid and vapour.

Equation of state for water vapour
Water vapour can be treated as an ideal gas to a good approximation and thus from the gas law it follows that

$$e = \rho_v R_v T, \tag{42}$$

where ρ_v is the density of water vapor, and R_v is the specific gas constant for water vapour which is equal to 461.5 J kg^{-1} K^{-1}.

In the literature the ratio between the gas constants for dry air and water vapour is used:

$$\epsilon = \frac{R_d}{R_v} = \frac{m_v}{m_d} \tag{43}$$

where $\epsilon = 0.622$ from the values of the gas constants.

Atmospheric air is a mixture of the ideal gases of dry air and water vapour. From Dalton's law, the total pressure of moist air is the sum of the partial pressures of the dry air and the vapour

$$p = p_d + e. \tag{44}$$

3.1 Saturation

Imagine a closed system consisting of a water body and a vacuum above. The water molecules in the water body are in a state of thermal agitation and the most energetic ones will overcome the intermolecular attraction and break free of the water body. The rate at which vapor molecules leave the surface depends upon the characteristics of the surface. The process is known as *evaporation*. The vapour vapour pressure increases as a result, which will be denoted e. Some of the water molecules will subsequently collide with the water surface and stick to the surface. This process is known as *condensation*, and decreases the vapour pressure. The rate at which vapor molecules arrive at a surface of liquid (cloud drop) or solid (ice crystal) depends upon the *vapor pressure*. Since the condensation depends on the vapour pressure, it is apparent that in the absence of external perturbations a state of dynamic equilibrium will eventually be reached in which the rates of *condensation* and *evaporation* equal each other (considering only liquid for now). The vapour is said to be *saturated* in this case, and the vapour pressure e is equal to the so-called *saturation vapour pressure e_s with respect to water.*

As the evaporation rate is only dependent on temperature, and the condensation rate on the vapour pressure, there are two important consequences to note concerning e_s:

1. e_s depends on T and T *only.*
2. Saturation is *independent* of the pressure of other gases

Supersaturation
If the saturation vapour pressure exceed the saturation value $e > e_s$ then the air is said to be *supersaturated* with respect to liquid water. We shall see that greatly supersaturated states *with respect to liquid water* in the atmosphere are not observed, as the excess water vapour quickly condenses to form liquid cloud droplets. The phrase *liquid water* is emphasized as the situation is not the same when it comes to cloud ice crystals as we shall see.

We now derive the dependence of e_s on T. Heat must be supplied to change a unit mass of liquid to vapour at a constant temperature; this is known as the *Latent Heat of Vaporization*, denoted L_v. Throughout the process of evaporation the e_s remains constant as it is a function of T only. For the transition from liquid phase q_1 to vapour phase q_2,

$$L_v = \int_{q_1}^{q_2} dq = \int_{u_1}^{u_2} du + \int_{v_1}^{v_2} p dv = u_2 - u_1 + e_s(v_2 - v_1). \tag{45}$$

However, since temperature is also constant we can write

$$L_v = T\int_{q_1}^{q_2} \frac{dq}{T} = T(\phi_2 - \phi_1) \tag{46}$$

Equating (45) and (46) shows

$$u_1 + e_s v_1 - T\phi_1 = u_2 + e_s v_2 - T\phi_2. \tag{47}$$

Gibbs Function
This implies that the so-called *Gibbs Function*

$$G = u + e_s v - T\phi \tag{48}$$

of a system is constant during isothermal, isobaric changes of phase.

The Gibbs function does vary however as a function of temperature and pressure, and differentiating (48) gives:

$$dG = du + v de_s + e_s dv - T d\phi - \phi dT. \tag{49}$$

But $Td\phi = dq = du + e_s dv$ giving

$$dG = v de_s - \phi dT. \tag{50}$$

The Gibbs function is independent of phase, such that $dG_1 = dG_2$:

$$v_1 de_s - \phi_1 dT = v_2 de_s - \phi_2 dT. \tag{51}$$

Clausius Clapeyron Equation
We can now rearrange (51) to derive the *Clausius Clapeyron Equation*:

$$\frac{de_s}{dT} = \frac{\phi_2 - \phi_1}{v_2 - v_1} = \frac{L_v}{T(v_2 - v_1)}, \tag{52}$$

where the last relationship uses (46). Under ordinary conditions the specific volume for water vapour is much greater than that of liquid, $v_2 \gg v_1$ allowing the Clausius Clapeyron equation to be approximated as

$$\frac{de_s}{dT} \approx \frac{L_v}{T v_2} = \frac{L_v e_s}{R_v T^2}, \tag{53}$$

where the final relationship uses the Gas Law once again.

At first sight it would appear to be straightforward to integrate (53) to give e_s as a function of T, but this is complicated by the fact that the Latent heat of vaporization L_v is itself a function of temperature. Fortunately this dependence is weak, with L_v varying by 6% from -30°C to +30°C. Neglecting this dependence as a first approximation, integrating (53) gives

$$e_s = e_{s0}\exp\left[\frac{L_v}{R_v}\left(\frac{1}{T_0} - \frac{1}{T}\right)\right]. \tag{54}$$

e_{s0} is the vapour pressure at temperature T_0, and at $T = 0$°C we have e_{s0} =6.11 hPa, and a value of 2.50×10^6 J kg^{-1} can be assumed for L_v. Substituting these values gives an approximate for for e_s as

$$e_s(T) = Ae^{\frac{-B}{T}} \tag{55}$$

where the constants are $A = 2.53 \times 10^8$ kPa and $B = 5.42 \times 10^3$ K. e_s doubles for every 10°C increase in temperature. Note that the nonlinearity of the saturation vapour pressure has important consequences for mixing of air parcels as is thus relevant for processes such as atmospheric convection. Below the freezing point at $T = 0$°C the Clausius Clapeyron equation describes the saturation pressure of *supercooled* liquid water (liquid water at temperatures below 0°C), and this is still relevant as we will see later that ice crystals do not form at $T = 0$°C and supercooled liquid cloud droplets are common. Of course at temperatures below freezing ice crystals may be present, and the saturation vapour pressure of ice, denoted e_i is also described by (53) but with L_v replaced

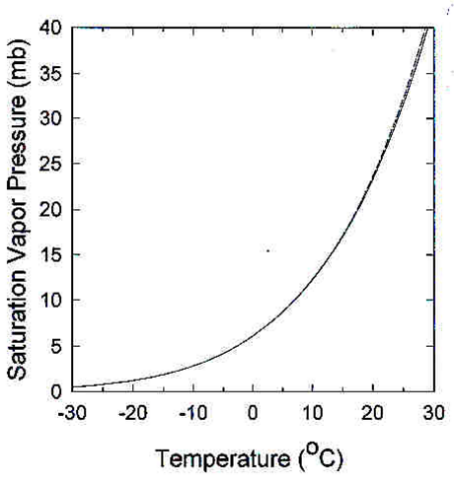

Figure 6: The saturation vapour pressure as a function of temperature

by L_s, which is the *Latent heat of Sublimation*, for which a value of 2.83×10^6 J kg^{-1} can be used. The ratio between the two at subfreezing temperatures is

$$\frac{e_s(T)}{e_i(T)} = \exp\left[\frac{L_f}{R_v T_0}\left(\frac{T_0}{T} - 1\right)\right], \tag{56}$$

where L_f is the *Latent Heat of Fusion* and is equal to $L_s - L_v$.

The dependency of the latent heat of vaporization on the temperature
To calculate the dependency of L_v on T we use (45) and note again that $v_2 \gg v_1$ and that $e_s v_2 = R_v T$. Then differentiating we get

$$\frac{dL_v}{dT} = \frac{du_2}{dT} - \frac{du_2}{dT} + R_v \tag{57}$$

Now $\frac{du_2}{dT} = c_{vv}$ which is the *specific heat capacity of water vapour at constant volume* and $\frac{du_2}{dT} = c_{vl}$ is the *specific heat capacity of liquid water at constant volume.*

We again note the relationship that the *specific heat of water vapour at constant pressure* $c_{pv} = c_{vv} + R_v$, and then integrate to get

$$L_v(T) = L_0 - (c_{vl} - c_{pv})(T - T_0), \tag{58}$$

where $L_0 = L(T_0)$ is the constant of integration. Both c_{vl} and c_{pv} vary as a function of temperature and pressure, but this variation is weak amounting to less than 3% over the full range of tropospheric conditions, and the constant values of c_{pv} =1870 J kg^{-1} K^{-1} and c_{vl} =4187J kg^{-1} K^{-1} will be assumed here, while $c_{vv} \simeq$1410 J kg^{-1} K^{-1}. For a complete list of gas constant and specific heat values refer to Appendix 2 of Emanuel (1994).

3.2 Other measures of water vapour

In addition to the *vapour pressure* e and the *vapour density* ho_v, there are alternative ways to describe the water vapour content of air that are more commonly used in Meteorology.

Mixing Ratio r_v
This is defined as the mass of water vapour per unit mass of *dry* air

$$r_v = \frac{M_v}{M_d} = \frac{\rho_v}{\rho_d}. \tag{59}$$

From the equation of state, $\rho_d = \frac{p-e}{R_d T}$, so that

$$r_v = \frac{\epsilon e}{p - e} \tag{60}$$

The saturation mixing ratio r_s, *with respect to liquid water*, is defined by replacing e with e_s, and is a function of both pressure and temperature.

Specific Humidity q_v
This is defined as the mass of water vapour per unit mass of *moist* air

$$q_v = \frac{\rho_v}{\rho} = \frac{\rho_v}{\rho_d + \rho_v}, \tag{61}$$

and using the same substitution as above

$$q_v = \frac{\epsilon e}{p - (1-\epsilon)e} \tag{62}$$

The saturation specific humidity is defined by replacing e with e_s. At all normal atmospheric conditions $e \ll p$, implying that in practice

$$q_v \approx r_v \approx \frac{\epsilon e}{p}, \tag{63}$$

The difference between r_v and q_v is greatest at the surface in the tropics and roughly 2% there[4].

Relative Humidity RH
The ratio of the vapour pressure to its saturated value:

$$RH = \frac{e}{e_s}. \tag{64}$$

Note that the relative humidity can be approximated as

$$RH \approx \frac{r}{r_s}, \tag{65}$$

however often this is used as an exact relationship in the literature. Some texts such as Rogers and Yau (1989) break this convention altogether and define RH in terms of mixing ratio and state (64) as an approximate relationship

Virtual Temperature T_v
A *hypothetical temperature*, the virtual temperature is the temperature a sample of dry air would have to have the same density as the same of moist air in question, at the same pressure.

To derive T_v we recall:

$$p = p_d + e = \rho_d R_d T + \rho_v R_v T = \frac{R^* T}{V}\left(\frac{M_d}{m_d} + \frac{M_v}{m_v}\right), \tag{66}$$

and using the gas law we get

$$p = \frac{\rho R^* T}{(M_d + M_v)}\frac{M_d}{m_d}\left(1 + \frac{M_v}{M_d}\frac{m_d}{m_v}\right). \tag{67}$$

Recalling the definitions of $\epsilon = m_v/m_d$ and $r_v = M_v/M_d$, (67) can be simplified to (*Exercise: Show*)

$$p = \rho R_d T\left(\frac{1 + \frac{r}{\epsilon}}{1 + r}\right) \tag{68}$$

Thus the equation of state for moist air can be written as the equation of state for dry air, but using the adjustment factor in brackets. We thus define the virtual temperature as

$$T_v \equiv T\left(\frac{1 + \frac{r_v}{\epsilon}}{1 + r_v}\right) \tag{69}$$

[4]This similarity leads to the two terms being used almost interchangeably in meteorology, not good practice, and one that is not helped by the fact that the notation for the specific humidity and mixing ratio are not standard, with q_v often used for mixing ratio in the literature. Note also that the subscript v is not always used.

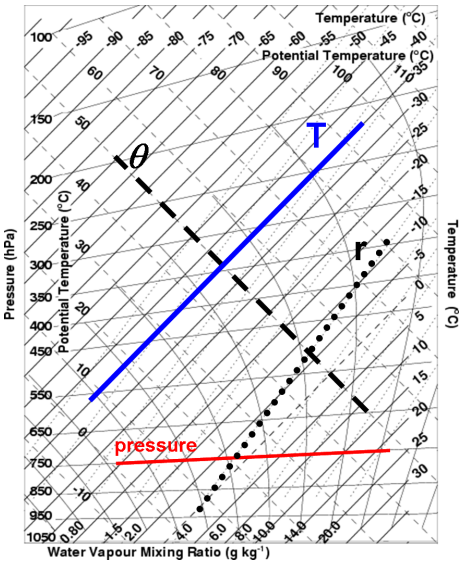

Figure 7: A blank tephigram with isopleths of r_s highlighted.

Allowing us to write the equation of state for moist air as

$$p = \rho R_d T_v. \tag{70}$$

Since $r_v \ll 1$, by ignoring second order terms the definition of T_v can be simplified to *Exercise: show*

$$T_v = T(1 + \frac{1-\epsilon}{\epsilon} r_v) \tag{71}$$

We can see that for moist air $T_v > T$ always since a unit volume of moist air is less dense than a unit volume of dry air. Thus for moist air it is T_v that should be used in the definition of buoyancy to account for this effect. We define the *virtual* potential temperature in terms of T_v

$$\theta_v \equiv T_v \left(\frac{p_0}{p}\right)^{\frac{R_d}{c_p}}. \tag{72}$$

and this quantity is conserved in adiabatic motion of moist air. We can apply the equation of state to moist air by replacing T with T_v, or we can alternatively use the gas constant for moist air R_m:

$$pv = R_d T_v = R_m T \tag{73}$$

Thus we can see that R_m is related to R_d by

$$R_m = R_d \left(\frac{1 + \frac{r_v}{\epsilon}}{1 + r_v}\right). \tag{74}$$

Take care not to confuse R_m with R_v.

Water Vapour in Tephigrams

We now return to the tephigram introduced in the previous section and add lines of constant (isopleths of) saturation mixing ratio to the tephigram, recalling from (60) that r_s is a function of pressure and temperature (Fig.7). *Q: This tephigram has an error, such that it is not a true thermodynamic chart. What is it?*

As an aside we reproduce a scanned correct tephigram in Fig. 8, as used and produced by the UK Meteorological Office, unfortunately only for the lower half of the troposphere to 500 hPa. Thus if at a pressure of 950 hPa we measure a temperature of 20°C, we can plot this on the tephigram, marked as a cyan star in Fig. (9. Likewise if we measure a mixing ratio of $r = 10gkg^{-1}$ we can also plot this using the mixing ratio isopleths, marked as an orange star. Making measurements through out the atmosphere (e.g. by a balloon) we can plot a sounding of temperature and humidity, as show by the yellow and blue stars.)

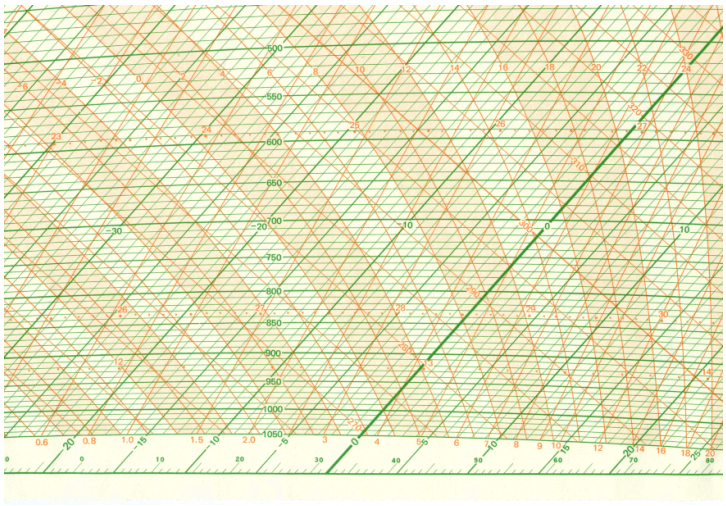

Figure 8: A *correct* tephigram. Courtesy EWG at McGill.

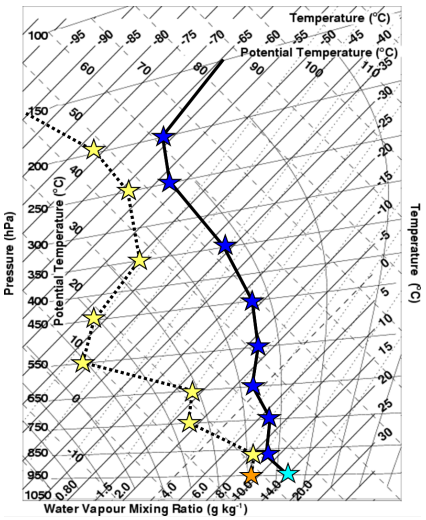

Figure 9: tephigram with T and r soundings plotted

3.3 Tephigram Exercises

Tephigram Ex 1 Using the correct tephigram shown in Fig. (8) plot the sounding data given in table 2.

1. How deep is the planetary boundary layer (PBL) in hPa?
2. Is the PBL neutral, stable or unstable ?
3. What is the RH at 1000 hPa and 900 hPa?
4. What is T_d at 1000 hPa?
5. Is the PBL "well mixed" in humidity?
6. What is the potential temperature θ of an air parcel at p=800hPa?
7. If this air parcel undergoes adiabatic ascent until it reaches a pressures of p=700hPa. What is its new T and θ?

We will now return to the Cabauw profiles (Fig. 1) and examine the humidity measurements taken during the balloon ascent, which are shown in Fig. 10. These show the sharp drop in humidity at the boundary layer top at 400m and that the humidity is roughly constant through the boundary layer. From the RH profile, we can see relative humidity increasing through the boundary layer and that the top of the boundary layer is almost saturated.

$p(hPa)$	T (°C)	r (g kg^{-1})
1000	10.0	5.0
950	6.5	4.7
900	3.1	4.5
850	2.5	3.2
800	0.0	2.8
700	-5.1	1.4
600	-12.0	1.3
500	-17.6	0.9

Table 2: An arbitrary atmospheric sounding

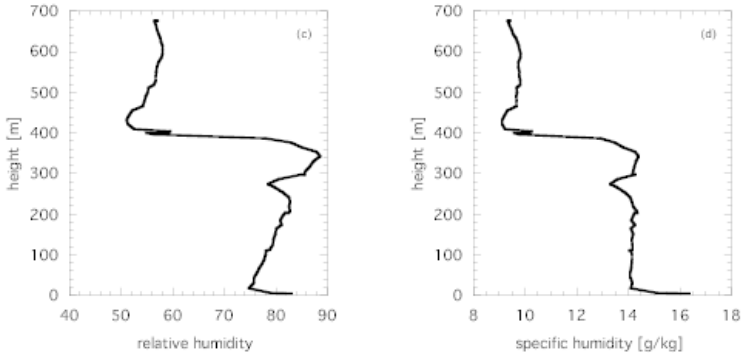

Figure 10: Vertical profile of RH and θ for the Cabauw profile in Fig. 1.

Tephigram Ex 2

Assuming that $r_v \approx q_v$ plot the tephigram of the Cabauw balloon ascent reading T (or θ) and q values at the levels of 50m, 200m, 260m, 300m, 350m, 400m, 450m and 650m from Figs. 1 and 10. To convert height into a pressure coordinate simply assume that $p = 1000$ hPa at the surface and that pressure drops with a scale-height of 7km, i.e. $p = p_0 \exp(-z/7000)$. You will see how the profiles of T and q in the boundary layer lie close to their respective isopleths of conserved quantities. What is happening at $z = 260m$ do you think?

3.4 Water variables in the liquid and ice state

Analogous to the water vapour variables described above we can define similar variables that describe the quantity of liquid water or ice in air

- Absolute liquid (ice) water ice density[5] : ρ_l or L kg m^{-3} (or ρ_i)
- Liquid (ice) water mixing ratio: $r_l = \frac{\rho_l}{\rho_d}$ kg kg^{-1} (or r_i)
- Specific liquid (ice) water content: $q_l = \frac{\rho_l}{\rho}$ kg kg^{-1} (or q_i)

The total water mixing ratio is the sum of the three phases $r_t = r_v + r_l + r_i$. Additionally, analogous to the T_v we can define the density temperature[6] T_ρ which is the temperature dry air would have to have equal density to moist cloud air

$$T_\rho \equiv T \left(\frac{1 + \frac{r_v}{\epsilon}}{1 + r_t} \right) \tag{75}$$

Similarly to T_v, if we assume $r_l \ll 1$ and $r_i \ll 1$ and ignore second order terms we get

$$T_\rho \simeq T(1 + \frac{1-\epsilon}{\epsilon} r_v - r_l - r_i) \tag{76}$$

The last two terms show how liquid and ice make a parcel more dense, and this effect is referred to as the *water loading effect*.

[5]Attention! The absolute liquid water density here is the total mass of liquid water droplets divided by a unit volume of cloudy air - this is not to be confused with the density of liquid water which will denoted ρ_L. To avoid confusion, the rest of this course always uses liquid water mixing ratio or specific water content, or we will use the notation L instead of ρ_l

[6]Again, there is not agreement in the literature concerning the virtual temperature T_v which is sometimes defined to include liquid and ice. Here we follow the notation of Emanuel (1994)

Figure 11: We will now start to consider processes relevant to deep moist convection so here is a superfluous photo to motivate you (source unknown)

3.5 Specific heat of moist air

Specific heat of moist air c_{vm} and c_{pm}
The presence of moisture alters the specific heat capacity of air. We add heat to a sample of air consisting of a unit mass (1kg) of dry air and r kilograms of water vapour

$$(1+r)dq = c_v dT + r c_{vv} dT \tag{77}$$

this gives

$$c_{vm} = \frac{dq}{dT} = c_v \left(\frac{1 + \frac{c_{vv}}{c_v} r}{1+r} \right) \tag{78}$$

As $c_{vv}/c_v = 1.96 \approx 2$ then ignoring second order terms,

$$c_{vm} \approx c_v(1+r) \tag{79}$$

Likewise the *specific heat at constant pressure* can be approximated

$$c_{pm} \approx c_p(1+0.9r) \tag{80}$$

As $r < 10^{-2}$ these correction factors can generally be neglected.

Reminders:

- What does it mean for air to be saturated?
- What is e_s a function of?
- What was one of the problems to get an expression $e_s = F(T)$?
- *Q: Can you think of some processes by which air can become saturated?*

3.6 Ways of reaching saturation

Ways of reaching saturation
There are several processes by which a parcel of air may become saturated which are all relevant to cloud physics:

- Diabatic cooling (e.g. radiation)
- Adiabatic cooling (e.g. ascent)
- Evaporation (e.g. of precipitation falling through parcel)

Diabatic Cooling: Dew Point Temperature T_d
As air is cooled isobarically, r is conserved, and the air will reach saturation when T is such that

$$r_s(T) = r. \tag{81}$$

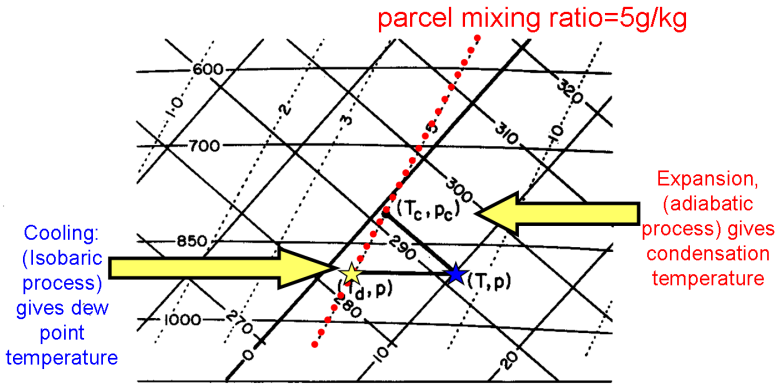

FIG. 2.2. Temperature, dew point, and isentropic condensation temperature, indicated on a tephigram. In the example shown the sample of air at 10°C, 900 mb, is assumed to have a mixing ratio of 5 g/kg. Its dew point, found from the intersection of the 900 mb isobar and the 5 g/kg vapor line, is 2.2°C. Its isentropic condensation point, found from the intersection of the adiabat through (T, p) with the 5 g/kg vapor line, is at 0.7°C and approximately 800 mb.

Figure 12: Figure from Rogers and Yau (1989) showing the dew-point and condensation temperatures. See text for details

Figure 13: Schematic of parcel ascending and reaching saturation, with condensed water falling out instantaneously in the so-called *pseudo-adiabatic* assumption.

This temperature is known as the *Dew Point Temperature* T_d. One can write equivalently $e(T) = e_s(T_d)$.

Adiabatic Cooling: Condensation Temperature T_c
As air is cooled adiabatically, θ_v is conserved, and the air will reach saturation at the *isentropic condensation temperature and pressure*. This pressure level is sometimes referred to as the *lifting condensation level* or LCL.

If ascent and expansion continues condensation will occur (we will see why air does not become supersaturated with respect to liquid later), *thus the temperature will decrease at a slower rate*. Now in this conceptional model of a parcel of air undergoing ascent in a cumulus cloud, we need to decide what happens to the condensed water: Does it remain in the parcel or will it fall out? *Q: If the droplets remain in the parcel what do we need to consider?*

Pseudo-adiabatic process
If it is assumed that the condensed water remains in the parcel of air then we would need to account for its *water loading* effect and its modification of the *heat capacity*. Moreover when the freezing point is reached we need to consider if and how some of the liquid droplets will freeze, invoking ice processes which are complex, as we shall see. These are issues concerning *microphysics* and *cloud dynamics*, thus involving a *cloud model*.

For now we take the simplest case and assume that all condensate is immediately lost as precipitation, known as the *pseudo-adiabatic* assumption (Fig. 13).

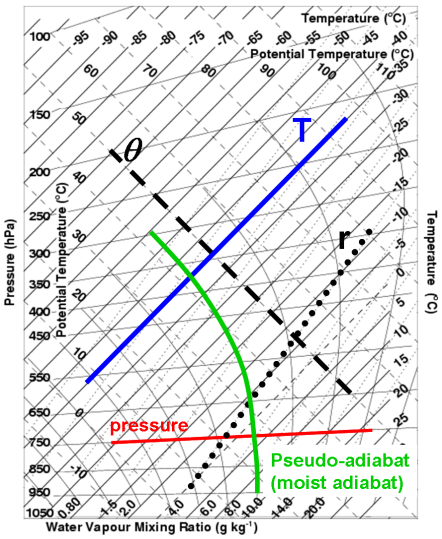

Figure 14: A blank tephigram with moist adiabats highlighted.

For moist saturated ascent and neglecting correction factor for the specific heat (so we can use c_p),

$$c_p dT - vdp + L_v dr_s \simeq= 0 \tag{82}$$

Thus the saturated moist adiabatic lapse rate Γ_s is

$$\Gamma_s = \frac{dT}{dz} = \frac{v}{c_p}\frac{dp}{dz} - \frac{L_v}{c_p}\frac{dr_s}{dz} = \Gamma_d - \frac{L_v}{c_p}\frac{dr_s}{dz} \tag{83}$$

As temperature falls with height, $\frac{dr_s}{dz}$ is negative implying that $\Gamma_s > \Gamma_d$. Recalling that Γ_d = -9.8 K km^{-1}, Γ_s is generally between -3 to -4 K km^{-1} in the lower troposphere. *Q: In the upper troposphere $\Gamma_s \sim \Gamma_d$, why is this the case?*

Isobaric Equivalent temperature T_{ie}
Let us take two parcels of air at the same pressure, but that differ in both their temperatures and humidity contents; how can we compare them energetically? One measure is the *isobaric equivalent temperature*, T_{ie}. T_{ie} is the temperature that a parcel would have if all of the humidity would condense isobarically.

As this is an isobaric process then it is clear that

$$T_{ie} = T + \frac{L_v}{c_p} r_v \tag{84}$$

neglecting the temperature dependence of L_v as always.

Adiabatic Equivalent temperature T_e
As this isobaric process of T_{ie} can not occur in the atmosphere, we can instead define the tephigram related *adiabatic equivalent temperature* T_e, by raising the parcel to the upper-troposphere and then descending to the original pressure.

From (82), we divide by $c_p T$, use the first law, and then assume T is constant in the humidity term (a fairly reasonable approximation as T varies by at most 30%) will allows us to integrate to get

$$T_e = T \exp\left(\frac{L_v r_v}{c_p T}\right). \tag{85}$$

Sometimes you will see T set to T_c in the humidity term, giving T_c in the exponential term on the RHS.

Equivalent potential temperature θ_e

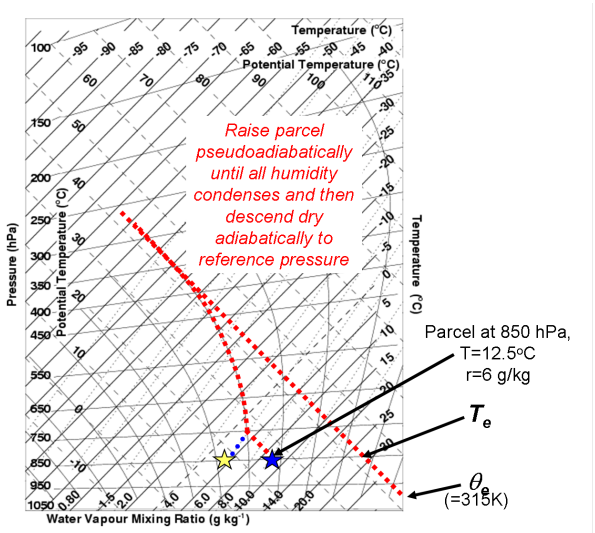

Figure 15: A blank tephigram showing the definition of T_e and θ_e.

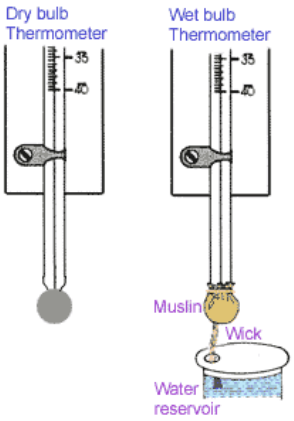

Figure 16: Method of measuring the wet-bulb temperature

We found it useful to derive θ_v which was conserved in dry adiabatic motions. An analogous quantity (approximately) conserved in moist adiabatic motions is the *equivalent potential temperature* θ_e.

We will see that each moist adiabat is uniquely labelled by one value of θ_e. The graphical determination of this is given in Fig. 15: after condensation the parcel follows a moist adiabat until all moisture is condensed, and then descends dry adiabatically to the reference pressure. θ_e can be approximated by

$$\theta_e = \theta \exp\left(\frac{L_v r_v}{c_p T}\right) \tag{86}$$

Evaporation: Wet Bulb Temperature T_w
In a Stevenson screen there is usually a wet bulb thermometer to measure the wet bulb temperature T_w, and determine the atmospheric water vapour content. The thermometer bulb is wrapped in a muslin clothe kept damp by a wick to a liquid reservoir, and the bulb is thus cooled by the evaporation process (Fig. 16). T_w is the temperature reached if water vapour is evaporated into it until it becomes saturated, with the latent heat provided by the air. Note that $T_d \leq T_w \leq T$, and that the difference between T_w and T_d provides a measure of the saturation of the atmosphere

To calculate the wet-bulb temperature we consider an air parcel consisting of unit mass of dry air with r_v mass of water vapour. The heat associated with the evaporation of dr_v is $-L_v dr_v$. Thus

$$(1 + r_v) C_{pm} dT = -L_v dr_v \tag{87}$$

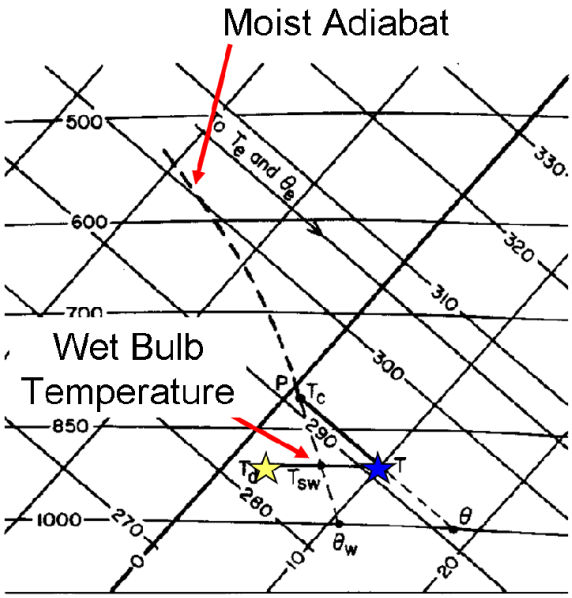

Figure 17: Figure from Rogers and Yau (1989) showing the calculation of wet-bulb temperature from a tephigram. This is known as **Normand's Construction**.

Using the definition of C_{pm} we get

$$C_p dT \simeq \frac{-L_v dr_v}{(1+r_v)(1+0.9r)} \tag{88}$$

For most purposes, we can neglect the correction factors and assume

$$C_p dT \approx -L_v dr_v \tag{89}$$

Treating L_v as constant we can integrate to get

$$T_w = T - \frac{L_v}{C_p}(r_s(p, T_w) - r_v) \tag{90}$$

To get T_w we substitute (55) to give a form that can be solved by interaction:

$$T_w = T - \frac{L_v}{C_p}(\frac{\epsilon}{p} A e^{\frac{-B}{T}} - r_v) \tag{91}$$

However we can estimate T_w directly from the tephigram as we shall see now. Figure 17 shows the construction to derive the wet bulb temperature T_w from a tephigram by lifting a parcel adiabatic to reach saturation and then following a moist adiabat back down to the original pressure. If the moist adiabat is followed to a reference pressure P_0 =1000 hPa, then the resulting temperature is known as the *wet bulb potential temperature* θ_w. Note that there is a one-to-one unique mapping between θ_w and $theta_e$. With each referring to a unique moist adiabat.

Tephigram Exercises III
Return to the sounding you plotted using the data in Table 2.

1. For a parcel of air at 1000 hPa, what is the condensation temperature T_c and pressure ?
2. For a parcel of air at 1000 hPa, what is the dry bulb or dew point temperature T_d?
3. If rainfall is evaporated into this parcel, at what temperature will it become saturated and what is this temperature called?
4. What will be the parcel's mixing ratio at this point?
5. What is the parcel's equivalent potential energy θ_e?
6. What is θ_e for a parcel at 900 and 700 hPa?
7. Is θ_e increasing or decreasing with height?

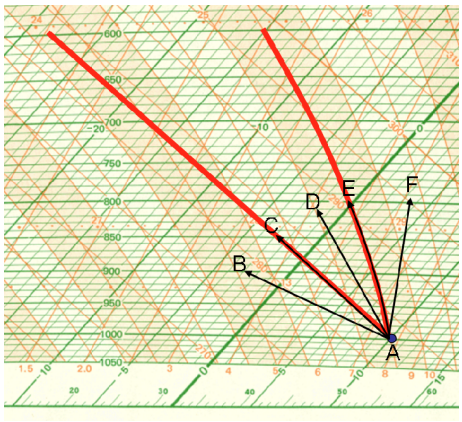

Figure 18: Tephigram showing 5 possible stability categories for environmental lapse rate. The red lines highlight the parcel dry and moist adiabats.

.

3.7 Static stability in a moist environment

The presence of instability is of great importance in weather forecasting and to understand the various climatic regimes. Earlier we classified three stability states in a dry environment. For a moist environment there are five stability categories.

- AB: Absolutely unstable (even if unsaturated, parcel is warmer),
- AC: Dry Neutral (parcel is neutral to dry ascent),
- AD: Conditionally unstable (for unsaturated ascent profile is stable, while it is unstable for saturated ascent),
- AE: Saturated Neutral (for saturated ascent parcel neutral),
- AF: Absolutely stable

Key convective parameters
We now examine the case of conditional instability further to define a range of parameters that are important for describing the potential for and eventually characteristics of, convection

. Let us examine the case of the surface parcel in the blown up tephigram in Fig. 19. The parcel is unsaturated and thus if lifted follows a dry adiabat. The profile is stable to dry adiabatic ascent, but let us assume that the mechanical lifting and/or the parcel initial momentum is sufficient such that ascent can continue. The parcel continues until it reaches the condensation temperature and pressure that we defined earlier. This pressure level is called the *lifting condensation level*, or LCL.

If ascent continues, after the LCL the parcel follows a moist adiabat. Since the profile is conditionally unstable, the moist adiabat must eventual cross the environmental temperature profile, implying that the parcel becomes warmer than the environment. After this point the saturated parcel accelerates upwards, undergoing *free convection* in meteorology terminology. Thus the level at which the parcel becomes positively buoyant is called the *level of free convection* or LFC.

Convective inhibition, CIN
The area enclosed on the tephigram between the parcel trajectory and the environmental profile when the parcel is negatively buoyant (i.e. colder than the environmental) is equal to the energy that the parcel must be supplied to overcome this inhibition barrier to undergo free convection. This area is thus called the *convective inhibition*, more commonly abbreviated to *CIN*.

After the LFC, the parcel accelerates upwards following a moist adiabat. *Reminders: What assumptions does this make concerning the parcel?* The ascent may continue to the upper troposphere where it recrosses the environmental temperature line. This level is called the *level of neutral buoyancy* or LNB. The parcel will overshoot and undergo oscillatory motion, but the LNB marks the cloud top approximately.

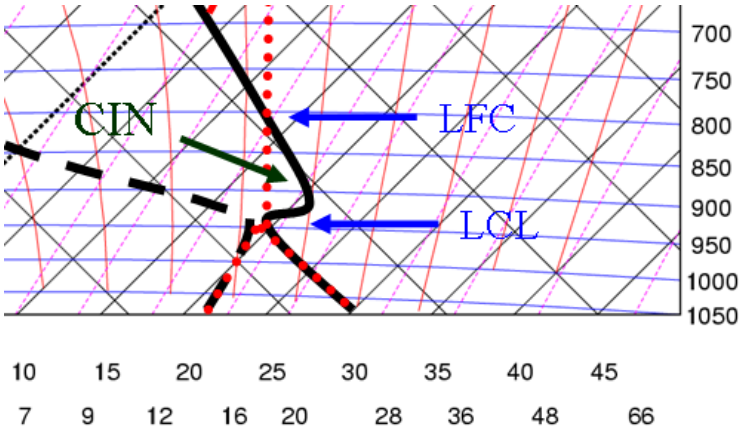

Figure 19: Tephigram showing the boundary layer profiles of temperature and humidity and the pseudo-adiabatic ascent of the surface parcel. See text for details of definitions.

.

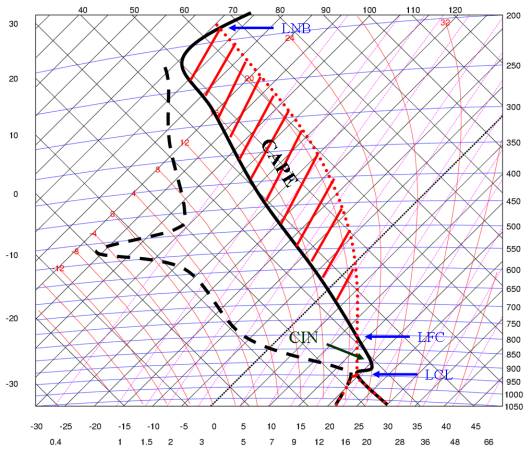

Figure 20: Full tephigram from Fig. 19 additionally showing the full parcel ascent and the positive energy area of CAPE.

.

Figure 21: View from space of a convective even over Mali (image courtesy of NASA)

CAPE

The positive area demarked equates to the energy that can be potentially gained by the parcel. We will call the *total*[7] energy available to a parcel starting from level i the *convective available potential energy* or CAPE.

If we concern ourselves only with the motions in the vertical then CAPE calculated from level i is thus the integral of the buoyancy force

$$CAPE_i = \int_i^{LNB} F_B dz, \tag{92}$$

and substituting (41) we get

$$CAPE_i = g \int_i^{LNB} \left(\frac{T_u - T_{env}}{T_{env}} \right) dz, \tag{93}$$

where T_u is the updraught parcel temperature.

To summarize this, we have defined

- LCL: Lifting Condensation Level
- LFC: Level of Free Convection
- CIN: Convective Inhibition
- LNB: Level of neutral buoyancy
- CAPE: Convective available potential energy

Figure 21 shows the anvil cloud spreading out from a thunderstorm over Mali in West Africa. Notice how flat the anvil top is, marking the LNB. Over the convective updraught region, the cloud top is undulating and higher, revealing the over-shooting updraughts. We can see from the tephigram in Fig. 20 that surface parcels are stable to small displacements, but unstable for large displacements. This is why the profile is termed *conditionally unstable* when $\Gamma_d < \Gamma_{env} < \Gamma$.

There are a number of mechanisms by which air can be mechanically lifted:

- Flow over orography
- Surface convergence due to low pressure perturbation
- Air lifted over colder, denser air masses at fronts or cold-pools from other convective events.

[7] i.e. including CIN. Often the literature refers to the CAPE of a sounding as *only* the positive area, as marked in Fig. 20, but here we follow Emanuel (1994).

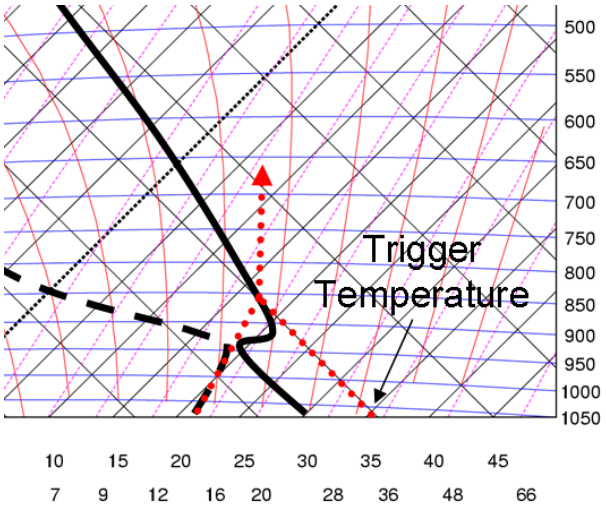

Figure 22: Tephigram showing the derivation of the convective trigger temperature

Convective Trigger Temperature
The convective trigger temperature is the temperature the surface layer would have to be heated to in order to remove all CIN, assuming no change in boundary layer mixing ratio during this heating process (*Q: is this a good assumption and when is the trigger T relevant?*)

. The convective trigger temperature is found by tracing a humidity isopleth of the surface layer mixing ratio to the environmental temperature curve and then following a dry adiabat back to the surface pressure (Fig. 22). For this particular example the trigger temperature is 35°C, requiring a warming of roughly 5°C. The convective trigger temperature is more relevant for cases where convection is not mechanically forced, for example whether convection will occur in undisturbed conditions as a result of the diurnal heating, particularly over land in the tropics over mid-latitude summers. If the soil conditions are wet then the surface heating can also lead to a significant latent heat (humidity) flux, which will lower the trigger temperature. It is thus clear to see why dry situations over land can become "locked-in" through a positive feedback. If a blocking high causes persistent dry conditions, the soil will dry out and the trigger temperature will be higher, making future convective storms less likely. Such a feedback has been shown to be relevant in Africa (Taylor et al., 1997) and has been also highlighted as playing a role in increasing the severity of the 2003 summer heatwave over Europe (Fischer et al., 2007).

Tephigram Exercises IV
Return to the sounding you plotted using the data in Table Tab:sounding1.

1. What is the LCL of a surface parcel of air?
2. What is the LFC?
3. What is the convective trigger temperature?
4. Do you think deep moist convection is likely to occur here?

Tephigram Exercises V
A 50hPa thick layer of air residing between has the values $T = 0°C$ and $r_v = 4.8$ g kg^{-1} at its lower boundary at 700 hPa, and $T = -2.5°C$ and $r_v = 3.0$ g kg^{-1} at the upper boundary at 650 hPa.

1. Is the layer absolutely stable/unstable, or conditionally unstable?
2. The layer is lifted by 100 hPa such that the lower boundary is at 600 hPa, what are the new temperatures at its boundaries?
3. Will the lifted layer be unstable to overturning?
4. Can you think of a criterion for this layer instability ?

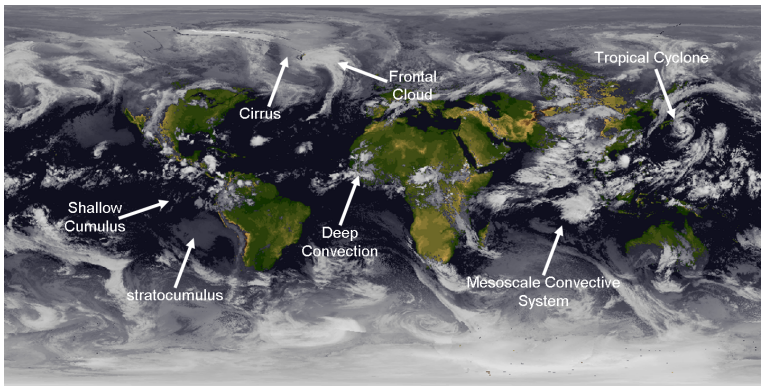

Figure 23: A composite infra-red cloud image where bright white indicates cold cloud tops. Some example convective cloud regimes/types are highlighted

Convective Instability
If a layer of the atmosphere is lifted that is absolutely stable, but which becomes conditionally (or absolutely) unstable through lifting then the layer is termed *Convectively unstable*

Examining the tephigram it is clear that a criterion for convective instability can be understood in terms of θ_e (or equivalently θ_w).

Three criteria for convective Instability:
$\frac{d\theta_e}{dz} < 0$: *Convectively Unstable*
$\frac{d\theta_e}{dz} = 0$: *Convectively Neutral*
$\frac{d\theta_e}{dz} > 0$: *Convectively Stable*

This kind of layer instability can lead to altocumulus or cirrocumulus clouds, which can be signs of impending arrival of a front, and are illustrated in Fig. 28.

Conclusions to thermodynamics
In the previous two sections we have introduced variables that described the thermodynamic state of air and allow us to compare the energetics of two air masses equivalently that may have differing properties of temperature and humidity. We discussed a number of conserved variables, that act as "markers of air" and are conserved under adiabatic motion. θ was conserved in dry adiabatic ascent of a dry air parcel, and for a moist air parcel undergoing unsaturated ascent θ_v and r_v were conserved. For an air-mass undergoing moist saturated ascent θ_e or equivalently θ_w are (approximately) conserved. If the condensed water falls out of the air parcel instantaneous the process is called pseudo-adiabatic. If the condensed water remains in the parcel, r_t is conserved, and the water loading and condensate heat capacity must be accounted for. The vertical gradients of θ and θ_e indicate the likelihood of convection.

4 Atmospheric Convection

In this section we will briefly introduce various types of convection that can occur. The detailed study of the dynamical equations concerning the each regime type is beyond the scope of this introductory course, however it is important to be able to place the convection regime types into context, which are given in Fig. 23.

The chart of vertical cloud types (Fig. 24) illustrates common cloud types as a function of height. It is seen that many of these are of type "cumulus" which are associated with vertical atmospheric instability and thus are vertically extended.

4.1 Shallow convection regimes

If the turbulent boundary layer becomes deep enough to cause saturation then cloud will form. We saw an example of this fair-weather cumulus earlier in the course. If the well mixed layer is capped by a strong stable temperature inversion then the buoyant turbulent updraughts will be stunted quickly when rising into the base of the stable layer. Thus strong temperature inversions forming

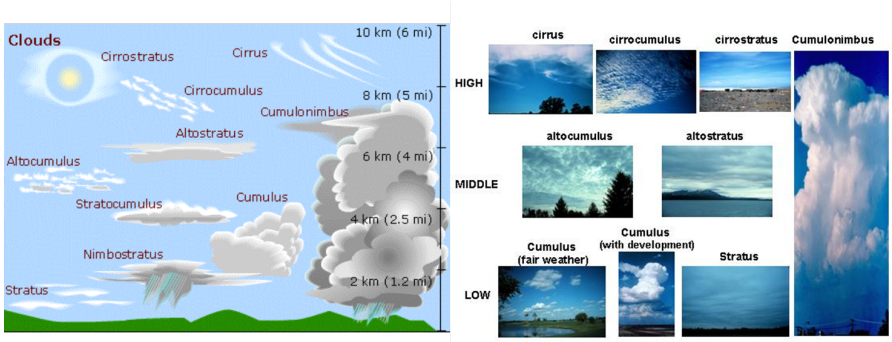

Figure 24: Chart of cloud types as a function of height (left) schematic chart with height scale and (right) photos (source unknown)

Figure 25: Example stratocumulus

under regions of subsidence (such as associated with anti-cyclone or over the Eastern Pacific) lead to stratocumulus with a high cloud cover In the literature we talk of stratus or stratocumulus; the accepted division being based on the optical thickness (i.e. thickness measured in radiative terms) being greater (less) than 23. However the terms are used interchangeably in reality. Here we examine the difference in the thermodynamic structures between cumulus and stratocumulus layers The following schematic shows the large scale circulation associated with the Walker and Hadley cells. *Q: why does subsidence lead to a temperature inversion?* To answer this question we return to the tephigram again and plot the imaginary trajectory of a parcel of air starting in the boundary layer over the Western Pacific (which we will assume is on the left side of the schematic in Fig. 27. The boundary layer parcel has $T = 25°$C and a RH equal to 85%. The parcel undergoes deep pseudo-adiabatic convective ascent until it reaches the upper troposphere, and we shall assume it leaves the deep convective cloud (this process is call *detrainment*) at 200hPa. As the parcel is advected across the Pacific it is also descending[8] *Q: Neglecting other processes what would be its temperature and RH when it arrives at p=900 hPa?* We can see that the parcel arrives at the top of the boundary layer extremely dry, and also much warmer than the typical surface temperature in the Eastern Pacific. However, this simple trajectory model massively exaggerates this, since in reality the air detrained from convection is not 'just' saturated as in the pseudo-adiabatic model, but also contains cloud ice, increasing the total water r_t, and the air will be subject from moistening by nearby deep convection during its descent. Moreover we know that the warming must be approximately balanced by radiative cooling during its journey across the Pacific. The trajectory plot is also a vast over simplification itself of course, since air will get recirculated in other convective events and so on. The trajectory pattern in the schematic crudely represents an averaged mean flow.

4.2 mid-level and upper-level convection

The lifting of convectively unstable layers can lead to the commonly observed cloud types of altocumulus (mid tropospheric, up to around 6000m) and cirrocumulus (upper tropospheric). The vertical division between the two cloud types is not purely taxonomic as cirrocumulus are cloud consisting purely of ice crystals while altocumulus are generally mixed phase clouds (consisting of both liquid and ice). Altocumulus normally occurs when a large air mass is lifted to middle levels

[8]hence the schematic in Fig 27 is a poor one since the arrow is horizontal indicating no subsidence.

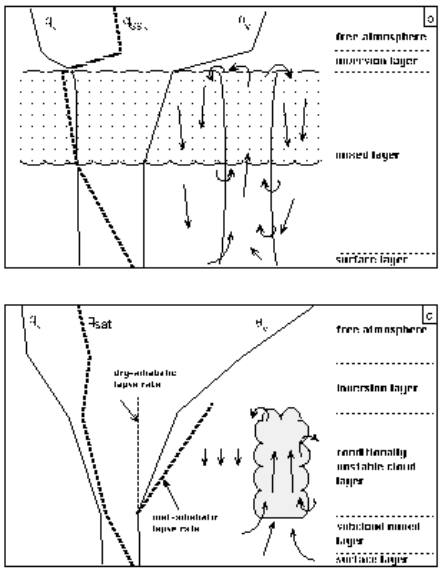

Figure 26: Schematic thermodynamic structure of (top) clear PBL layer (middle) stratocumulus cloud layer and (lower) shallow convective layer (source: S. De Roode cloud lecture notes).

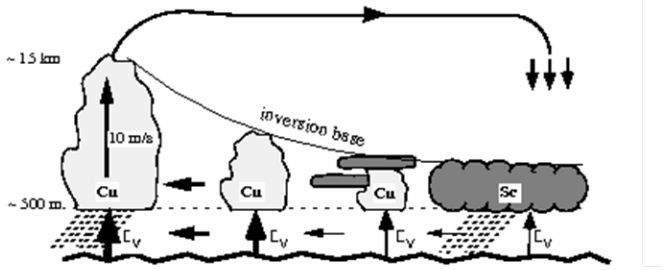

Figure 27: Schematic of the Walker/Hadley circulations, showing Stratocumulus forming under the strong capping inversions associated with the subsidence that balances deep convection. (source: S. De Roode cloud lecture notes)

Figure 28: Examples of clouds formed by convectively unstable layers. (a) Altocumulus (b) Altocumulus undulus, resulting from vertical wind shear (c) cirrocumulus (source: www.theairlinepilots.com)

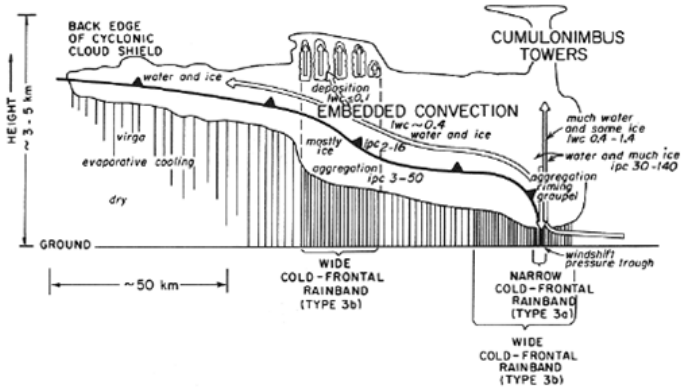

Figure 29: Schematic cross section of convection embedded in a front (source).

by a landmass or an incoming frontal system. If the unstable layer is deep enough, as is often the case in frontal lifting then the mid and upper level convection can lead to schematic here shows the role that mid or upper level cumulus

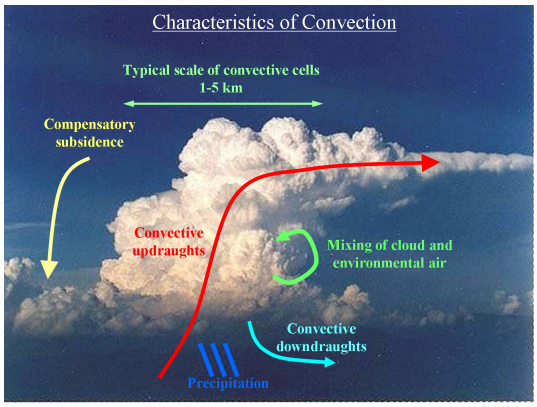

Figure 30: Schematic of other processes to consider in deep convection

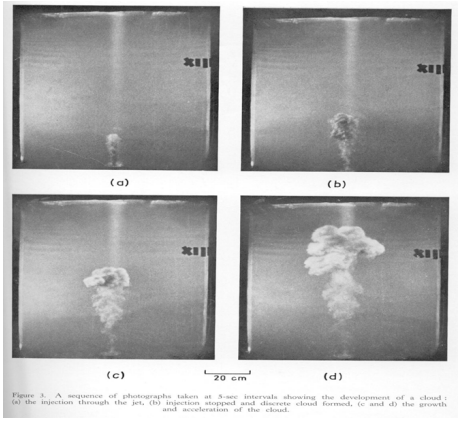

Figure 31: Example of a laboratory experiment of buoyant plumes in a tank experiment of Turner 1963. **?**

4.3 Deep convection

Processes in deep convection
We will now consider some other processes that have been neglected so far in our simple model of deep convection, summarized in Fig. 30.

We saw from the tephigram study that convective elements can penetrate all the way to the tropopause. However, our model of convection was extremely simple, considering a parcel that undergoes ascent without mixing.In reality the billowing turbulent motions indicate that mixing of air between the cloud and environment occurs. Indeed the process of mixing was proven in early laboratory studies using buoyant plumes of dyed liquids mixing, however these studies were unable to adequate represent the effect of latent heating. The understanding and representation of mixing in convection is a long-standing problem. The highly turbulent nature of clouds was evidenced in the first aircraft measurement that were taken after the second world war, such as by (Byers and Braham Jr., 1948; WARNER and Newnham, 1952; Warner, 1955). Here we reproduce slightly later examples from Telford and Warner (1962) we a photograph of the wet-bulb and dry-bulb instruments (Fig. 32). Note the turbulent nature of the cloud and the main updraught is towards the centre of the cloud region while the main (saturated) downdraught areas are at the edge of the cloudy region. This led to the bubble model of cumuli development.

Mixing in Cumulus clouds
Consider two masses of moist air at pressure p with diverse properties (we use subscripts 1 and 2) of temperature and humidity and are subsequently thoroughly mixed isobarically.

The specific humidity of the mixture is

$$q_v = \frac{M_1}{M_1 + M_2} q_{v1} + \frac{M_2}{M_1 + M_2} q_{v2} \tag{94}$$

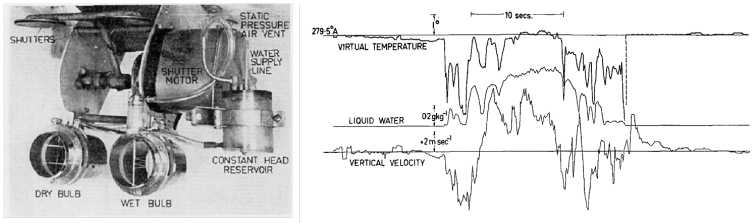

Figure 32: Some of the instrumentation and an example transect through a fair weather cumulus cloud from Telford and Warner (1962).

We can write this relationship approximately using mixing ratios and vapour pressure

$$r_v \approx \frac{M_1}{M_1 + M_2} r_{v1} + \frac{M_2}{M_1 + M_2} r_{v2} \tag{95}$$

$$e \approx \frac{M_1}{M_1 + M_2} e_1 + \frac{M_2}{M_1 + M_2} e_2 \tag{96}$$

We will assume that there is no net loss of gain of heat during mixing so that the change in heat of the two parcels is equal

$$M_1(c_p + c_{pv} r_{v1})(T - T_1) + M_2(c_p + c_{pv} r_{v2})(T - T_2) = 0. \tag{97}$$

If we neglect the contribution of water vapour in the heat capacities then we can see that temperature also approximately is linearly mixed:

$$T \approx \frac{M_1}{M_1 + M_2} T_1 + \frac{M_2}{M_1 + M_2} T_2 \tag{98}$$

As the saturation vapour pressure is a nonlinear function of temperature, then the approximate linear mixing property of vapour pressure and temperature imply that the mixing of two unsaturated parcels of air can result in a mixed parcel that is saturated (draw sketch). This phenomenon is commonly seen when your breath is visible on a winter's day. In fact it was from this observation that James Hutton deduced in 1784 the concave shape of the Clausius Clapeyron curve a century before it was derived according to **?** Middleton(1966).

Convective Downdraughts
From the transect through a fair weather cumulus cloud it was seen that clouds consist of both updraught and also *downdraught* components. In deep convective systems these saturated downdraughts form at mid-tropospheric levels and can penetrate all the way to the surface, spreading out to form a convective *coldpool*.

Downdraughts and coldpools can be dangerous for aircraft landings (Fig. 33) and thus their short-term prediction is a crucial task of short-term aviation *nowcasting* in potentially convective situations. Severe events are sometimes referred to as microbursts. Downdraughts and their associated coldpools are an important component of convective systems since the spreading coldpools can lift environmental air and trigger new convective events, as shown in the schematic of Fig. 34.

Mesoscale convective systems
Thus convection becomes self propagating and one can speak of organised *mesoscale convective systems* (or MCS) consisting of numerous convective cells. Such systems can have a life time that greatly exceeds the life-span of an individual convective events.

In the presence of wind shear the convective can become linearly organised and is referred to as a *squall line*, with examples shown in Fig. 35. In addition to the saturated convective downdraughts, larger mesoscale downdraught also play a thermodynamical and dynamical role in squall line evolution. Of course there are many other examples of organised convection such as tropical cyclones, convectively coupled Kelvin waves, convection associated with monsoon circulations and African Easterly waves, and the madden Julian oscillation to name a few. However, a full description of these is beyond the scope of this course.

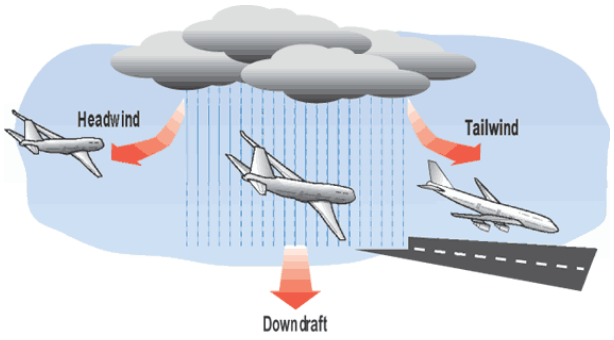

Figure 33: Schematic showing how a downdraught or severe microburst can cause an aircraft stall on approach (source: electronicdesign.com)

.

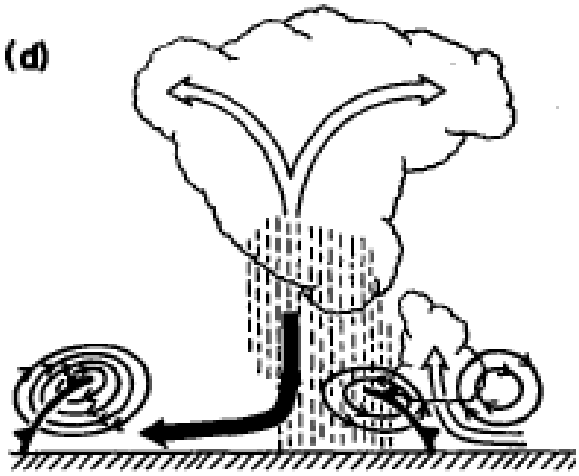

Figure 34: Schematic from Rotunno et al. (1988) showing how air lifted by spreading coldpools can lead to new convective cells being formed

.

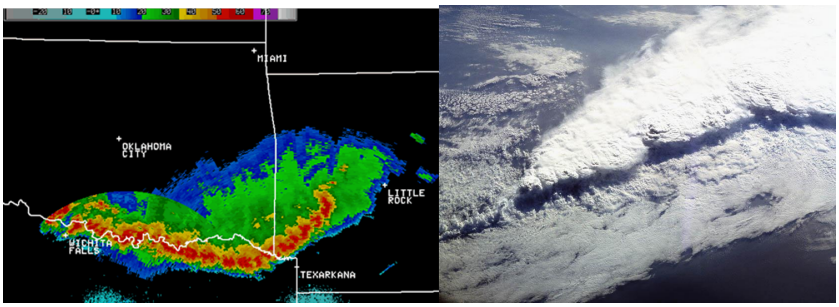

Figure 35: Left: Radar image of a squall line over the United States (source: NOAA). Right: Photo of a squall line over Mexico taken from the Space Shuttle (source: NASA)

.

GATE Sounding

P (hPa)	T (C)	T_d (C)
1010	24.5	21.6
950	20.2	19.2
900	17.5	16.1
800	13.2	11.0
700	7.2	5.1
600	0.0	-1.6
500	-7.6	-11.0
400	-17.5	-21.8
300	-34.3	-38.9
250	-43.4	-49.3
200	-50.6	-71.2

Downdraughts and coldpools
Downdraughts are formed both by the frictional drag of falling precipitation and are also buoyancy driven. The following tephigram example shows how important the mixing and precipitation evaporation (wet bulb) processes are to forming convective downdraughts.

Tephigram Exercises VI
Plot this (slightly doctored) GATE profile on the tephigram.

1. Determine the Lifting condensation level (LCL) for the surface parcel
2. Determine the Trigger temperature for the surface parcel
3. Draw the temperature profile for a moist adiabatically (no mixing) ascending parcel
4. Determine the level of neutral buoyancy (LNB)

An updraught air parcel mixes with the cloud environment in a single entrainment event at $p = 700hPa$, such that the mixture is composed of equal amounts of cloudy and environmental air. Precipitation then passes through the parcel and evaporates, bringing the mixed parcel to saturation.

1. What is the final temperature of the mixed parcel?
2. Can the parcel form a convective downdraught?
3. Recalculate this for a mixing event between updraught at 600 hPa.
4. If a downdraught can form, we assume it is keep at saturation during its descent by further precipitation evaporation. What temperature does it have at the surface?
5. Finally compute the CAPE of the surface parcel (you will probably find it easier to use pressure coordinates for this, assume hydrostatic balance)

4.4 The parametrization problem

What are numerical models?
In the modelling of the atmosphere, we assume that the behaviour of interest is as if the matter (the gas or liquid) were continuous - We ignore the molecular structure. Thus we introduce the idea of the modelling of a material volume, which has bulk properties of e.g. density $\rho(\underline{x}, t)$, temperature $T(\underline{x}, t)$, velocity $V(\underline{x}, t)$ and so on.

A numerical model numerically integrates the equations for momentum, conservation of mass and the thermodynamic equation for a volume of the atmosphere, which is divided into a series of material volumes, called the grid mesh. If we are interested in modelling the atmosphere for a region that is small compared to the earth, we can solve the equations using a Cartesian grid. For a global the equations have to be transformed into polar stereographic coordinate system, and then the equations will be solved on a grid mesh like that depicted in figure 36.

For a given mesh, we can obviously only model scales of motion down to the size of that mesh. Remember that all fluid in one "grid-box" is considered to be a continuum, and is considered to have one uniform mean property for temperature, velocity etc. The finer the grid-scale we use, the greater the range of spatial scales of motion we can represent, but at the same time the model becomes much more expensive to run.

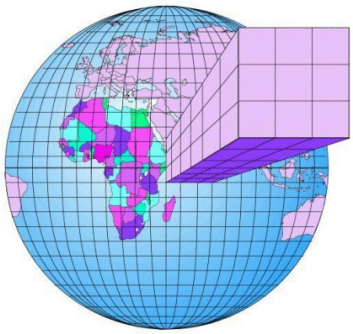

Figure 36: Schematic of a low resolution grid mesh for a global model.

How fine a mesh can we use to solve our equation set? It depends on many factors, the length of the integration, the power of the computer facility available, the efficiency and complexity of the numerical model. But in general a global climate model that must run for many tens of years uses a horizontal mesh size of 100 to 300km, while global numerical weather prediction models that run for days to weeks use mesh sizes of 30 to 100km. For regional modelling the mesh size is of course related to the domain chosen for the integration, with smaller domain allowing for higher resolution to be used. The use of a finite grid mesh implies that there are some processes that will occur on smaller scales. *Q: Can you think what some of these processes may be?*

The use of a finite grid mesh implies that there are some processes that will occur on smaller scales. Some examples (see schematic Fig. 37) are

- subgrid-scale motions such as local turbulence and non-local convection
- clouds
- radiative transfer processes
- surface exchange

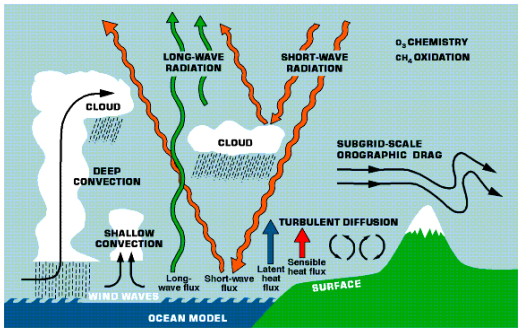

Figure 37: Schematic of a processes that occur on small scales and generally require parametrization in regional or global models

The problem is that these small-scale processes can reflect back on the large-scale equations of dynamics and thermodynamics, and thus can not be ignored. We therefore attempt to construct physical models (that can be simple or very complicated) that use the large-scale grid resolved parameters (T, q, u, v, w etc) as *input* to determine these subgrid-scale processes (e.g. the strength of turbulence). These models are called *parametrizations* since the process is not explicitly modelled. The ultimate output of the parametrization scheme is the tendency of the the large-scale model equations due to the parametrized process.

To illustrate the concept, let us consider the barotropic vorticity equation; the first numerical weather prediction models were based on this.

$$\frac{\partial \xi}{\partial t} + \nabla.(\underline{v}\xi) + \beta \underline{v} = 0, \tag{99}$$

where ξ is the relative vorticity and $\underline{v}$ the horizontal velocity vector and β is the poleward gradient of the Coriolis parameter.

Reynolds Averaging
Now we will perform Reynolds averaging. Let

$$\xi = \overline{\xi} + \xi' \tag{100}$$

where $\overline{\xi}$ is the mean of ξ in our discretised gridbox for a given model timestep, and ξ' is the *local* deviation from the average. Similarly $\underline{v} = \overline{\underline{v}} + \underline{v}'$.

Substituting into the vorticity equation we get

$$\frac{\partial \overline{\xi}}{\partial t} + \frac{\partial \xi'}{\partial t} + \nabla.(\overline{\underline{v}}\overline{\xi}) + \nabla.(\overline{\underline{v}}\xi') + \nabla.(\underline{v}'\overline{\xi}) + \nabla.(\underline{v}'\xi') + \beta\overline{\underline{v}} + \beta\underline{v}' = 0 \tag{101}$$

We now average this equation over the gridbox () and timestep, and thus applying the Reynolds averaging assumptions that (i) $\overline{A'} = 0$ (ii) $\overline{\overline{A}A'} = 0$ (ii) $\overline{\overline{A}} = \overline{A}$ the barotropic vorticity equation reduces to

$$\frac{\partial \overline{\xi}}{\partial t} + \nabla.(\overline{\underline{v}}\overline{\xi}) + \nabla.(\overline{\underline{v}'\xi'}) + \beta\overline{\underline{v}} = 0 \tag{102}$$

We note that the equation for $\overline{\xi}$ looks identical to that of ξ, except for the addition term $\nabla.(\overline{\underline{v}'\xi'})$. *This term* $\nabla.(\overline{\underline{v}'\xi'})$ *represents the unresolved subgrid-scale processes.*

The purpose of parametrization is to give an expression for the subgrid-scale terms as functions of the resolved values.

4.5 parametrizations for turbulence

4.5.1 Constant K diffusion

Constant K diffusion turbulence parametrization
For simplicity we consider the the subgrid-scale flux in one direction only, the x-direction:

$$\frac{\partial}{\partial x}\overline{(u'\xi')}. \tag{103}$$

Let us suppose that the effect of fluctuations on the subgrid fluctuations is simply to smooth out fluctuations of ξ (down-gradient mixing by analogy to molecular diffusion). We could represent this is a simple *parametrization* by

$$\overline{(u'\xi')} = -K\frac{\partial \xi}{\partial x}, \tag{104}$$

where K is a constant, which we shall call the *diffusion coefficient.*

Thus

$$\frac{\partial}{\partial x}\overline{(u'\xi')} = -K\frac{\partial^2 \xi}{\partial x^2} \tag{105}$$

Note that this parametrization is scale-selective in that the term is larger for smaller wavelengths. This means that if the advected field in question (in this case relative vorticity) is initially smooth, then this term is small, and might appear to be negligible.

However, small scales are generated by the flow (see diagram). This idea can be quantified by looking at enstrophy, $0.5\overline{\xi^2}$, as a function of scale (geostrophic turbulent theory) (see diagram). There is a cascade of enstrophy from the forcing scale to smaller scales. Even if the model is stable, the solution is increasingly contaminated by noise on the grid-scale. The effect of the diffusion term is to smooth out this noise. In other words, the diffusion term is artificially removing some of the enstrophy that should have cascaded to smaller scales. There is no theory that predicts exactly what smoothing is required.

It is of course possible to extend the simple constant K diffusion concept to make K a function of atmospheric stability for example, and the handout notes now proceed to explain one such approach based on the Richardson number. Due to time limitations, this material is for interest only and does not form part of the syllabus for this course.

4.5.2 Improvements on the constant K diffusion

To devise a better turbulent scheme than a simple analogy to molecular diffusion, we must consider the source of the subgrid-scale fluctuations.

We start by examining the equation for the *turbulent kinetic energy* TKE, which we denote by e.

$$\overline{e} = \frac{1}{2}(\overline{u'^2} + \overline{v'^2} + \overline{w'^2}) \tag{106}$$

Here we state the rate equation for e, but you may like to attempt to derive this from first principles, starting from the momentum equation and applying Reynolds averaging.

$$\frac{\partial e}{\partial t} + \underline{\overline{v}}.\nabla e = \frac{g}{\overline{\theta}}\overline{w'\theta'} - \overline{u'w'}\frac{\partial \overline{u}}{\partial z} - \overline{v'w'}\frac{\partial \overline{v}}{\partial z} - \frac{\partial \overline{w'e}}{\partial z} - \frac{1}{\overline{\rho}}\frac{\partial(\overline{w'p'})}{\partial z} \tag{107}$$

The terms are as follows:

- $\frac{\partial e}{\partial t}$ local rate of change of TKE, the storage term,
- $\underline{\overline{v}}.\nabla e$ advection by the grid-scaled average velocity,
- $\frac{g}{\overline{\theta}}\overline{w'\theta'}$ buoyant production or destruction of TKE,
- $-\overline{u'w'}\frac{\partial \overline{u}}{\partial z}$ (and similar v term) production of TKE by shear in the flow,
- $-\frac{\partial \overline{w'e}}{\partial z}$ advection of TKE by the perturbation velocity,
- $-\frac{1}{\overline{\rho}}\frac{\partial(\overline{w'p'})}{\partial z}$ pressure correlation term, how TKE is redistributed by pressure perturbations, often associated with gravity waves.

There are two terms that represent sources/sinks of TKE, the buoyancy term and the shear term. Their ratio is an indication of the amount of turbulence to be expected, known as the flux Richardson number

$$R_{if} = \frac{-\frac{g}{\overline{\theta}}\overline{w'\theta'}}{\overline{u'w'}\frac{\partial \overline{u}}{\partial z} + \overline{v'w'}\frac{\partial \overline{v}}{\partial z}} \tag{108}$$

If R_{if} is large it implies that the atmosphere is local stable, and buoyancy suppresses turbulence. If R_{if} lies between zero and one shear instabilities occur creating turbulence. If R_{if} is negative, then there is an unstable lapse rate and buoyancy generates turbulence through convection.

We can now use the definition of Richardson number to create an improved parametrization for subgrid-scale turbulence that is related to the local stability of the atmosphere.

We will accomplish this by relating K to the shear deformation rate S and a typical eddy length scale l such that

$$K = l^2 S \tag{109}$$

where

$$S^2 = \frac{1}{2}\sum_{ij}\left(\frac{\partial \overline{u_i}}{\partial x_j} + \frac{\partial \overline{u_j}}{\partial x_i}\right)^2 \tag{110}$$

To determine the length scale we assume that there is a local equilibrium between sources and sinks of TKE (i.e. no storage) such that the TKE equation reduces to

$$-KS^2 + K\frac{g}{\theta}\frac{\partial \overline{\theta}}{\partial z} = -\epsilon \tag{111}$$

where ϵ is the viscous rate of dissipation of TKE due to molecular friction, and on dimensional grounds can defined as $\epsilon = \frac{K^3}{{l_0}^4}$ where l_0 is the length scale typical of the most energetic eddies (Here we are invoking dimensional analysis, where the viscosity has units energy/time $= \frac{L^2}{T^3}$ and K has units L^2/T and l of course L). We have also assumed the earlier parametrization of the eddy flux $\overline{w'\theta'} = K\partial\overline{\theta}/\partial z$.

Combining the above we find

$$-l^2S^3 + l^2S\frac{g}{\theta}\frac{\partial\overline{\theta}}{\partial z} = \frac{-l^6S^3}{l_0^4} \tag{112}$$

combining these formulae we find

$$l = l_0(1 - R_i)^{0.25} \tag{113}$$

where R_i is the gradient Richardson number

$$R_i = \frac{\frac{g}{\theta}\frac{\partial\overline{\theta}}{\partial z}}{S^2} \tag{114}$$

This is subject to the condition that l is positive-definite. So now we have a parametrization (equations 109, 110 and 113) for turbulence which increases subgrid-scale mixing in regions subject to wind-shear and/or buoyancy driven turbulence. Sometimes, the formula for l is replaced by empirical stability functions derived separately for stable and unstable conditions.

When such a scheme is used in practice, the scheme mostly mixes strongly in the boundary layer (buoyancy driven), in the vicinity of convection draughts (if the model is able to model such motions), and in the region of strong jets (shear driven). In the free troposphere often such a scheme will produce no mixing in low-shear stable conditions. Depending on the model, the mixing of such a scheme can sometimes be insufficient to prevent numerical instabilities from arising, and therefore an ad-hoc minimum value of K may be required to smooth the fields and prevent this from happening. This will depend on a number of factors, the main one being the artificial diffusivity of the model's numerical advection scheme, and whether this scheme is designed to be absolutely stable (e.g. total variational diminishing scheme).

The above schemes for turbulence are known as *local* schemes, since sub grid transport of heat and momentum occurs between adjacent gridcells of the model. If schemes instead transport mass and heat on the subgrid-scale across many layers then these are non-local. Some schemes for shallow convection and all so-called *mass flux schemes* for deep convection are non-local.

5 Cloud Physics

5.1 Introduction

Introduction to cloud physics
In all our discussions so far of convection, we have readily assumed that in updraught motions, once saturation is reached cloud drops readily form. However it is not obvious that this is the case. Indeed, we shall see that this is not the case for the formation of ice crystals.

In this part of the course we move to the small scale physics that occurs on the *microscale* of droplets within clouds, known as *cloud microphysics*. What are the processes that we need to consider in clouds therefore?

Cloud processes
We will consider the

- change of phase from water vapour to liquid droplets or ice crystals
- transformation of small cloud droplets to larger rain drops
- freezing of cloud droplets
- formation of ice crystals from water vapour
- advection/falling of the larger sized droplets (precipitation)
- evaporation/sublimation of precipitation and cloud

Cloud particle modes
Condensed droplets of water can obviously have a range of sizes, or droplet radius. However the probability density function describing the droplet sizes is not a smooth function from the very small to the very large (large being a relative term!), but instead we shall see that diverse and discrete cloud processes contrive to produce distinct peaks in the droplets size spectra, termed *modes*. We shall follow the convention of considering each mode as a *bulk quantity*.

We will consider modes of

- cloud drops
- rain drops
- ice crystals
- snow flakes

For ice processes the division is less obvious since ice crystals can form many different shapes or *habits*, with differing radiative and microphysical (e.g. fall-speed) properties despite similar particle sizes which may be treated as a separate category. It is always possible to divide each mode into finer size categories of course, for instance considering small and large cloud ice particles separately. Cloud models that treat many size categories are often termed *bin resolving* as they divide each mode into a number of size *bins* Figure 38 shows a schematic of the typical sizes of cloud particles in *warm phase* (i.e. no ice processes involved) clouds. The cloud droplet has a typical radius of 10μm, (a micron=1 μm), 100 times smaller than a typical raindrop. In general we will consider cloud microphysical processes as pathways that can either convert particles from one or more discrete modes to a different particle mode, or can change the mass or size distribution within one particular mode. Figure 39 reveals a bewildering array of such processes. A full description of clouds at this level of complexity is beyond the scope of this course, but the diagram reemphasizes the complexity of the task to represent such small-scale complex processes in global climate models with 100km size grid-boxes.

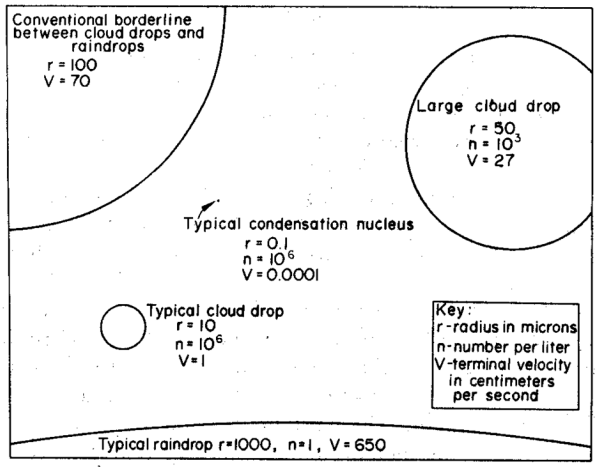

Figure 38: Typical drop sizes, from Mcdonald 1958 **?**, reproduced from Rogers and Yau (1989).

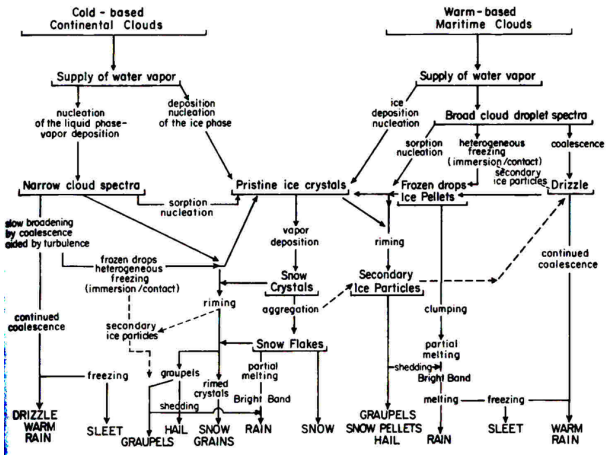

Figure 39: Schematic of cloud process pathways between various cloud particle modes (source unknown)

5.2 Cloud drop formation

In our earlier lecture we assumed that supersaturated states could not exist and water vapour in excess of the saturation mixing ratio was immediately condensed into cloud droplets. It is not obvious that this should be the case. We will now consider the effects imports for cloud particle activation.

Saturation over a curved surface

The first aspect is that the relationships given earlier for the saturation vapour pressure was for a *planar water surface*. On the scale of a cloud droplet the curvature of the surface is sufficient to reduce the number of (attracting) neighbouring molecules.

The saturation vapour pressure is thus lower over a *curved surface*, with the saturation vapour pressure of a liquid droplet of radius r given by:

$$\frac{e_s(r)}{e_s(\infty)} = \exp\left(\frac{2\sigma}{rR_v\rho_L T}\right), \tag{115}$$

where σ is the surface tension, which is the free energy per unit surface area of the liquid and can be viewed as the work per unit area required to extend the surface of liquid at constant temperature[9]. $\sigma \approx 7.5 \times 10^{-2} Nm^{-1}$ for usual conditions. This is known as the *Thomson* or *Kelvin* effect. We can simplify this to

$$\frac{e_s(r)}{e_s(\infty)} = \exp\left(\frac{a}{rT}\right), \tag{116}$$

[9]We will use notation $e_s(r) = e_s^r$ interchangeably.

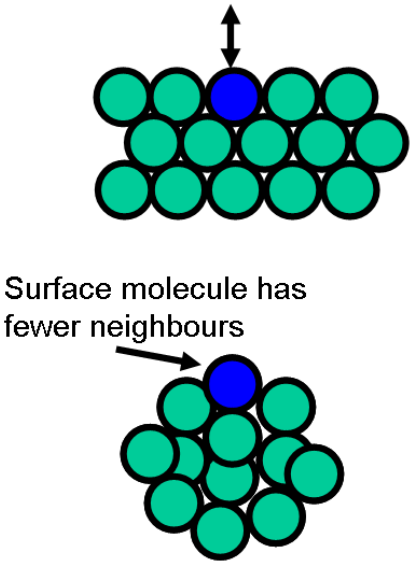

Figure 40: Schematic of evaporation process showing how water molecules have fewer neighbours in a curved drop relative to a planar surface.

where $a = \sigma/R_v\rho_L$ which is (almost) constant at 3.3×10^{-7} m K.

The right hand side of the expression can be usefully approximated to

$$\frac{e_s(r)}{e_s(\infty)} \approx 1 + \frac{a}{rT}, \tag{117}$$

The rate of growth is proportional to the difference $e - e_s(r)$. If $e < e_s(r)$ then the droplet will evaporate, while it will grow if $e > e_s(r)$.

Homogeneous nucleation of liquid droplets

A chance collision of molecules to form a droplet is called *homogeneous nucleation*. Such an event involving 183 molecules of water vapour forming a droplet of radius of approximately 10^{-3} μm at a temperature of 273K would require a saturation ratio of S =3, where S is the *saturation ratio*, $S = \frac{e}{e_s(\infty)}$ (so that S =3 equates to a relative humidity of 300%) to survive and grow.

Such high values are never measured in the atmosphere, thus homogeneous nucleation is not a relevant mechanism for cloud formation. So what is it?

Aerosols

Aerosols in the atmosphere can range in size from 10^{-4} to 10 μm radius with particle concentrations also widely varying from 10^3 cm^{-3} in a remote location to $> 10^5$ cm^{-3} in an urban environment such as London.

There are a number of *natural and anthropogenic* sources for aerosols:

- mineral soil dust
- sea salt
- gas to particle conversion SO_2 →sulphate aerosols
- combustion of fossil fuels / biomass burning

Small aerosols with radii < 0.2 μm are referred to as *Aitken particles*, $0.2 < r < 2$ μm are *large aerosols*, and $r > 2$ μm are *giant aerosols*. Both *dry deposition* (sedimentation) and *wet deposition* (removal by precipitation) are the sinks of aerosols, with a typical aerosol lifetime being around 1 week.

Heterogeneous nucleation of liquid droplets

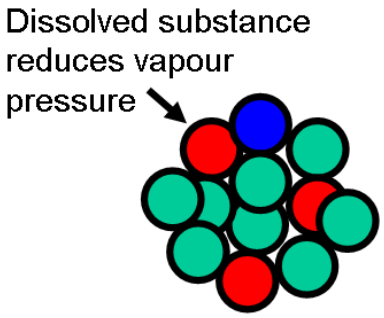

Figure 41: Schematic showing how saturation vapour is instead reduced when there are molecules of dissolved substance (red) present in the droplet.

Many aerosols in the atmosphere are hydrophilic and thus water molecules can collect on their surface. Clouds can thus form by a process known as *heterogeneous nucleation*, where water molecules collect on a foreign substance. These hydrophilic aerosols are called *Cloud Condensation Nuclei* or CCN. These CCN are always present in sufficient numbers in the lower and middle troposphere to initiate cloud growth.

CCN aerosols can be insoluble but *wettable*, which means that the surface tension between their nucleating surface and water is sufficiently low and water can form a spherical cap completely surrounding the aerosol. Thus the physics of drop nucleation is the same as for pure water, and only large or giant aerosols ($r > 0.2$ μm) generally have a low enough curvature to form cloud droplets at observed supersaturations. However, aerosols can instead be *soluble*, in which case aerosols with much smaller radii can act as CCN.

The solution term

The presence of dissolved substances implies that the some water molecules are replaced from the droplet surface (Fig. 41). Thus the saturation vapour pressure is reduced for a *solute*.

If $e_s(sol)$ is the saturation vapour pressure over a solute and n_w and n_s are the number of water and solute molecules, respectively, then the fraction of surface which is occupied by water molecules is simply:

$$\frac{e_s(sol)}{e_s^\infty} = \frac{n_w}{n_w + n_s} = \left(1 + \frac{n_s}{n_w}\right)^{-1} \simeq 1 - \frac{n_s}{n_w}, \tag{118}$$

where the final approximation assumes $n_s \ll n_w$. In a droplet the number of water molecules is proportional to r^3, thus for a fixed mass of aerosol this effect adjust the saturation vapour pressure by a factor

$$\frac{e_s(sol)}{e_s^\infty} = 1 - \frac{b}{r^3} \tag{119}$$

where b is a constant that depends on the aerosol mass and type. The curvature (117) and solute (119) effects can be combined to give the resultant equilibrium curve referred to as the *Köhler curve* given by:

$$\frac{e_s^r(sol)}{e_s^\infty} = \left(1 - \frac{b}{r^3}\right) \exp\left(\frac{a}{r}\right) \approx \left(1 + \frac{a}{r} - \frac{b}{r^3}\right) \tag{120}$$

Figure 42 shows a normalized curve, and the actual shape depends on the mass and type of solute. For a solute formed with 10^{-16} g of ammonium sulphate the solution term is ineffective for radii above 0.3 μm. Due to the r^3 factor the solute term dominates at small droplet radii.

If RH increases starting from a low value, water vapour start to condense on aerosol parcels as RH reaches about 80% (S =0.8), referred to as *haze* particles. At these small radii the droplet is stable as an increase in RH will cause the haze particle to grow until a new equilibrium radius is reached. However, if the RH continues to increase a critical radius R^* is reached at the critical supersaturation S^* value at which the droplet becomes unstable, and grows rapidly by diffusion. The droplet is said to be *activated*. It is the haze particles that are responsible for reducing visibility on a sunny (humid) day.

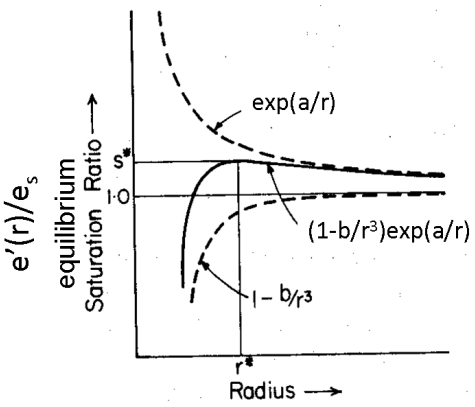

Figure 42: Köhler curve for the equilibrium saturation vapour pressure for a liquid solute droplet.

In summary, about 10 to 20% of aerosols over oceans can act as CCN, while over land only about 1% can act as CCN. Nevertheless, the total concentration of CCN is still higher over land with a typical value of 500 cm^{-3} compared to 100 cm^{-3} over oceans, but these numbers are highly temporarily and spatially variable. Therefore a cloud air parcel brought to saturation over ocean shares the available water between fewer CCN, so we would expect fewer but larger cloud droplets. The consequence of this is that maritime clouds are more likely to rain. We will see that with larger droplets it is easier to grow raindrops.

5.3 Diffusional growth

Diffusional Growth of droplet
Once a cloud particle is activated it grows rapidly by diffusion of water vapour, and the flux F (kg s^{-1}) is given by the standard diffusion expression (see sketch):

$$F = 4\pi n^2 D \frac{d\rho_v}{dn}, \tag{121}$$

where D is the diffusion coefficient ($\approx 2.2 \times 10^{-5}\text{m}^2 s^{-1}$ at 273K) and ρ_v is the vapour density.

In a steady state the diffusion rate is balanced by rate of increase of mass of droplet M:

$$\frac{dM}{dt} = 4\pi n^2 D \frac{d\rho_v}{dn}. \tag{122}$$

We will assume that the growth is constant. Thus

$$\frac{dM}{dt} \int_r^\infty \frac{dn}{n^2} = 4\pi D \int_{\rho_v(r)}^{\rho_v(\infty)} d\rho_v. \tag{123}$$

giving

$$\frac{dM}{dt} = 4\pi D r(\rho_v(\infty) - \rho_v(r)) \tag{124}$$

We want the rate of change of radius, so we need the expression

$$M = 4/3\pi r^3 \rho_L, \tag{125}$$

which we differentiate to give

$$\frac{dM}{dt} = 4\pi r^2 \rho_L \frac{dr}{dt}. \tag{126}$$

Substituting (126) into (124) gives

$$\frac{dr}{dt} = \frac{D}{\rho_L r}(\rho_v(\infty) - \rho_v(r)). \tag{127}$$

We now use the ideal gas law to change the density to vapour pressure:

$$\frac{dr}{dt} = \frac{D}{\rho_L r R_v T}(S e_s^\infty - e_s^r(sol)) \tag{128}$$

Now we use our earlier approximate expression for the Köhler curve given in (120):

$$\frac{dr}{dt} = \frac{D e_s^\infty}{\rho_L r R_v T}(S + \frac{a}{r} - \frac{b}{r^3} - 1) \tag{129}$$

For $r > 1$ micron this simplifies to

$$\frac{dr}{dt} \simeq \frac{D e_s^\infty}{\rho_L r R_v T}(S - 1) \tag{130}$$

This expression is approximate and ignores an important effect. We have neglected the fact that latent heat is warming the droplet, and to be strict the expression should account for the diffusion of heat *away* from the droplet. This "complication" reduces the droplet growth rate very roughly by a factor of 2.

Availability of water vapour
For a hypothetical cloud parcel there are two main terms that affect the supersaturation (or equivalently relative humidity):

- increase due to the parcel cooling: rate proportional to the parcel velocity
- decrease due to the diffusion process

The evolution of an air parcel containing a spectra of diverse CCN can be calculated numerically using a Lagrangian *parcel model* (see Ren and Mackenzie, 2005, for an example in ice clouds). We will consider the hypothetical evolution of the parcel:

1. All CCN start to form haze particles at $RH \approx 80\%$,
2. the larger droplets formed on giant CCN (and thus have lower activation S) become activated first.
3. These giant nuclei are few, thus have limited effect on the water availability, RH continues to increase,
4. and we start to activate drops with higher activation S^*. There are many of these and thus water vapour is consumed, eventually balance is reached where S is at a maximum.
5. After this point particles with $S^* < S_{max}$ will continue to grow, while those with $S^* > S_{max}$ will decay as S decreases.

The final points to note are that

- The maximum supersaturation between (0.1 to 0.5%) occurs within 10 to 100 metres of cloud base,
- S_{max} defines the number concentration of cloud droplets, and is thus also determined close to cloud base,
- higher updraught speeds give higher S_{max}, thus higher number of activated droplets leading to a higher number of final cloud droplets,
- Growth of cloud droplets from an initial aerosol of 0.5 μm takes only a few seconds explaining well cloud base is *well defined*,
- Calculated drop size spectra from modelling this process are *narrower* than observed (i.e. less size variability). This is because we have neglected the processes of cloud mixing and coalescence of droplets

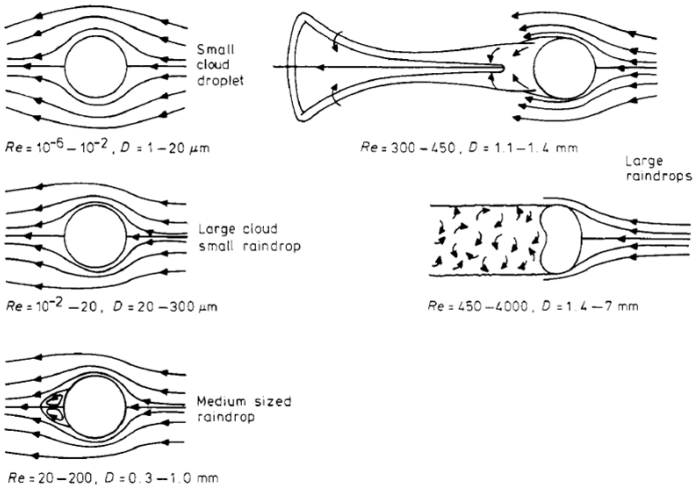

Figure 43: Changes in the air flow patterns round falling water drops as the Reynolds number increases (source: Mason, 1978)

Time taken for diffusional growth
We have an expression for the rate of change of r as a function of time and supersaturation. If we assume S is time-independent we can find out how long it takes to grow cloud droplets of a certain size by the diffusion process by integrating (130).

This gives (*exercise: check!*)

$$t = \frac{\rho_L R_v T}{2De_s^\infty(S-1)}(r^2(t) - r^2(0)). \tag{131}$$

If we take an example of T=284K and $r(0)$=0.5 μm and $S-1$ =0.002 (a *supersaturation* of 0.2%) then table 3 gives the time taken to grow a cloud droplet of the given sizes We recall that 10 μm

r (μm)	1	5	10	100
t (seconds)	1	36	150	15000

Table 3: Time taken to grow a cloud drop of given radius by diffusion.

was a typical cloud radius and thus growth by diffusion *is* fast enough to produce such droplets. However 100 μm is a small raindrop size, and it is seen that over 4 hours are required to achieve this initial raindrop, far longer than the observed life-cycles of precipitating clouds.

5.4 Terminal velocity of particles

Terminal velocity
We now introduce the concept of the terminal fallspeed of particles in a simplified way. The terminal velocity is achieved when the force due to gravity $F = 4/3\pi r^3 g(\rho_L - \rho)$ is balanced by the drag on the droplet.

However the drag strongly depends on the drop size, as seen in Figure 43. The drag on a droplet is related to the particle velocity V and the radius r and can be divided into three regimes, leading to three distinct terminal fall speed V_t relationships:

- $r < 30\mu$m: Drag $\propto Vr$ giving $V_t = X_1 r^2$ where $X_1 \sim 1.2 \times 10^8 \text{s}^{-1}$ m^{-1}.
- $30 < r < 1000\mu$m: Drag $\propto Vr^2$ giving $V_t = X_2 r$ where $X_2 \sim 8 \times 10^3 \text{s}^{-1}$.
- $r > 1000\mu$m: Drag $\propto V^2 r^2$ giving $V_t = X_3\sqrt{r}$ where $X_3 \sim 250 \text{s}^{-1}$ m$^{0.5}$.

Table 4 gives typical fallspeeds as a function of radius. From these fallspeeds we notice two facts:

r (μm)	1	10	20	100	1000
V_t (m s^{-1})	1.2×10^{-4}	0.012	0.048	0.8	8

Table 4: Time taken to grow a cloud drop of given radius by diffusion.

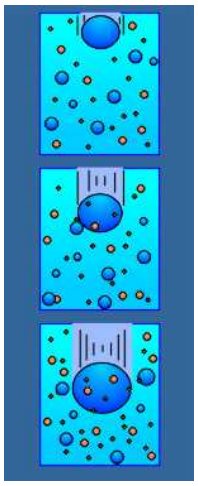

Figure 44: Schematic of larger raindrops colliding with smaller drops during descent (source islandnet.com)

- The fallspeed of typical cloud droplets (2 to 20 μm) is negligibly small compared to typical updraught and downdraught velocities, with a 10 micron droplet requiring a day to fall 1km. This means that to a good approximation we can assume that cloud droplets are in suspension in the air.
- The differential terminal fallspeeds also implies that larger droplets falling faster than smaller ones may collide and collect smaller droplets during their descent.

5.5 Collision and coalescence

We consider a large drop of radius R is falling through a cloud of smaller droplets radius r. If we take a simple view and assume that any small droplet in the path of the large droplet comes into contact and is *collected* (as in the sequence of Fig. 44, the volume of droplets collected per unit time is $\pi(R+r)^2(V-v)$. The liquid water content of the small droplets is $L = q_l\rho$ in kg m^{-3}, giving a mass accumulation rate of

$$\frac{dM}{dt} = L\pi(R+r)^2(V-v) \tag{132}$$

We will simplify the equation by assuming $R >> r$ and $V >> v$, and then use (126) which we recall states $\frac{dM}{dt} = 4\pi R^2 \rho_L \frac{dr}{dt}$ to give

$$\frac{dR}{dt} = \frac{LV}{4\rho_L} \tag{133}$$

If we take the case of the initial growth of small droplets ($r < 30$ μm) then the terminal velocity was given by $V = X_1 R^2$ giving

$$\frac{dR}{dt} = \frac{LX_1R^2}{4\rho_L} \tag{134}$$

We recall that the radius rate change due to the diffusive process was proportional to the inverse of radius. This implies that there is a changing balance between the competition of these two processes, with the dominance of diffusion overcome by the importance of the collection process as the radius increases (see sketch) We can simply integrate (134) to show that for $L = 10^{-3}$ kg m^{-3} a drop can grow from 20 to 30 μm in approximately 10 minutes. We then need to introduce the relationship $V_t = X_2 R$ into (133) and integrate to calculate that the raindrop can attain a radius of around 300 μm in 20 minutes.

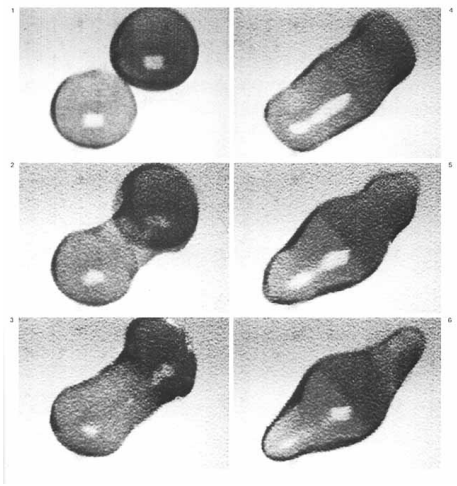

Figure 45: Sequence of shots showing droplet collision and subsequent cohesion (source unknown)

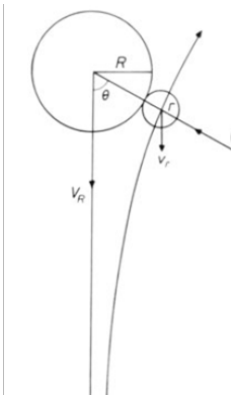

Figure 46: Schematic showing more realistic path of small droplet (source Mason (1978))

These times appear to be reasonable compared to cloud lifetimes, but we have ignored two effects in this simple view, *Q: Can you think what they might be?* We assumed simplistically that all droplets with in the large droplet trajectory collided with the large drop and that all collisions led to coalescence. Neither of these two assumptions are very accurate.

Collection efficiency $E(R, r)$
We saw earlier in Fig. 43 how the streamlines around various raindrop sizes looked. The lack of inertia of very small droplets implies that they will tend to get swept around the larger droplets if r/R is small (see Fig. 46). To describe this we introduce the *collision efficiency parameter* $E(R, r)$. For small r/R, $E(R, r)$ can be as low as 0.1, while when $R \sim r$ the flow fields can interact in a complex way and result in $E(R, r) > 1$.

Coalescence efficiency, ϵ
The *Coalescence efficiency* ϵ is often assumed to be $\sim$1, but observations show that it can be lower than 0.5.

Figure 47 shows two methodologies for the calculation of $E(R, r)$ from Klett and Davis (1973) which differ greatly for $R < 30$ μm in this case. Taking the *collision efficiency* and *Coalescence efficiency* into account modifies our radius growth rate equation to

$$\frac{dR}{dt} = \frac{LV\epsilon E(R, r)}{4\rho_L} \tag{135}$$

and growing a droplet from 20 to 30 μm can now take as much as *100 minutes* instead of 10 minutes, and we no longer grow rain drops in the observed time of cloud development. There are a number of mechanisms that lead to an accelerated growth rate to get us out of this impassé:

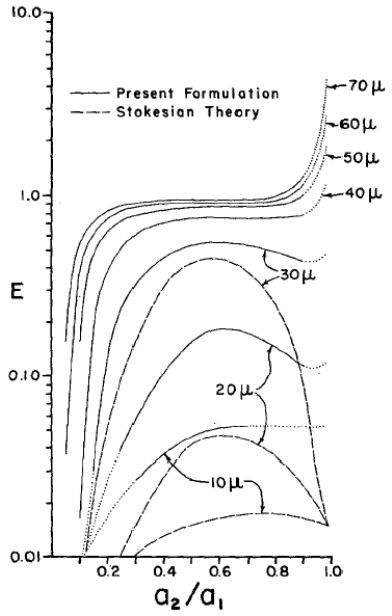

Figure 47: Graph of theoretical collection efficiencies $E(R, r)$ for two calculation methodologies with the x-axis showing the radii ratio r/R. Each line is labled with the radius of the larger droplet. (source Klett and Davis (1973))

- *Statistical models of raindrop growth*: we assumed that droplet growth was a discrete function of time, whereas it consists of a serious of discrete events. If in a time Δt 10% of raindrops collide and coalesce then after time $2\Delta t$ there will be one large drop from 100 initial droplets (see Fig. 48). But this larger droplet will then be favoured for further growth as the growth rate is $\propto r^2$. *A spectrum of drop sizes, often bimodal, is therefore generated* (see Fig. 49).
- It was also assumed that droplets were evenly distributed within the cloud, whereas in reality cloud are *inhomogeneous*, and regions of higher liquid water content will favour droplet growth.
- The process of *entrainment* cause the partial evaporation of droplets broadening the droplet size distribution.

5.6 Ice crystal nucleation

Introduction to ice processes
The first thing that should be emphasized when considering the ice phase is that *ice phase processes in clouds are far more complicated (Fig. 50) and consequentially poorly understood* relative to the warm phase cloud processes. This course can only skim the surface of the relevant mechanisms.

5.7 Ice saturation

Saturation over a plane surface of pure ice
Before we continue with the discussion of ice we must first consider the concept of saturation over a planar ice surface. Analogous to the liquid water saturation, the air is said to be saturated if the *deposition* (vapour→ice) rate equals the *sublimation* (ice→vapour) rate.

As the intermolecular bonding energy of molecules in ice is greater than that in liquid water, at a given temperature, the evaporation rate is larger than the sublimation rate. Thus it is clear that $e_{si}(T) < e_{sw}(T)$ (see Fig. 51) where the saturation vapour pressures are

- e_{si} over ice
- e_{sw} over liquid water.

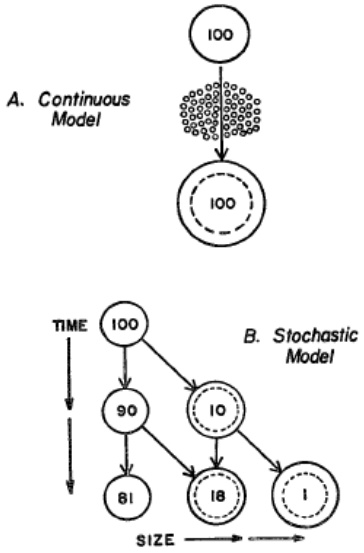

Figure 48: stochastic model of sweep out (source Berry (1967))

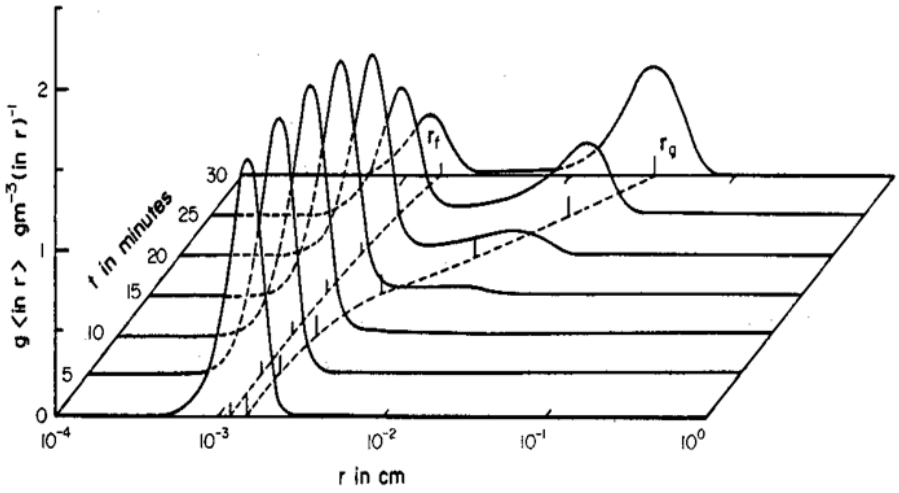

Figure 49: Example of the development of a droplet spectrum by stochastic coalescence (source Berry and Reinhardt (1974))

5.8 Ice nucleation mechanisms

When the temperature falls below 0°C there is no guarantee that freezing of liquid cloud droplets will occur. *Q: Why is it then that ponds freeze over in winter with slightly sub-zero temperatures?*

Homogeneous nucleation of ice from liquid
Ice particles can be nucleated from either the liquid or vapour phase *in theory*. The homogeneous nucleation of ice from the liquid phase is analogous to the nucleation of liquid drops from vapour. An initial crystal or *ice germ* is formed by statistical fluctuations of the liquid molecular arrangement to form a stable ice-like lattice structure. If the germ is over a critical size, which depends on the temperature, then other water molecules will bind to the ice germ rapidly and the water body will freeze rapidly.

It is clear that a pond therefore freezes more readily than a cloud of liquid droplets as the formation of an ice germ of critical size only has to occur once in the pond, while the event needs to occur in each cloud droplet which is far less likely. Thus it is possible and indeed very common to find liquid cloud drops existing at temperatures much below the freezing point; referred to as *supercooled droplets*. Theoretical results imply that a liquid drop of 5 μm will spontaneously freeze at temperature of around -40°C, and measurements inside real clouds show that they contain no

Figure 50: Example of an ice crystal from http://www.its.caltech.edu/)

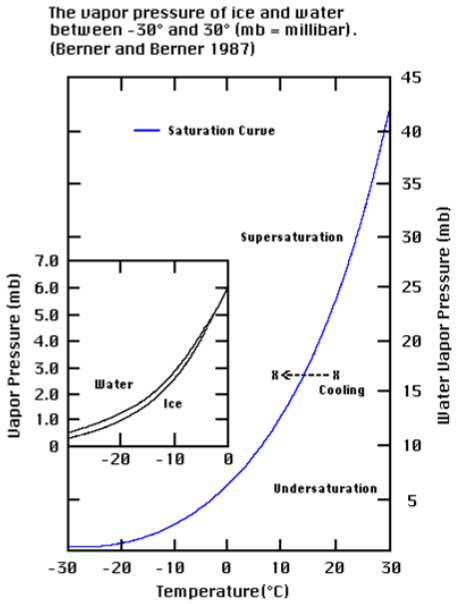

Figure 51: Water and ice saturation vapour pressures (from Berner and Berner 1987)

ice once temperatures of around -35°C to -40°C are attained (depending on the cloud drop size spectra). Such clouds are said to be completely *glaciated*.

Homogeneous nucleation of ice from vapour
It is also theoretically possible to nucleate ice crystals directly from the vapour phase, however theory shows that very high supersaturations (> 1000%) with respect to ice would be required. At these high supersaturations, air would also be supersaturated with respect to liquid water, forming droplets that would freeze. Thus *homogeneous nucleation of ice directly from the vapour phase is not a relevant mechanism* for creating ice cloud.

Ice supersaturation in the upper troposphere
One consequence of the above is that cloud-free air can be supersaturated with respect to ice and not form ice cloud. However there is an upper limit to the amount of ice supersaturation set by e_{sw} since at this point liquid droplets form which will homogeneously freeze *if* the temperature is below -40°C. A common sign of the upper troposphere being supersaturated is the presence of *permanent contrail cloud* (Fig. 52).

As temperature get colder, e_{sw} and e_{si} diverge, and larger ice supersaturations are possible. In fact it is more complicated and the limit is below e_{sw} since we recall that aqueous solution droplets (haze) forms at RH with respect to water substantially below 100%.

Koop et al. (2000) investigates this limit in detail and shows an upper limit of 45% ice supersaturation at $T = 235$ K increasing to 67% at $T = 190$K.

In Fig. 53 Spichtinger et al. (2003) shows using retrievals from microwave limb sounder data that ice supersaturated states are quite common in the upper troposphere. We have seen that homogeneous ice nucleation occurs at temperature below -40°C and that supercooled liquid water

Figure 52: Photo and satellite picture of permanent contrails over the UK. (source unknown).

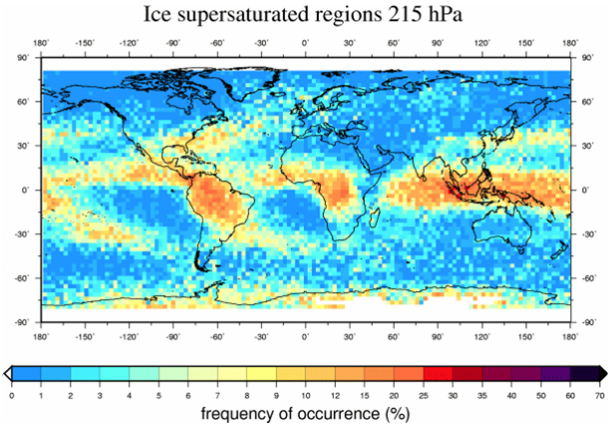

Figure 53: Frequency of ice supersaturation at 215hPa (source Spichtinger et al., 2003)

is very common below 0°C. However it is also true that ice is observed in clouds between 0°C and -40°C. Clouds *Q: How could it get there?*.

- Air was previously at much colder temperatures: *parcel history*
- Ice has fallen from above: *ice sedimentation*
- Ice has nucleated in-situ: *how?*

Heterogeneous nucleation of ice

Aerosols in the atmosphere can also act as *ice nuclei* (IN) if their molecular structure is close enough to the lattice structure of ice. The first point to emphasize is that it is much less common for aerosols to have this property and therefore ice nuclei are much less common than CCN.

At $T = -20$°C a typical number concentration (NC) of ice nuclei might be 10^{-3} cm^{-3} compared to CCN of roughly 10^{2} cm^{-3}.

Whether an aerosol can act as a cloud nuclei depends on the *ice supersaturation* and the *temperature*.

As ice supersaturation increases and temperature reduces more aerosols take on the property of being ice nuclei. **?** found that for each 4°C of cooling the number of ice nuclei increases by a factor of ten (Fig. 54).

Common ice nuclei

Some ice nuclei are given in table 5 along with their maximum nucleation temperature.

Demott et al. (2003) tested air samples taken from mountain top in mid-Western USA and documented the distribution of IN depicted in Fig. 55. It should be emphasized that knowledge of which aerosols can act as ice nuclei is uncertain and the subject of current research. Ice nuclei concentrations are highly variable, and although the Fletcher curve may be accepted as typical, concentrations can vary by orders of magnitude. Aerosols may also be carried a long distance in the atmosphere before being involved in ice cloud nucleation events. Demott et al. (2003) and others have shown that mineral aerosols from Western Africa are a significant source of ice cloud

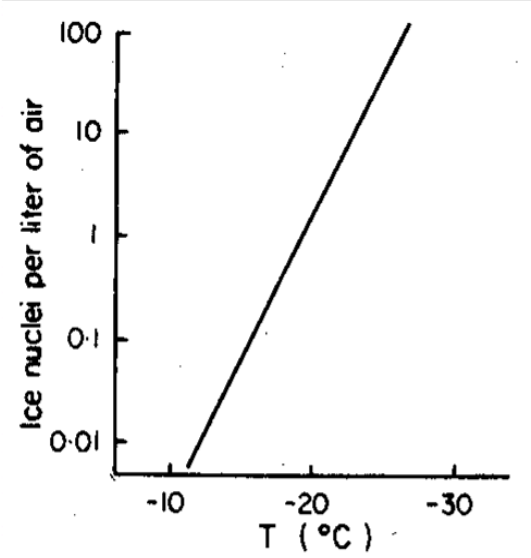

Figure 54: Ice nuclei concentration as a function of temperature (source **?**)

Substance	Nucleation T (°C)	Notes
ice	0	
silver iodide	-4	used in cloud seeding
clay	-9	often seen in snow crystals
cholesterol	-2	
bacteria(!)	close to 0	used in snow machines

Table 5: ice nuclei and their nucleation temperature maximum

nuclei over the United States for example! In fact many snow or ice particles contain clay mineral aerosols indicating that the desert regions of the world are in general an important source of IN (see Fig. 56).

General properties of ice nuclei
Observations and laboratory experiments indicate that aerosol particles usually satisfy a list of criteria if they are to serve as IN (Pruppacher and Klett, 1997).

- **Insolubility criterion:** In general, IN must be very insoluble. The disadvantage of a soluble substrate is that it disintegrates under the action of water. Hence the molecular structural requirement for ice nucleation can not be maintained.

- **Size criterion:** IN must have a size comparable to, or larger than, that of a critical ice embryo. Generally speaking the radius of the IN must be greater than 0.1 μm; i.e. Aitken particles do not tend to be ice nuclei. At sizes less than this critical radius (0.1 μm), the nucleating ability of the particle decreases rapidly (and becomes increasingly more temperature dependent).

- **Chemical Bond criterion:** The chemical nature of an IN, that is the type and strength of the chemical bonds at the IN surface, affect nucleation. Since an ice crystal lattice is held together by hydrogen bonds it is very reasonable to assume that an IN must have similar hydrogen bonds available at its surface for nucleation to occur.

  In view of this bond criterion, certain complex organic molecules (i.e. aerobic bacteria) exhibit good ice nucleation abilities. The hydrogen bonding groups in ice are similar to the hydrogen bonding groups in many organic molecules.

- **Crystallographic criterion:** Since ice nucleation on a substrate is actually an overgrowth of ice on the substrate, it is reasonable to expect the nucleating ability of the substrate to increase when the lattice structure of the substrate is similar to the hexagonal lattice structure

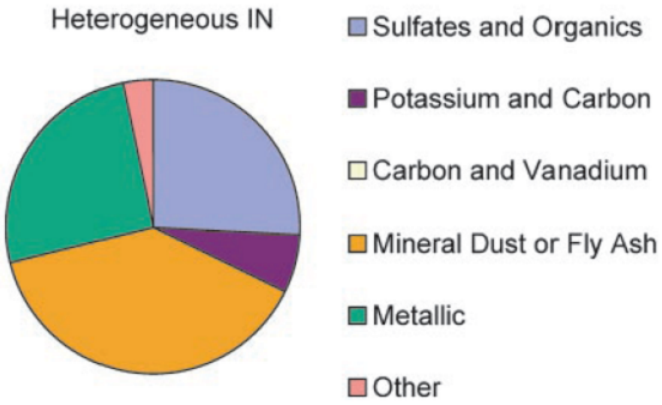

Figure 55: From Demott et al. (2003), distribution of IN type from air samples taken over the mid-West USA.

What kind of cloud is this figure showing?

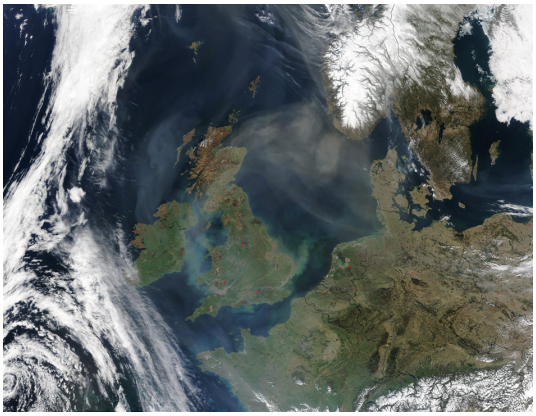

Figure 56: Modis image over Europe (source MODIS website)

of ice. In this way, molecular matching between the molecules of ice and the substrate may be achieved (Fig. 57). The crystallographic matching reduces the *"misfit"* and *elastic strain* in the ice.

Both of the properties of misfit and elastic strain reduce the nucleating ability of the substrate. Kaolinite forms good ice nuclei because it has a *pseudo-hexagonal structure.* AgI (silver iodide) also has a hexagonal form. Other molecules have a non-hexagonal shape (e.g. cubic), but still have crystal structures close enough to ice to aid nucleation. The crystallographic requirement has to do with the arrangement of molecules and is distinct from the chemical bond criterion.

- **Active Site criterion:** Ice nucleation generally occurs at distinct sites on the substrate. Laboratory studies have indicated that ice nucleation is preferred on those substrates which have pits and steps on their surfaces. Those nuclei that have smooth surfaces are less efficient nuclei, that is, nucleation occurs at *lower temperatures.* An example is shown in Fig. 58 where ice crystals preferentially formed on steps etched onto the surface of a cadmium iodide crystal.

Mechanisms for Heterogeneous Nucleation

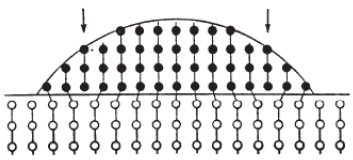

Figure 57: An ice-embryo (dark points) growing upon a crystalline substrate with a misfit of 10%. The interface is dislocated, dislocations being indicated by arrows. (from Fletcher, 1969) **?**.

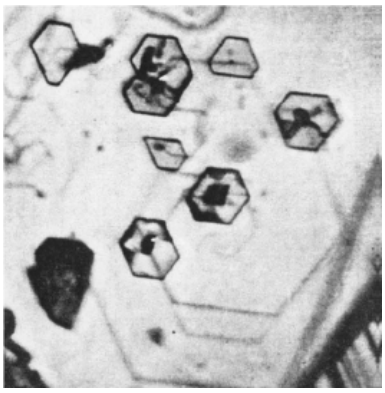

Figure 58: An epitaxial deposit of ice crystals growing at the steps of a hexagonal growth spiral on cadmium iodide. (source Briant et al., 1959 **?**)

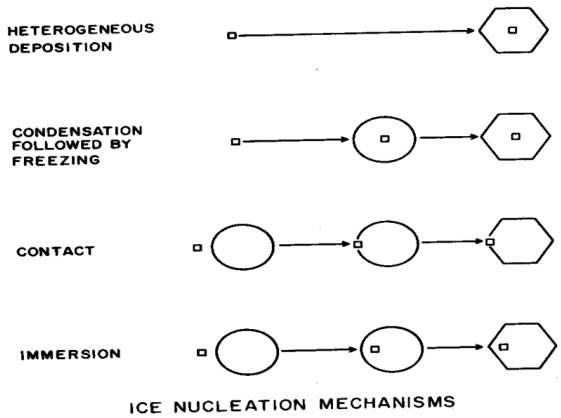

Figure 59: Schematic of heterogeneous nucleation pathways (source: Rogers and Yau, 1989).

There are several mechanisms for ice crystal nucleation, schematically illustrated in Fig. 59. These are

- heterogeneous deposition nucleation
- condensation nucleation
- contact nucleation
- immersion nucleation

5.9 Ice crystal growth

We divide the consideration of ice crystal growth by diffusion of water vapour into two regimes: *mixed phase* and *glaciated* clouds. For *mixed phase clouds* we recall that at subfreezing temperatures the ice and water vapour saturation pressures diverge, and thus an air volume at water saturation is supersaturated with respect to a planar ice surface, reiterated in Fig. 60.

Bergeron-Findeison Effect
The *Bergeron-Findeison effect* is an important growth enhancing mechanism in mixed phase clouds. In a supercooled liquid water cloud imagine one liquid droplet freezes (Fig. 61):

- The cloud is initially saturated *with respect to liquid water*.
- It is thus *ice* supersaturated.
- The ice crystal will grow by diffusion of water vapour towards the crystal,

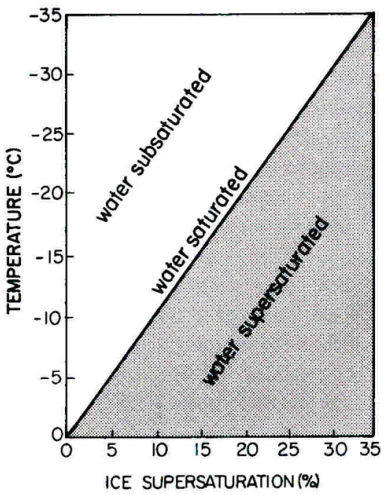

Figure 60: Diagram showing relative degrees of ice and liquid water super or sub-saturation as a function of temperature (source: Pruppacher and Klett, 1997))

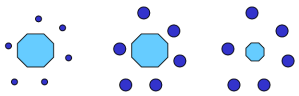

Figure 61: Schematic of Bergeron-Findeison process, with the cyan hexagon representing an ice crystal in a liquid water cloud

- This reduces the vapour pressure below the liquid water saturation value.
- The liquid droplets evaporate on a fast timescale maintaining the vapour pressure close to the liquid water saturation.

The outcome of the Bergeron-Findeison effect is that the growth rate of the ice crystal is faster than it would be in the absence of liquid cloud droplets. For a water saturated environment the growth rate is fastest when the difference between the saturation limits is largest *in absolute (not relative!) terms*. This occurs around $T = -15°\text{C}$.

A laboratory photo shows the result of the BF-effect, with the lack of liquid droplets surrounding the ice crystal on the plate (Fig. 62)

Ice Habits

Ice habits can be very complex and depend on the temperature and ambient ice supersaturation at which ice nucleation takes place (Fig 63). The crystal shape has a strong impact on radiative properties (Macke et al., 1996) and the fall speeds of the ice particle.

A classification of ice shapes in shown in Figure 64.

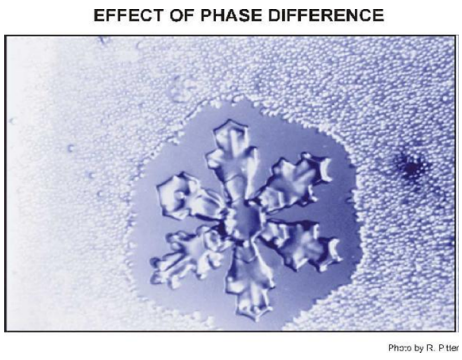

Figure 62: Photo of BF-Effect (source R. Potter from ?)

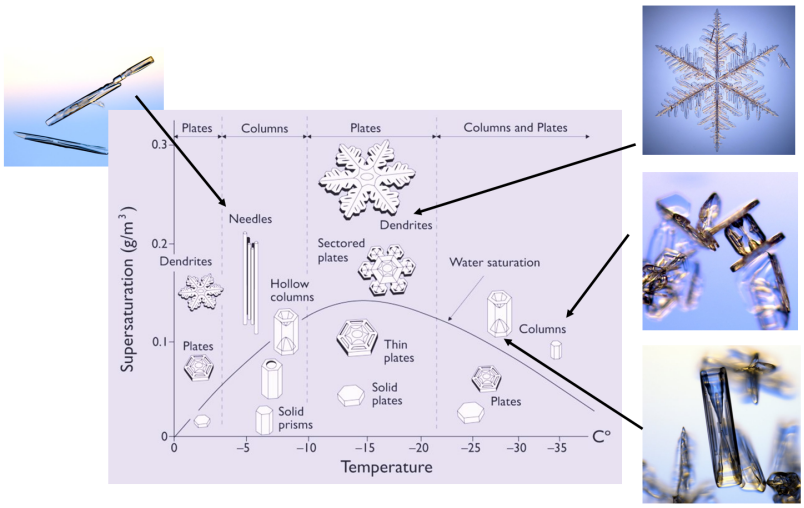

Figure 63: Ice crystal types as a function of S_i and T (source www.its.caltech.edu)

5.10 Competition between ice nucleation mechanisms

Competition between ice nucleation mechanisms
At temperatures warmer than -40°C the only nucleation mechanism is heterogeneous. However at temperatures colder than this both heterogeneous and homogeneous nucleation can occur contemporaneously.

As many IN become active at ice supersaturations of 10 to 30%, well below the threshold range for homogeneous nucleation, then homogeneous nucleation has the potential to be the dominant nucleation mechanism, *if and only if* IN are present in sufficient numbers to prevent the RH reaching the homogeneous nucleation threshold in a rising (cooling) parcel of air.

Q: Both mechanism create ice crystals, so why do we care which one dominates? Demott et al. (2003) (Fig. 65) documents the concentration of nucleated ice crystals as a function of water saturation for air samples collected over the western United States. For $T > -35$°C the NC increases with supersaturation as more aerosols become active. However at cold temperatures there is a step jump close to water saturation to much higher concentrations due to homogeneous nucleation. . *Homogeneous nucleation thus has the potential to create a much higher concentration of cloud ice crystals - Q: Why?* The homogeneous nucleation process creates more ice particles since it is due to the freezing of aqueous solution droplets and thus related to the number of CCN. The particles nucleated by homogeneous process are much smaller in size therefore.

Whereas in warm clouds the droplet concentration was related directly to the CCN number, in ice clouds the relationship between IN and ice particle number concentration is more complicated and nonlinear, falling into two distinct regimes, illustrated schematically in Fig 66. The figure shows three cases of an lifted hypothetical parcel of air at cold temperature ($T < -40$°C). The left case is for a clean sample of air with no IN. The parcel rises until the RH attains the threshold for homogeneous nucleation, 160% in this example. Many ice particles ensue. These rapidly grow by depositional growth as the air is highly ice supersaturated and the water vapour content returns rapidly (in seconds to minutes) to the ice saturation vapour pressure.

The middle column shows a parcel of air with a low number of IN. These nucleate ice at lower supersaturation thresholds (say 30%) but the number is too small to "use up" (by deposition) much vapour and the homogeneous threshold is still reached. Nevertheless the "overshoot" over this threshold and number of aqueous particle formed will be less due to the take-up of vapour by the IN, and thus the final total number of ice crystals will be less. This also implies that the return of the vapour content to the ice saturation value will be slower.

Finally the right hand column shows air with a high enough content of IN such that the ice particles nucleated are sufficiently numerous to prevent the RH from even reaching the threshold for homogeneous nucleation and the latter mechanism is effectively inhibited. The final number of ice particles is orders of magnitude lower than in the clean air case and the return to ice saturation is much slower and may take on the order of an hour or longer.

Figure 64: Ice crystal categorization (source www.its.caltech.edu)

After this point further increases of IN will increase the ice particle concentrations as in warm phase clouds, but always at much lower concentrations than produced by homogeneous nucleation.

The final number of ice crystals will be dependent on the both the IN concentration of the air and the updraught velocity of the air parcel. As in warm clouds, parcel models are used to study this, as in this example of Ren and Mackenzie (2005) in Fig.67. *In a weather or climate model, what are the issues involved in representing this relationship?* The following points should be noted about the parcel model results in Fig.67:

- The *overshoot* past S_{cr} for homogeneous nucleation determines the *number* of ice crystal nucleated.
- The overshoot has a timescale of seconds, and thus is not temporarily resolved by numerical models (parcel models use sub-second timesteps to resolve this),

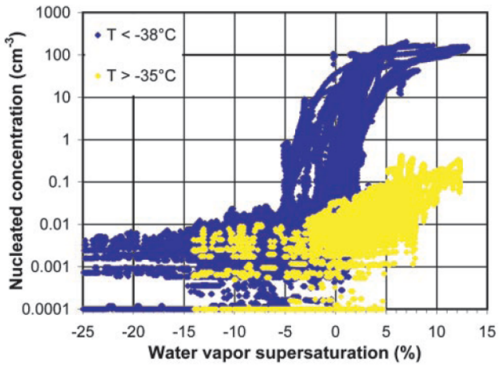

Figure 65: Nucleated ice crystal number in air samples as a function of water saturation at two temperatures. (source: Demott et al., 2003).

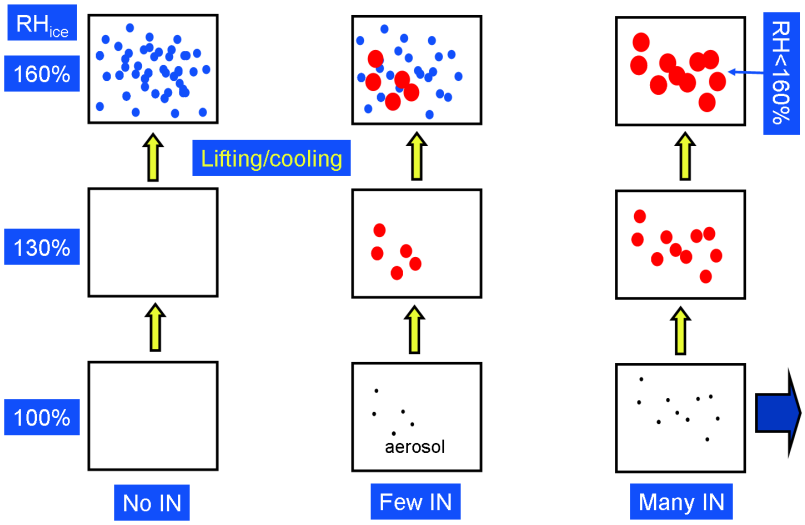

Figure 66: Schematic of homogeneous and heterogeneous nucleation competition, see text and lesson for details

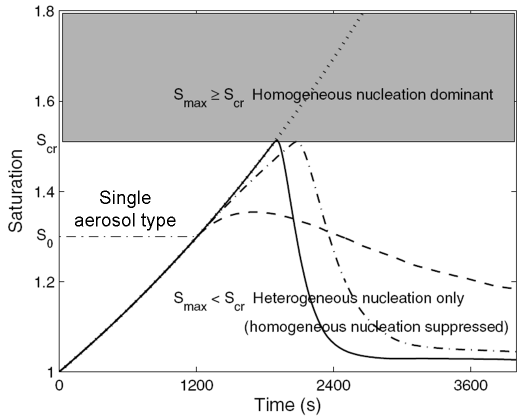

Figure 67: Results from parcel model of Ren and Mackenzie (2005) using a single aerosol type with a IN property threshold of $S = 1.3$

- The overshoot depends on the updraught velocity and also the number of aerosols present and their own nucleation (S_{cr}) properties.
- A numerical model needs to be able to resolve the updraught velocity of the parcel *on the scale of the cloud*
- A numerical model needs to have accurate information concerning the aerosol quantities present.
- In many cases the diffusional growth timescale is also less than the timestep of a typical global model (O(1 hour)).

Another example of this work is Gierens (2003). To pick up on the point concerning the model vertical velocity, Fig. 68 gives typical PDFs observed and also modelled using a global model. It is seen that the coarse resolution of the model truncates the spectra and does not resolve the highest velocities occurring on small spatial scales. Some success at reproducing the statistics of the vertical velocity spectrum is achieved with a simple parametrization. Some of my own work (Tompkins et al., 2007) has attempted to implement a modified cloud scheme into a weather forecast model that takes the zero-order effect of the elevated homogeneous nucleation threshold into account.The schematic in 69 shows the RH evolution of a air parcel undergoing homogeneous nucleation and model assumptions the dotted line add shows the assumptions made

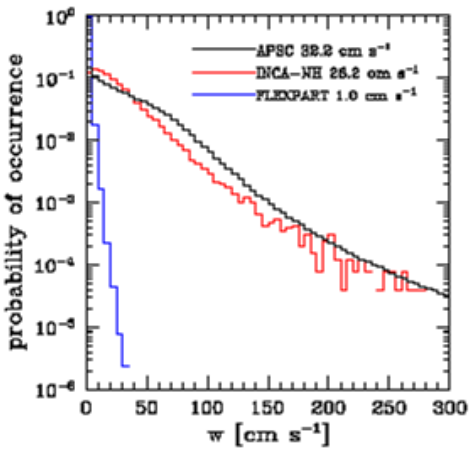

Figure 68: Results from Lohmann (citation needed) showing PDF of vertical velocity from (blue) a global model (red) aircraft observations and (black) model results corrected with a simple turbulence based parameterization for use in a ice-cloud model.

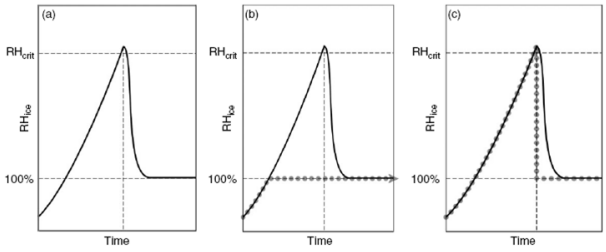

Figure 69: Schematic from Tompkins et al. (2007) showing (left) the *RH* evolution of a air parcel undergoing homogeneous nucleation and model assumptions.

in many models (middle panel) and the new scheme (right). The new scheme allows the clear air to be supersaturated, but assumes that once ice crystals are nucleated they grow instantaneously by diffusion to return the vapour to ice saturation within a model timestep. The *zero order* effect of the ice nucleation threshold and *hysteresis* behaviour is captured.

Such a simple scheme is able to reproduce the distribution of frequency of occurrence of supersaturation from satellite retrievals and the PDF of *RH* from aircraft well (Fig. 70). Errors in the map reflect errors in the convection occurrence in this version of the model known from other sources. We note (1) that model error sources may be remote and are not easy to track down (cancellation of errors) and (2) parametrization complexity does not need to exceed that necessary to represent the zero-order effect of the process, your knowledge of the process, or the complexity of the models' other components!

5.11 Aggregation

Aggregation
The ice particle that form from diffusional growth from an ice crystal are called *pristine*. However pristine ice particles can clump together to form *snowflakes* in a process known as *aggregation*.

The efficiency of this process increases as the temperature exceeds -5°C, when ice surfaces becomes *sticky*. There is also a secondary peak between -10°C and -16°C when dendrite arms get entangled. Figure shows an example of 71 of aggregates of bullet rosettes.

5.12 Riming

Riming to form graupel

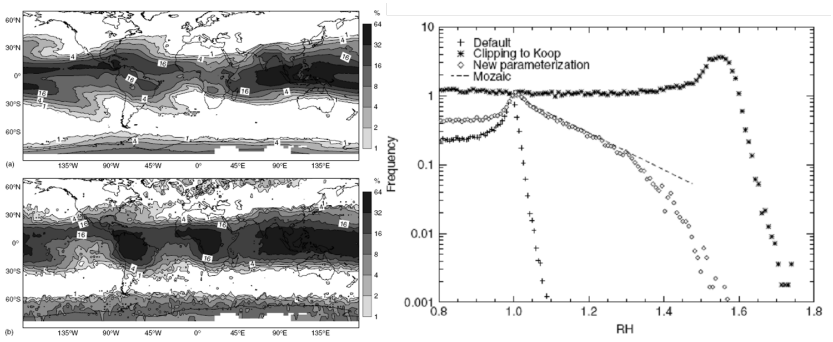

Figure 70: Results from Tompkins et al. (2007) showing (left) freq of occurrence of supersaturation compared to retrievals of Spichtinger et al. (2003) and (right) PDF of RH compared to Mozaic data of Gierens et al. (1999)

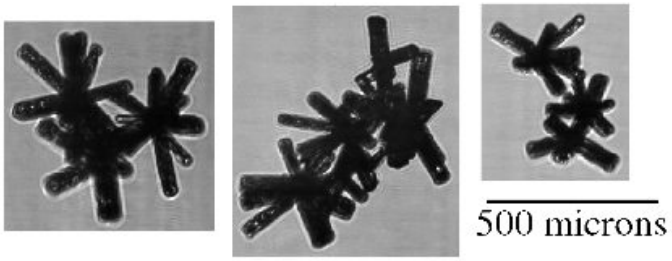

Figure 71: Bullet Rosette aggregates aggregates (source Dr. Chris Westbrook, Reading University, UK)

If vapour exceeds the water saturation mixing ratio (in strong updraughts) then water can condense on ice crystals, and then subsequently freeze to form *graupel*, which are round ice crystals of higher densities.

Graupel and Hail are also formed by aggregating liquid drops in mixed phase clouds (see schematic in Fig. 72).

Some examples of lightly and heavily rimed ice are given in Fig. 73. If the latent heat of condensation and fusion keeps temperature close to 273K then high density *hail* particles can form, since the liquid water *"spreads out"* before freezing. Hail is dense and thus has high terminal velocities (up to 40 m/s) implying that it only forms in convection with strong updraught able to support the particle long enough for growth

5.13 Ice particle fall-speeds

The density and size of ice particles determines their respective fallspeeds and its dependence on particle radius (Fig. 74).

There are implications for numerical models that may become clear examining radar animations of cloud systems (see link). *can you think what these might be?*

5.14 Ice multiplication

Ice multiplication

In recent years it has become increasingly evident that concentrations of ice crystals in "real" clouds are not always represented by the concentrations of IN measured or expected to be activated in such environments. In particular, it has been found that at temperatures warmer than -10°C the concentration of ice crystals can exceed the concentration of IN activated at cloud top temperature by as much as three or four orders of magnitude

There have been a number of hypotheses which have been advocated to explain such discrepancies. In particular, these hypotheses attempt to account for the unexpectedly high concentrations

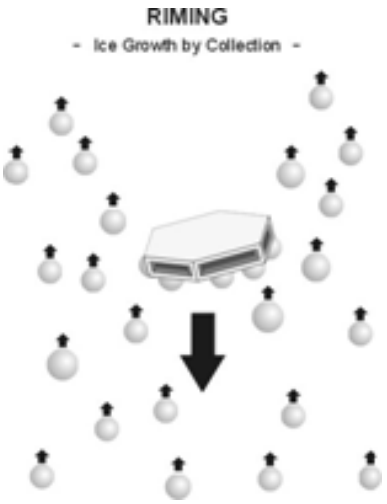

Figure 72: Schematic of riming process (source unknown)

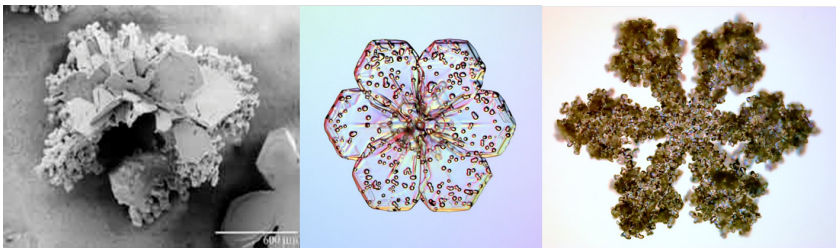

Figure 73: Photos of lightly and heavily rimed ice (source http://www.its.caltech.edu/)

at warm temperatures. Some of the leading hypotheses are:

1. Fragmentation of large drops during freezing.
2. Mechanical fracture of fragile ice crystals (i.e., dendrites and needles) caused by collision of these crystals with graupel and other ice particles.
3. Splinter formation during riming of ice crystals.
4. Artificial measurement artifact of ice crystals shattering on impact with aircraft measurement device inlet.

Aircraft observations of ice in mid-level clouds observed in aircraft campaigns by Fleishauer et al. (2002) are shown in Fig. 75. Although many models make simple assumptions such that ice particle size reduces with temperature, it is seen that this is not necessarily valid in clouds with strong mixing. The small particles may only appear circular due to instrument resolution limitations.

Raindrop size distributions

In many parts of the globe frozen precipitate melt before they reach the surface and thus precipitation reaches the surface in the form of rain. There is a natural limit to the raindrop size due to droplet breakup, and it is usually very rare to measure raindrops with radii larger than 3mm - with 2mm a more common limit.

Q: If you stand underneath a tree during a shower, you may get much larger drops fall on you. Why?

The reduction in occurrence with droplet size implies that raindrop radii (or diameters) tend to follow an inverse exponential distribution, known as the Marshall-Palmer distribution (Marshall and Palmer, 1948), after the first authors to suggest the relationship from observations

$$N(D) = N_0 e^{-\Lambda D}, \tag{136}$$

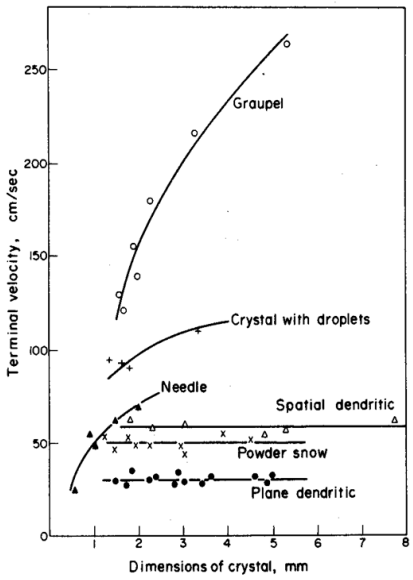

Figure 74: Fallspeeds of bulk ice particle categories (source: Rogers and Yau, 1989).

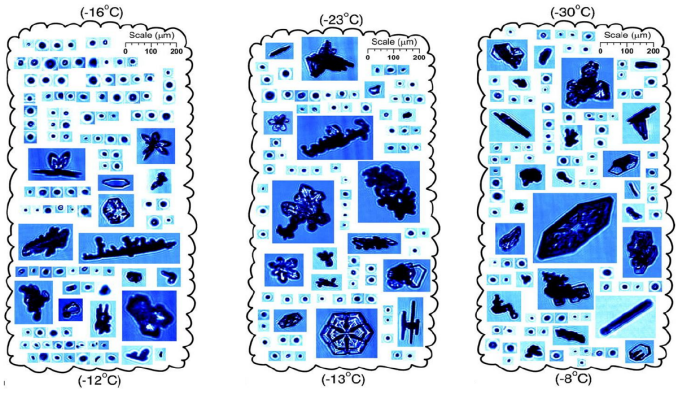

Figure 75: Example ice crystals from aircraft observations in mid-level cloud systems by Fleishauer et al. 2002 Fleishauer et al. (2002).

where $N(D)dD$ is the number of drops per unit volume with diameters between D and $D + \Delta D$.

The slope factor *Lambda* depends on rainfall rate R and is given by

$$-\Lambda(R) = 41R^{-0.21}, \tag{137}$$

where the units of R and *Lambda* are mm hour^{-1} and cm^{-1}, respectively. It was also found that N_0 was independent of rainfall rate, taking a value of $N_0 = 0.08$ cm^{-4}. Fig 76 shows the Marshall-Palmer distribution.

Of course, these relationships are empirical and valid over a large-number of observations. Exact relationships will vary with location and time and departures from the MP distribution will always occur (Fig. 77).

Snowflake size distributions

Most of the precipitation that reaches the ground does so as snowflakes and not pristine ice crystals.

Q: What conditions are most likely required for pristine ice precipitation?.

Since snowflakes are irregular aggregates of crystals there is no simple way to measure their dimensions, thus they are usually measured in terms of their mass or, equivalently, the diameter of the water drop that would form from their melting.

Gunn and Marshall (1958) found that the exponential approximation still fits the snowflake diameter well with the following parameters:

$$-\Lambda(R) = 25.5R^{-0.48}, \tag{138}$$

Q: what properties do you notice from the rainfall size distribution?

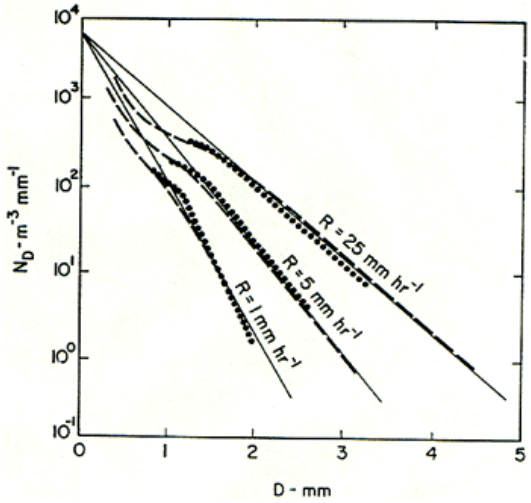

Figure 76: Marshall-Palmer distributions (from Marshall and Palmer, 1948)

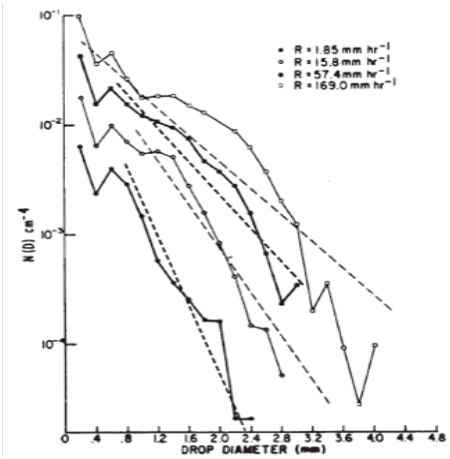

Figure 77: An example of raindrop size distributions from Willis (1984)

and

$$N_0 = 3.8 \times 10^{-2} R^{-0.87} \tag{139}$$

where the units of R and *Lambda* are mm hour^{-1} and cm^{-1} (Fig 78).

The final figure (Fig. 79) shows an intermediate complexity bulk scheme in use in numerical models.

Reminder Questions

- Take a look at the precipitation radar animation of 9/2/09 and explain what is going on.
- Explain with a sketch diagram what the LCL, LFC and LNB are, and graphically what CAPE and CIN are. Explain with a diagram how one graphically determines the wet-bulb temperature and with which process is it associated? How is the wet bulb temperature related to the equivalent potential temperature?
- explain at the board what it means for an aqueous aerosol solution droplet to become "activated".
- What are the main mechanisms of ice nucleation that are relevant for ice cloud formation?
- Explain why you can sometimes see your breath in winter.

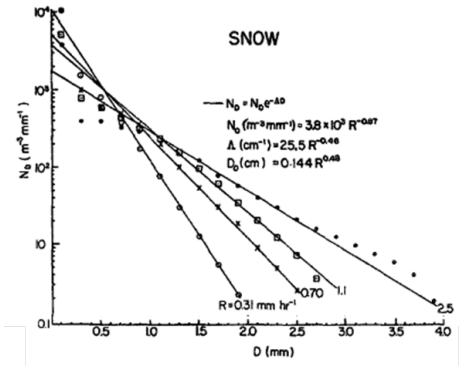

Figure 78: Snow flake size distributions (from Gunn and Marshall, 1958)

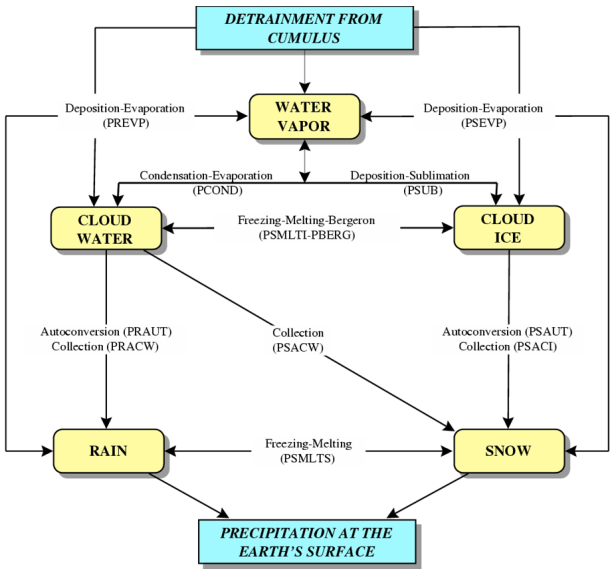

Figure 79: Typical intermediate complexity scheme of Fowler et al. (1996)

- How is a cloud called that consists only of ice, and one which consists of both liquid and ice? In roughly which temperature regimes does each cloud type exist? In the mixed phase explain what the Bergeron-Findeison effect is for ice growth
- Explain why we can find air that is supersaturated with respect to ice but not with respect to liquid water? What kind of cloud is an indication of supersaturated layers?
- Does the liquid cloud droplet radius increase or decrease with CCN number? Assuming that in a forming cloud, condensing liquid water is equally distributed among CCN, write down the relationship between droplet radius and cloud liquid water density in kgm^{-3}
- Does the ice crystal radius increase or decrease with ice nuclei (IN) number? What is a common source of IN?
- What are the two main mechanisms by which activated aerosols grow into raindrops, and under which droplet size radius do they operate and why? We made a number of approximations in our mathematical descriptions of the two processes, can you name some?
- What factor directly determines the number of ice crystals nucleated by each homogeneous nucleation, and what is this dependent on in turn?
- Explain what the criteria are for absolute convective stability and instability, and also conditional instability.

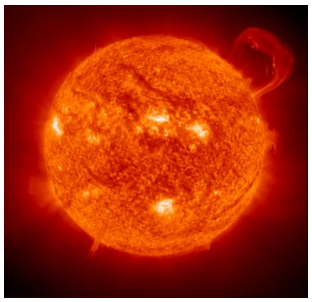

Figure 80: The sun! (http://z.about.com)

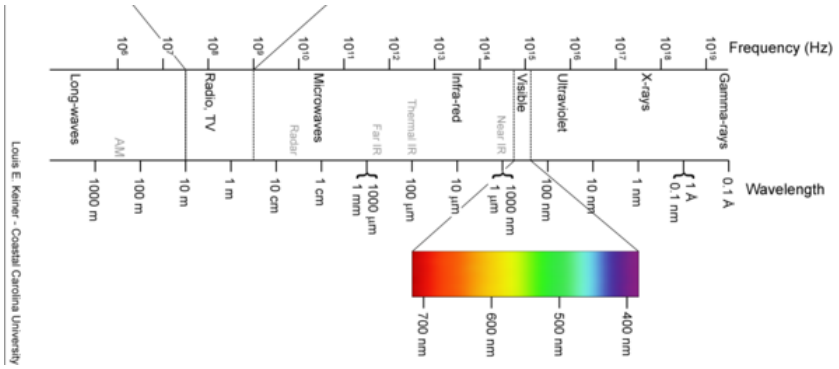

Figure 81: Electromagnetic spectrum with visible bands highlighted (source see caption).

6 Radiation

Why study radiative processes?

The sun (Fig. 80) is the fundamental energy source of the planet, and the uneven adsorption of solar radiation leads to the large-scale weather patterns that redistribute heat. Perturbations to radiative processes are responsible for climate variability through the greenhouse effect, volcanic eruptions and solar variability. Understanding radiative processes is also important for remote sensing of the atmosphere.

6.1 Definitions of the radiative field

Electro-magnetic spectrum

The electromagnetic (EM) spectrum is the range of all possible electromagnetic radiation frequencies. The "electromagnetic spectrum" of an object is the characteristic distribution of electromagnetic radiation from that particular object.

Bands that are important for atmospheric radiative processes are the ultraviolet, visible (400 to 700nm), near/thermal infra-red (Fig. 81).

Electro-magnetic wave

Electro-magnetic waves have a speed of $c = 3 \times 10^8$ m/s, (Fig. 82) with speed, frequency ν and wavelength λ related by

$$c = \nu\lambda \tag{140}$$

The Earth with radius[10] r_e orbits the sun (r_s) at a radius of r_d and intercepts a tiny fraction of the emitted energy (see sketch). We assume that the sun emits as a *black body.*

Black Body

A black body is an object that absorbs all electromagnetic radiation that falls on it. No electromagnetic radiation passes through it and none is reflected. It is also a perfect emitter of radiation.

[10]In the radiation section r is used for radius, not to be confused with mixing ratio! Other duplications of notation will also occur.

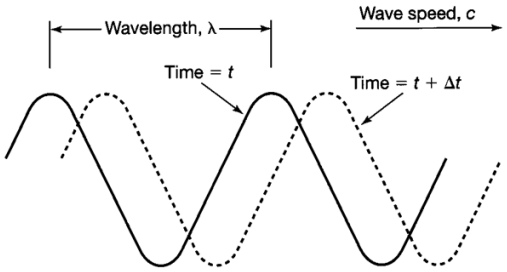

Figure 82: Propagating electromagnetic wave.

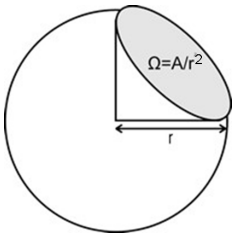

Figure 83: Definition of the solid angle.

A black body at temperature T emits exactly the same wavelengths and intensities which would be present in an environment at equilibrium at temperature T, and which would be absorbed by the body. Since the radiation in such an environment has a spectrum that depends only on temperature, the temperature of the object is directly related to the wavelengths of the light that it emits.

Irradiance and Radiant Emittance E
Irradiance and *radiant emittance* are radiometry terms for the power of electromagnetic radiation arriving or leaving a flat-plate surface, per unit area, integrated over the *hemisphere* above the plate (sketch). *Irradiance* is used when the electromagnetic radiation is incident on the surface while *radiant emittance* is used when the radiation is emerging from the surface.

The total energy per unit time is called the *radiant flux* and has units of J s^{-1} or W. As the irradiance and radiant emittance are measured per unit area they have units W m^{-2}. There is nothing in the definition of irradiance that tells us from which direction the radiation arrives or is emitted. We therefore introduce the *solid angle*.

Solid Angle Ω
The solid angle, Ω is the angle in three-dimensional space that an object subtends at a point. It is a measure of how big that object appears to an observer looking from that point. The solid angle is proportional to the surface area, A, of a projection of that object onto a sphere centered at that point, and inversely proportional to the square of the sphere's radius, r (Fig. 83).

We define the solid angle

$$\Omega = \frac{A}{r^2} \tag{141}$$

and it has units of *steradians* or *ster*. An important special case for radiation is the integration over a hemisphere of unit radius in spherical coordinates (Fig. 84). Following conventional spherical coordinate notation, the angle to the zenith is defined by θ, with $\theta = 0$ marking the vertical axis normal to the surface. The azimuth angle is defined by ϕ. We imagine integrating elements of solid angle $d\Omega$ over concentric circles starting in the horizontal direction. The radius of the circle element of width $d\theta$ from the vertical axis is $r\sin\theta = \sin\theta$. Thus the azimuth dimension of the solid angle element $d\Omega$ is $\sin\theta d\phi$. The vertical dimension of $d\Omega$ is simply $d\theta$. Thus:

$$\int_{\text{hemisphere}} d\Omega = \int_0^{2\pi} \int_0^{\frac{\pi}{2}} \sin\theta d\theta d\phi = 2\pi \quad \text{steradians} \tag{142}$$

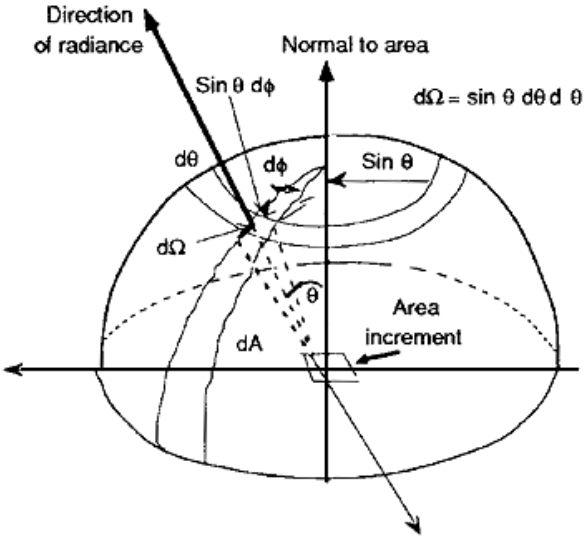

Figure 84: Integration of solid angle over a hemisphere

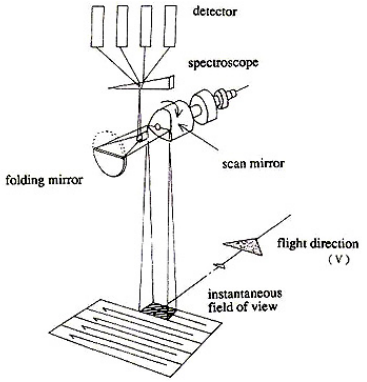

Figure 85: Schematic of why small solid angles measurements are required for remote sensing (source NASA website).

Radiance

The radiance tells us the radiant flux density per unit solid angle coming from a direction (θ, ϕ). For a surface area of ΔA_{norm} *normal* to the direction (θ, ϕ), the radiant flux received from the solid angle $\Delta\Omega$ will be $L(\theta, \phi)\Delta\Omega\Delta A_{\text{norm}}$ (*draw sketch*).

$L(\theta, \phi)$ is the *radiance* with units W m^{-2} ster^{-1} However, in general the receiving surface *will not be normal to* θ, ϕ. If we take the special case where the receiving surface of dimension ΔA is *horizontal*, then the projection of this area on to the surface normal to direction (θ, ϕ) is given by $\Delta A_{\text{norm}} = \Delta A\cos\theta$ (see sketch).

Thus in general the contribution to the radiant flux incident on a horizontal surface is given by: $L(\theta, \phi)\Delta\Omega\Delta A\cos\theta$. If we take $\Delta A = 1$ for a unit area, then the radiant flux per unit area from solid angle (i.e. the contribution to the *irradiance* from that solid angle) is $L(\theta, \phi)\cos\theta\Delta\Omega$ with units W m^{-2}. From now on we will assume the (θ, ϕ) angle dependence and simply write L for radiance. With remote sensing we need a device capable of measuring radiation from different directions with very small solid angles to achieve the best resolution possible (Fig. 85).

Irradiance E Definition

We are now able to return to the concept of *irradiance*, which is the total radiance integrated over all solid angles over a hemisphere.

Thus

$$E = \int_{\text{hemisphere}} L\cos\theta d\Omega = \int_0^{2\pi}\int_0^{\frac{\pi}{2}} L\cos\theta\sin\theta d\theta d\phi \tag{143}$$

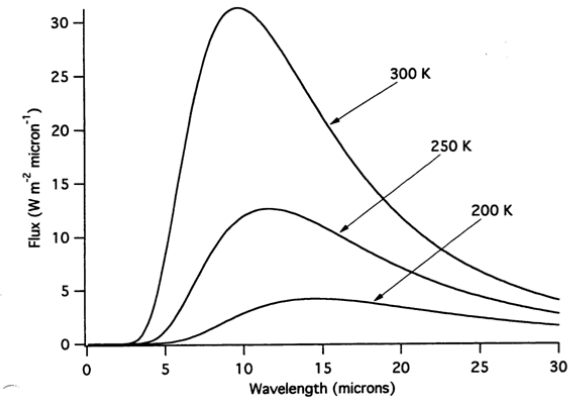

Figure 86: Black body emission at three tropospheric temperatures.

Isotropic radiation
An important special case is *isotropic radiation*, namely that the radiative flux has the same intensity regardless of the direction, and thus L is independent of direction. *Q: can you think of some examples?* Examples include:

- Emission from a black body.
- Solar radiation beneath a cloud of moderate thickness due to multiple scattering of photons.
- Background microwave radiation from big bang.

In this case we may write

$$E = L \int_0^{2\pi} \int_0^{\frac{\pi}{2}} \cos\theta \sin\theta d\theta d\phi = \pi L \tag{144}$$

Exercise: show! Q: What are the units of π in (144)? The units of π are steradians.

Planck Function
Planck's law describes the spectral radiance of electromagnetic radiation at all wavelengths from a black body at temperature T. The *Planck Function* giving the radiance for wavelength λ as a function of T is:

$$L_\lambda = \frac{c_1}{\lambda^5 (e^{\frac{c_2}{\lambda T}} - 1)} \tag{145}$$

where c_1 and c_2 are constants. The emitted power per unit area of emitting surface, per unit solid angle, and per unit wavelength.

At room temperature, black bodies emit mostly infrared light ($\lambda > 4\mu$m), but as the temperature increases past a few hundred degrees Celsius, black bodies start to emit visible wavelengths, from red, through orange, yellow, and white before ending up at blue, beyond which the emission includes increasing amounts of ultraviolet. Examples of the Planck function for temperatures between 200 to 300 K are given in Fig. 86.

Wein's Displacement Law
Note how the peak in Fig. 86 moves to shorter wavelengths as the temperature increases. The relationship describing the wavelength at which emission is at a maximum (i.e. where $dL_\lambda/d\lambda = 0$) is

$$\lambda_{\max} = \frac{2897\mu\text{K}}{T} \tag{146}$$

Integrating (145) across all wavelengths gives the total emitted energy *per unit solid angle*, in other words the radiance L. We will not enter the details of the mathematics here, but simply state the result that

$$L \equiv \int_0^\infty L_\lambda d\lambda = \frac{\sigma T^4}{\pi} \tag{147}$$

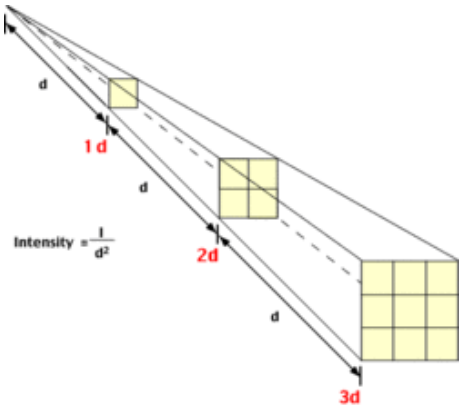

Figure 87: Inverse square law, radiation spread over increasing

where σ is the Stefan Boltzmann constant ($= 5.67 \times 10^{-8}$ W m^{-2} K^{-4}).

We now recall that the integral of L over the hemisphere gives us the Radiant Emittance E, which (144) tells us in the case of isotropic blackbody radiation is equal to πL. Thus combining (145) and (144) we get

$$E = \sigma T^4 \tag{148}$$

This is known as the *Stephan-Boltzmann Law.*

6.2 Energy balance models of the atmosphere

Energy balance models of the atmosphere

We are now in a position to construct a simple energy balance model of the earth-atmosphere system. If the sun is considered to be a black body (a good approximation) then its emittance is given by σT_{sun}^4 where T_{sun} is the surface temperature of the sun. This is emitted over a surface area of $4\pi r_s^2$ giving a total energy of $4\pi r_s^2 \sigma T_{\text{sun}}^4$.

The energy of the sun is spread over the surface of a sphere of area $4\pi r_d^2$ at a distance of r_d, known as the inverse square law (Fig. 87). The *irradiance* E (W m^{-2}) at a distance r_d is thus

$$E = \sigma T_{\text{sun}}^4 \left(\frac{r_s}{r_d}\right)^2. \tag{149}$$

If r_d corresponds to the distance of separation between the earth and the sun, then we define $S_0 \equiv E$, called the *solar constant.*

Solar Constant S_0

S_0, the average irradiance at the top of the earth's atmosphere, is known as the *Solar Constant.* Measurements from satellites show that $S_0 \simeq 1370$ W m^{-2}. The value varies by ≈ 1 W m^{-2} over a solar cycle that has an average length of 11 years.

Knowing the solar constant we can invert (149) to get the surface temperature of the sun:

$$T_{\text{sun}} = \sqrt[4]{\left(\frac{r_d}{r_s}\right)^2 \frac{S_0}{\sigma}} \tag{150}$$

giving T_{sun} as 5800K. The energy intercepted by the earth is (see Fig.88) $S_0 \pi r_e^2$, so that E_e, the average incident solar radiation on the earth's surface, which has a surface area of $4\pi r_e^2$, is

$$E_e = \frac{S_0 \pi r_e^2}{4\pi r_e^2} = \frac{S_0}{4} \tag{151}$$

which has a value of 340 W m^{-2}.

Planetary Albedo

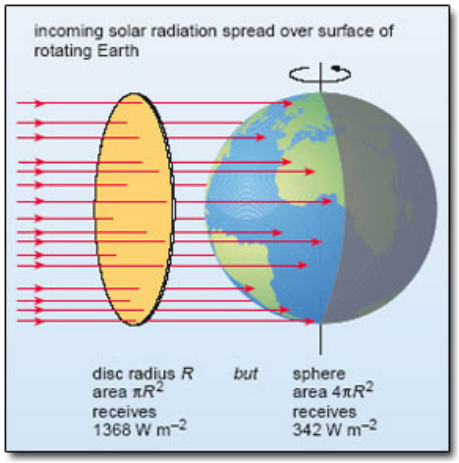

Figure 88: Shadow area of earth

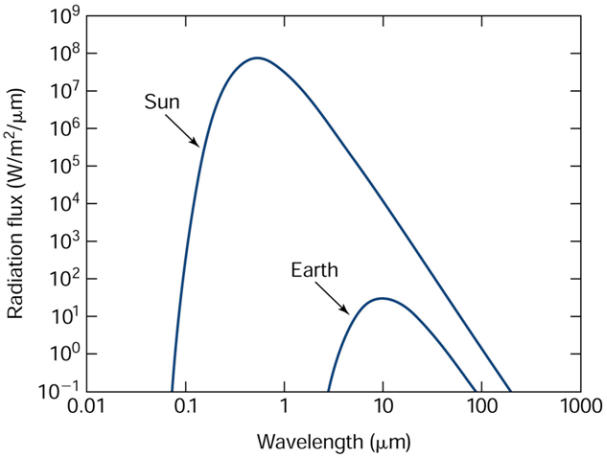

Figure 89: Radiative flux per micron for sun and earth's emitted temperatures (source unknown)

A proportion of this radiation is scattered back to space by clouds, atmospheric gases and the planet's surface. We thus introduce the parameter α_p as the *planetary albedo*. Which is defined as

$$\alpha_p = \frac{\text{Reflected solar irradiance (at top of atmosphere)}}{\text{Incident solar irradiance}} \tag{152}$$

Observations from Satellites put the earth albedo at $\alpha_p \simeq 0.3$. Thus the average irradiance absorbed is $\frac{S_0}{4}(1-\alpha_p)$ which is 240 W m^{-2}.

Effective Emitting temperature of the Earth
Earth/atmosphere is assumed to emit to space as a black body at some effective temperature T_e. Thus the rate of emission is $4\pi r_e^2 \sigma T_e^4$. We will assume that there is a *long term balance* (i.e. an equilibrium) between absorbed solar and emitted infrared radiation:

$$S_0 \pi r_e^2 (1-\alpha_p) = 4\pi r_e^2 \sigma T_e^4 \tag{153}$$

Thus

$$T_e = \sqrt[4]{\frac{S_0}{4\sigma}(1-\alpha_p)} = 255\text{K} \tag{154}$$

Thus we have two contrasting temperature of the sun (5800K) and the earth (255K). This is important since the peak wavelengths (λ) at which energy is emitted is a function of temperature. The Planck function L_λ is shown graphically for the sun and earth effective emitting temperatures in Fig. 89. We now plot λL_λ to give us the black body emitted radiation and reduce the solar

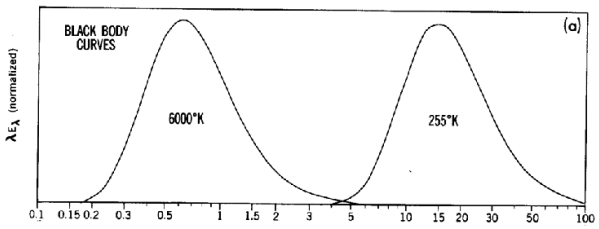

Figure 90: Blackbody spectra after normalisation at sun/earth temperatures. (x-axis in μm).

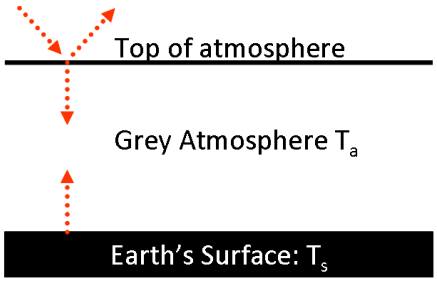

Figure 91: Sketch of the greenhouse slab model (source: me!)

curve by a factor of $\frac{r_s}{r_d}(1-\alpha_p)$ to get the normalized radiation at the earth, depicted in Fig. 90. It should be pointed out the solar radiation energy is *not* restricted to the visible (0.4 to 0.7 μm), rather 35% of the solar energy received at the earth is in this band, with 50% in the *near-infrared* and 15% in the *ultra-violet*. It is also clear that the result of the different emitting temperatures is that the radiation from the sun and earth are in *distinct wavelength regions* with little overlap.We found that $T_e = 255$ K and yet surface measurements indicate an average global temperature of roughly 288K. *Q: Why are these so different? Q: How does a greenhouse work?*

A simple model for the greenhouse effect

To illustrate the *Greenhouse Effect* we will now construct a simple radiative balance model for the earth surface with an overlying atmosphere which will be considered a single radiatively active *homogeneous slab*.

We make the following simplifying assumptions:

- The earth surface is a black body.
- The atmosphere does not absorb solar radiation.
- Atmosphere can be represented as a *grey body*.

Grey Bodies and Kirchoff's Law

A grey body emittance is one which emits radiation according to

$$E_{\text{grey}} = \epsilon\sigma T^4, \tag{155}$$

where ϵ is the fractional emittance ($\epsilon \leq 1$).

Kirchoff's Law states that, if at a given wavelength we know how good an emitter a body is, then we also know how good an absorber it is. Kirchoff's Law specifies:

- Absorptance $a = \epsilon$
- Transmittance $\tau = 1 - \epsilon$

We can now write down the radiative energy balance of each component (according to the sketch in Fig. 91), assuming a state of *radiative equilibrium*.

Q: Derive these components.

Top of atmosphere

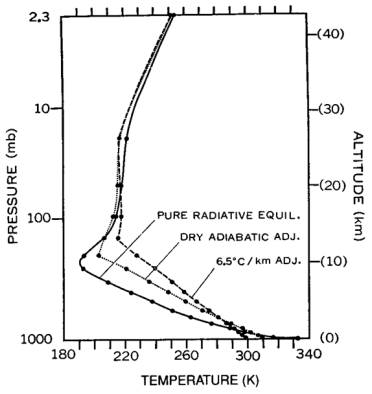

Figure 92: Temperature profiles resulting from a pure radiative equilibrium, or a radiative-convective equilibrium assuming a simple parametrization of convection that adjust the profile to a dry (9.8 C km^{-1}) or mean moist (6.5 C km^{-1}) temperature lapse rate. From Manabe and Strickler (1964).

$$\frac{S_0}{4}(1-\alpha_p) = \sigma T_s^4(1-\epsilon) + \epsilon\sigma T_a^4 \tag{156}$$

Atmosphere

$$\epsilon\sigma T_s^4 = 2\epsilon\sigma T_a^4 \tag{157}$$

Q: Why is there a factor 2 on the RHS?

Surface

$$\epsilon\sigma T_a^4 + \frac{S_0}{4}(1-\alpha_p) = \sigma T_s^4 \tag{158}$$

Q: Why isn't there an ϵ factor in the solar term?

We thus have 3 equations with 2 unknowns T_s and T_a, and can use any two to calculate these unknowns. For example, from (157) we have

$$T_a = \frac{T_s}{\sqrt[4]{2}}, \tag{159}$$

which if we substitute into (156) gives

$$T_s = \sqrt[4]{\frac{S_0(1-\alpha_p)}{2\sigma(2-\epsilon)}} \tag{160}$$

Exercise: Check this derivation and also try other equation combinations using (158)

If we assume that $\epsilon = 0$ then we get the same result we achieved earlier, namely $T_s = 255$K, *Q: Why?*.A more reasonable value is $\epsilon = 0.6$, which results in $T_s = 278$K and $T_a = 235$K. Thus we can see that introducing an atmosphere that can absorb in the thermal IR *causes a surface warming*. This is known as the *greenhouse effect*. We will later consider what determines ϵ and its variation in a continuous media.

We could take this approach further and divide the atmosphere up into many vertical slabs, each with its own emittance according to the absorbing gases present in the layer. This would provide a *vertical atmospheric temperature profile* of the earth-atmosphere system in a state of *radiative equilibrium* (sketch). However this would *not* be a good model of the atmosphere temperature structure, *Q: Can you think why this would be the case?*

If one calculates the vertical temperature structure that would arise from radiative equilibrium it turns out that it is *absolutely unstable* to both dry and moist deep convection. Thus convection can (and does) occur to transport heat from near the earth's surface to higher in the atmosphere. One of the earliest studies to examine this using a column model of the atmosphere was conducted by Manabe and Strickler (1964) (Fig. 92). *Q: in a state of radiative equilibrium, what would be the net radiative heating everywhere in the atmosphere?* In a radiative equilibrium the net heating rate would be zero everywhere by definition. Instead in the *troposphere* there is a net cooling rate of O(1 K day^{-1}) which is balanced by convective heating processes.

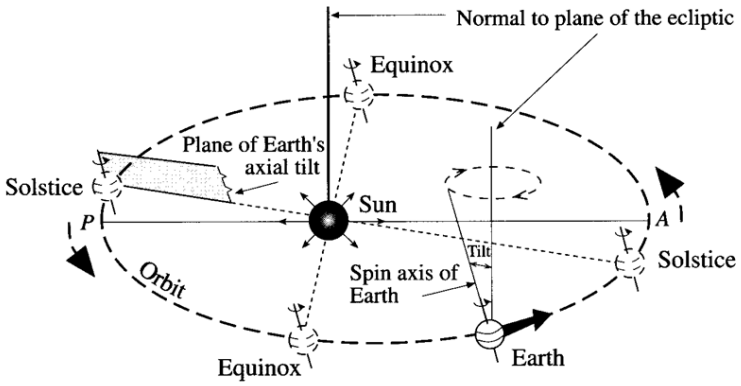

Figure 93: B

6.3 Sun and Earth Geometry

In the previous section we constructed a simple slab-atmosphere radiative balance model. We now briefly discuss the sun-earth geometry in more detail as this determines the insolation of the earth by the sun and the sun position in the sky needed for radiative transfer calculations.

Sun-Earth Geometry
The sun-earth geometry is shown in Fig.93. Note the

1. Declination angle of the earth ϑ
2. Eccentricity of the earth's orbit

Declination Angle ϑ

- $\vartheta = +23.5°$: at the summer solstice June 21st
- ϑ = -23.5° : at the winter solstice December 21st
- $\vartheta = 0°$: at the spring and Autumn Equinoxes

Eccentricity of orbit
The Earth's orbit is slightly elliptical with an *eccentricity factor* of $e = 0.0167$. Since the average sun-earth separation is $r_d = 149.6 \times 10^6$km, we can calculate:

- The *Perihelion* (distance of closest approach) is $r_d(1 - e) = 147.1 \times 10^6$km.
- Thus the *Aphelion* (distance of furthest approach) is $r_d(1 + e) = 152.1 \times 10^6$km.

Presently, the Perihelion occurs on January 3rd while the Aphelion July 4th, but the closeness of these dates to the solstices is a present-day coincidence.

Solar Zenith Angle
The solar zenith angle (θ) is a function of latitude, time of year and time of day. The *daily averaged* insolation is given in Fig. 94. *Q: At midsummer, at which latitude do you think Q_{av} is greatest: Tropics, subtropics, midlatitudes or at the north pole?*

In midsummer Q_{av} is maximum at the north pole. θ ranges from 0° at a latitude of 23.5°N to 66.5° at the north pole. *Q: If the sun is overhead at 23.5°N, why is Q_{av} is maximum at the north pole?* It is due to the day length which more than offsets the lower value of $S_0 \cos\theta$.

Variations in Earth's orbit (Milankovitch cycles)
There are variations in the Earth's orbit parameters, that affect the eccentricity of the earth orbit, the Axial tilt (obliquity) and Precession (wobble).

The variations in the solar insolation can strongly modulate climate (Fig. 96).

However, these variations are not thought to be the causes of ice-ages beginning or ending, as the forcing variability occurs at a higher frequency than the major glaciations (Fig. 97),

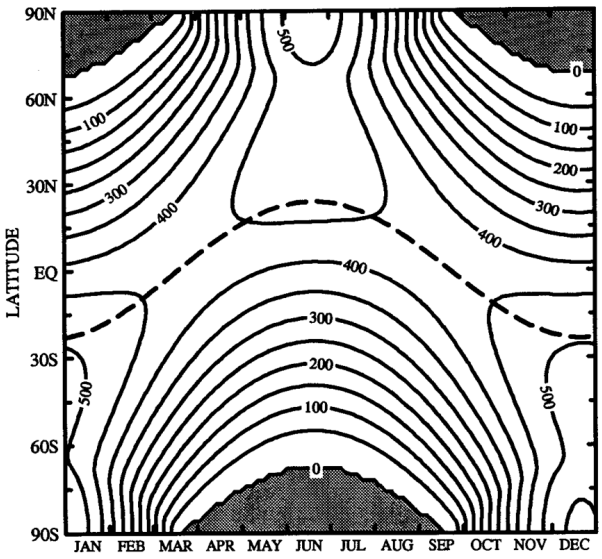

Figure 94: Day averaged insolation Q_{av} (W m^{-2}) at the TOA as function of season and latitude. The heavy dashed line marks the latitude of the subsolar point at noon **?**.

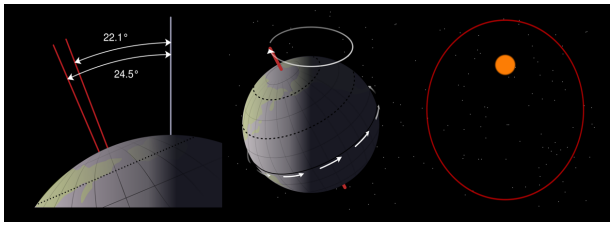

Figure 95: Schematic (Left) Axial tilt (obliquity), (middle)Precession and (right) eccentricity (source Wikipedia)

6.4 Radiation interactions with a slab

Radiation interaction with a slab
We now consider the interaction of radiation with a layer of the atmosphere in more detail, considering the processes depicted in the sketch. We imagine a layer that is homogeneous in the infinite horizontal direction, and has a finite vertical depth of Δz.

The radiance L_λ which we recall is a function of (θ, ϕ), can be divided into three distinct components (draw sketch):

1. The direct solar component: the radiative flux that passes unimpeded through the slab direction (θ, ϕ).

2. The scattered component: the radiative flux that originates from a different solid angle to (θ, ϕ), but undergoes scattering within the slab to emerge in direction (θ, ϕ).

3. Emission: Radiation that is emitted from the slab in direction (θ, ϕ).

6.4.1 Direction Radiation

Direct Radiation - Beer's Law
Beer's Law The law states that there is a logarithmic dependence between the transmission τ of the a radiative flux through a substance and the product of the absorption coefficient of the substance, a, and the thickness of the material (i.e. the path length).

To derive this, we note that the finite reduction in the direct component by the slab dL_λ will be directly proportional to (*draw sketch*):

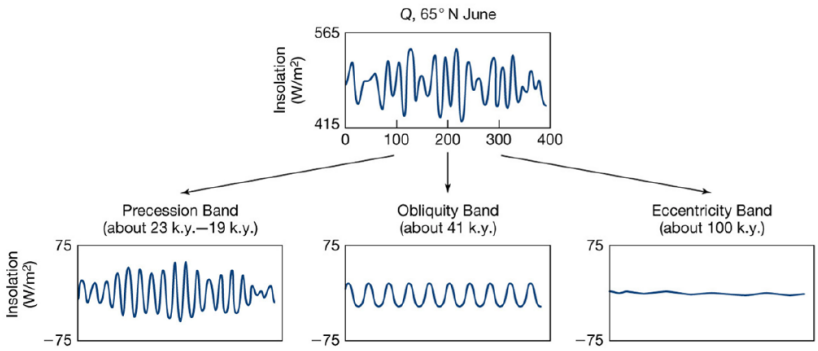

Figure 96: Solar flux variation as a result of earth orbit variations

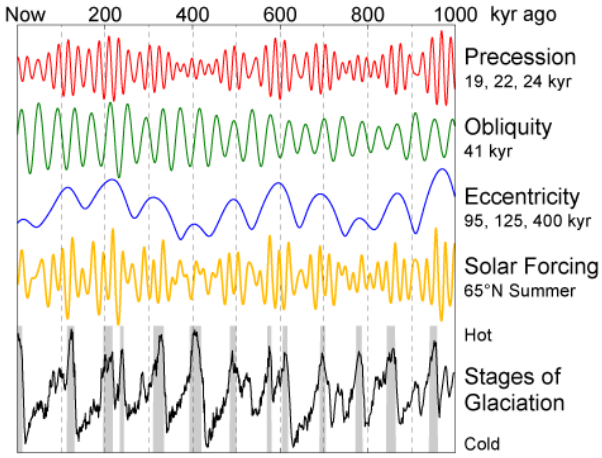

Figure 97: Solar flux variations as a result of earth orbit variations and the associated reconstructed temperature records (source Wikipedia)

- L_λ: The original intensity of the radiative beam
- $sec\theta dz$: The path length through the slab of the radiation.
- k^e_λ: The mass extinction coefficient at wavelength λ

Thus

$$dL_\lambda = -L_\lambda k^e_\lambda \rho sec\theta dz, \tag{161}$$

where ρ is the density of the material.

Mass extinction, absorption and scatter coefficients
For a specific material, it is useful to define the mass extinction k^e_λ. This specifies how strongly a unit mass of a medium depletes a direct beam of radiation of a given wavelength λ (or equivalently frequency ν) and has units m^2 kg^{-1}.

The mass extinction coefficient is the sum of the absorption k^a_λ and scattering k^s_λcoefficients.

$$k^e_\lambda = k^a_\lambda + k^s_\lambda \tag{162}$$

Single scattering albedo
The *single scattering albedo* is defined as the ratio

$$\omega = \frac{k^s_\lambda}{k^e_\lambda} \tag{163}$$

The two extreme regimes are

- $\omega = 1$: Pure scatter (conservative scatter)
- $\omega = 0$: Pure absorption

We now integrate (161) over a finite depth slab to get the direct component of radiation as

$$L_\lambda^{z_1} = L_\lambda^{z_2} exp\left(-\int_{z_1}^{z_2} k_\lambda^e \rho sec\theta dz\right). \tag{164}$$

Optical Thickness/Depth
If from (164) we set

$$\delta_\lambda = \int_{z_1}^{z_2} k_\lambda^e \rho sec\theta dz. \tag{165}$$

Then δ_λ is known as the *optical thickness* or *optical depth* of the layer between z_1 and z_2, essentially the integrated extinction coefficient.

Beer's (or Lambert's Law) then can be written

$$L_\lambda^{z_1} = L_\lambda^{z_2} e^{-\delta_\lambda} \tag{166}$$

showing us that the transmittance τ is related to optical depth by

$$\tau_\lambda = e^{-\delta_\lambda} \tag{167}$$

We lastly emphasize that the transmittance, absorptance, extinction and optical depth are *functions of wavelength* or equivalently frequency.

6.4.2 Emission from Slab

Emission from slab
The emission by a slab in direction (θ, ϕ) is simply

$$L_\lambda^{\text{emitted}} = L_\lambda k_\lambda^a \rho sec\theta dz \tag{168}$$

6.4.3 Scattering from other directions

Scattering from other directions
The scattering from other directions (θ', ϕ') is defined as

$$L_\lambda^{\text{scatter}} = \frac{\omega_\lambda}{4\pi} \int_0^{2\pi} \int_{\frac{-\pi}{2}}^{\frac{\pi}{2}} L_\lambda(\theta', \phi') P(\theta', \phi', \theta, \phi) \text{sin}\theta d\theta d\phi \tag{169}$$

We note

- The two integrals are to integrate over the sphere.
- 4π is a normalization factor, the solid angle integrated over a sphere.
- Recall $\text{sin}\theta d\theta d\phi$ is the element of solid angle.

Phase Function
$P(\theta', \phi', \theta, \phi)$ is called the *Phase Function* and gives the probability that a photon will be scattered from direction (θ', ϕ') into direction (θ, ϕ)

For solar radiation ($\lambda < 4\mu$m) *thermal emission* is unimportant as L_λ is very small. For thermal infrared ($\lambda < 4\mu$m) scattering can generally be neglected, thus only the extinction and emission are important.

We now examine these in turn.

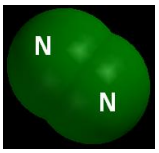

Figure 98: N_2 molecule

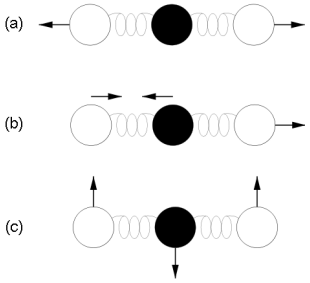

Figure 99: CO_2 molecule with its main vibrational modes

6.5 Absorption by atmospheric gases

Gases are not like black bodies that absorb equally and completely at all wavelengths. Rather, they absorb only at specific, often narrow ranges of wavelengths.

Absorption by atmospheric gases
In general molecules posses three kinds of quantized energy

- Electronic Energy (Visible and UV)
- Vibrational Energy (Near IR, Thermal IR 0.7-20 μm)
- Rotational Energy (Thermal IR)

To absorb or emit radiation the molecule must possess a permanent dipole, as it vibrates or rotates the electric field varies, allowing the interaction with the incoming/outgoing radiation.

N_2 and O_2
The major species of N_2 and O_2 are simple molecules that possess no permanent dipole (Fig. 98), and thus possess almost no vibrational or rotational absorption.

CO_2
Carbon dioxide CO_2 is a linear molecule, and thus from its symmetry possesses no dipole and thus no rotational spectrum. However, there are certain vibrational modes shown in (Fig. 99).

H_2O and O_3
H_2O and O_3 do possess a permanent dipole as the molecular structure is "bent" and hence asymmetric. They therefore also have a rotational spectrum. (Fig. 100),

Absorption Spectrum
The distribution of absorption lines with wavelength is very complicated. We have seen that the molecular states are defined by the molecule's modes of vibration and rotation and these modes are *quantized*, and may be excited by absorbing single photons (Fig. 101).

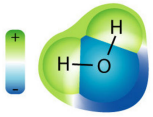

Figure 100: H_2O molecule and its charge structure

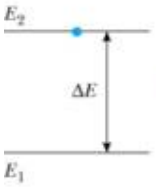

Figure 101: Quantized vibrational energy levels.

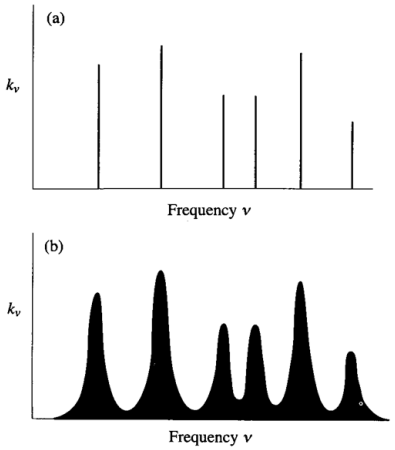

Fig. 3.5 Hypothetical line spectrum (a) before broadening, (b) after broadening.

Figure 102: (a) Hypothetical discrete absorption lines (b) actual absorption due to line broadening mechanisms

The excited states do not persist: after some random amount of time, the molecules revert back to their original, lower energy state. The vibrational or rotational mode decays, emitting a photon.

The energy associated with with a transition between two states is

$$\Delta E = h\nu = h\tilde{\nu}c \tag{170}$$

where h is the Planck Constant and $\tilde{\nu}$ is the *wavenumber* which is the reciprocal of the wavelength (λ^{-1}). Due to the existence of various rotational and vibrational discrete levels, molecules can absorb or emit at many different wavelengths or wavenumbers, with the strength of the absorption related to the probability of the transition between the relevant energy levels.

Line broadening
Due to the discretised nature of the molecular energy levels one might expect absorption and emission to occur at distinct set *delta function* wavelengths as in Fig. 102a. In reality the energy levels are slightly "fuzzy" due to *line broadening mechanisms* so that absorption is spread over a finite width of wavelengths (Fig. 102b).

Three mechanisms for line broadening are

- *Natural Broadening*: a fundamental limit to the narrowness of the spectral lines due to Heisenberg's uncertainty principle, which relates the uncertainty of the time spent in excited states to the energy of the state transition
- *Pressure Broadening*: The energy levels are perturbed by the presence of other particles nearby the emitting one, for example, collisions of other particles with the emitting particle interrupts the emission process.
- *Doppler Broadening*: the emitting particles will have a variety of motions towards and away from the observer leading to a Doppler shift in the radiation.

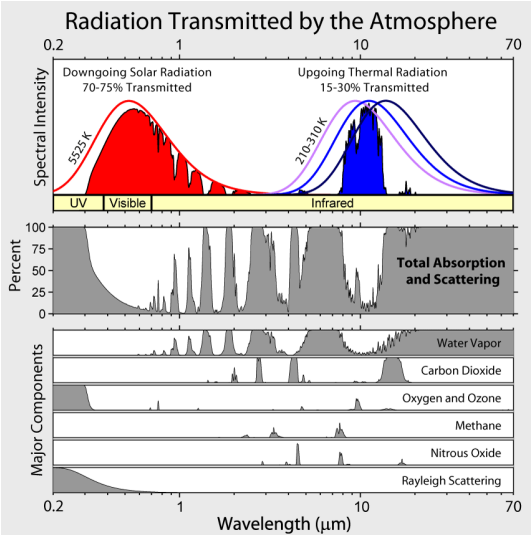

Figure 103: Upper panel shows the transmitted radiation in comparison to theoretical blackbody curves. Lower panels show the percentage absorptance due to the atmosphere and the contribution to this by the main active gases (source Wikipedia).

Natural Broadening is overwhelmed by the other two processes. *Q: Where in the atmosphere will pressure broadening dominate?* Pressure broadening dominates in the troposphere where p is relatively high and Doppler broadening is important in the upper stratosphere ($z > 30$km). We recall from earlier (167) that the transmittance is related to optical depth as $\tau_\lambda = e^{-\delta_\lambda} = \exp(-\int_{z_1}^{z_2} k_\lambda^e \rho sec\theta dz)$. If we assume a homogeneous material and a solar zenith angle of zero, then this simplifies to

$$\tau_\lambda = \exp(-k_\lambda^e \rho(z_2 - z_1)) \tag{171}$$

The absorption in a band depends on the product $-k_\lambda^e \rho(z_2 - z_1)$. If a particular gas is an efficient absorber (high $-k_\lambda^e$) and/or is present is high amounts (large $\rho(z_2 - z_1)$) then the incoming/outgoing radiation of a band of wavelengths around the line centre may be completely absorbed. We thus find that we can have two regimes of *absorption lines* (*draw sketch*):

- *Weak Limit*: Absorption is linear with absorber amount
- *Strong Limit*: Radiation is totally absorbed at line centre, adding more absorbed only increases absorption at band edges. Absorption increases proportionally to the *square root* of the absorber amount with the constant of proportionally depending on pressure.

This is important when considering the greenhouse effect of gases. Carbon dioxide CO_2 for example is present in substantially amounts and in the strong limit. Doubling CO_2 does *not* double its greenhouse affect. On the other hand CFCs are not present naturally and absorb in a part of the spectrum where other atmospheric gases are not active (referred to as an *absorption window*), and therefore their greenhouse effect increases linearly with concentration

The major absorption bands are shown in Fig. 103 with the contribution by the main active gases. It is seen that nearly all of the outgoing infra-red radiation from the earth's surface is absorbed by water vapour except for the window between 8 and approximately 15 μm. However, CO_2 is strongly active in this window with an absorption band between 14 and 16μm. We saw in Fig. 103 the existence of the water vapour window in the IR. *Q: In remote sensing what would this be useful for?* The window region of 8-13 μm is useful for remote sensing of the surface (e.g. SST).

In contrast to the earth's infra-red radiation, the majority of the solar radiation at the top of atmosphere reaches the earth's surface, with the atmosphere on average absorbing around 17% of solar radiation. We supplement Fig. 103 with Fig. 104, which has the specific gas absorption band marked and also gives the exact incoming solar radiation spectra in addition to the theoretical blackbody curve.

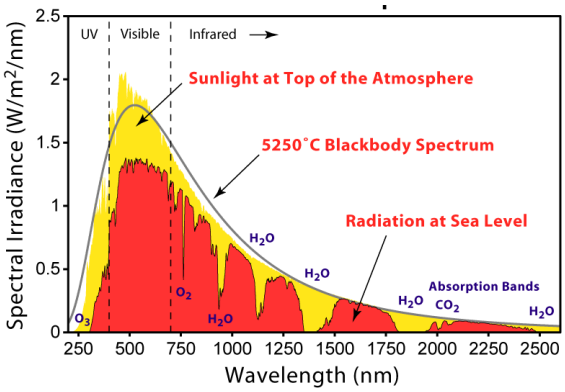

Figure 104: Solar incoming TOA and surface radiation spectra with the gases responsible for the major bands marked.

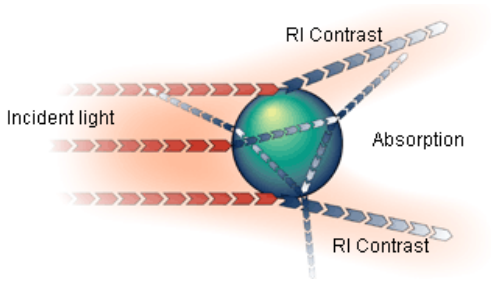

Figure 105: Schematic of mie scattering (source www.malvern.co.uk)

6.6 Scattering

The scattering of radiation by a particle, depends strongly on the ratio of the wavelength of the radiation to the radius of the particle. The theory that governs this is called Mie theory, involving the internal and external refraction of the radiation by the particle and the full description is beyond the scope of this course. (Fig.fig:mie)

The scattering regime has a large impact on the phase function $P(\theta', \phi', \theta, \phi)$ (Fig. 106, see also Maxwell animations online). The relevant parameter to determine the scattering regime is the ratio of the particle circumference to the radiation wavelength $2\pi r/\lambda$. One can see that in the regime $2\pi r/\lambda << 1$ the scattering is more regular in direction, with the phase function loosing its directional dependence in the limit $2\pi r/\lambda \to 0$.

Rayleigh Scattering

If we assume in the regime $2\pi r/\lambda << 1$ (the limit is about 5×10^{-3}) that phase function is independent of direction and the scattering is thus a function of λ only then this approximation is called *Rayleigh Scattering*. In this regime the scatterer can treated as a single dipole. The regimes where Rayleigh scattering approximation is valid are shown in Fig 107.

In general the radiatively "active" species are the trace gases such as CO_2, H_2O, O_3. Rayleigh

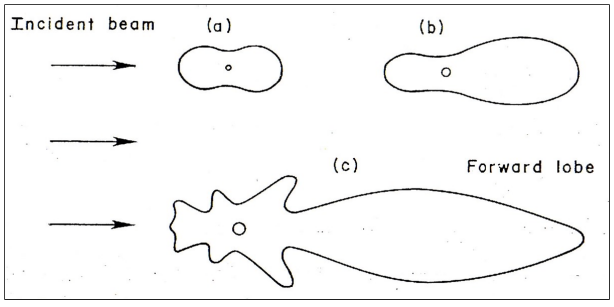

Figure 106: Scatter regimes as a function of $2\pi r/\lambda$ (a) $2\pi r/\lambda << 1$, (b)$2\pi r/\lambda \sim 1$ (c) $2\pi r/\lambda > 1$

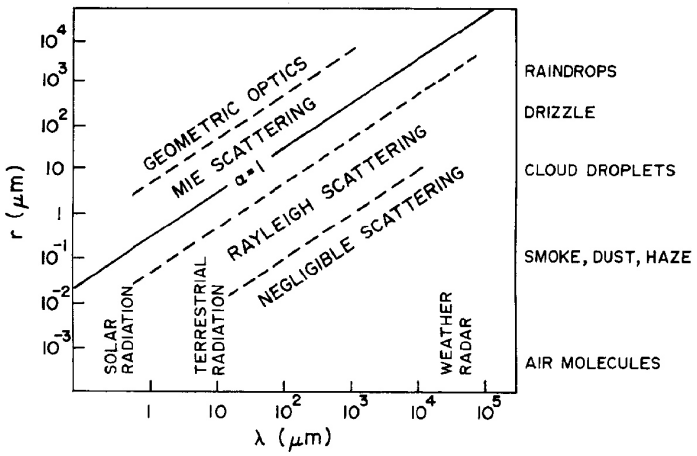

Figure 107: Scattering regimes as a function of wavelength and particle radius.

Scattering is one of the few examples where the major species such as N_2 and O_2 are "active". *Q: why is the sky blue?*

The scattering extinction coefficient in the Rayleigh regime is proportional to the inverse fourth power of the wavelength, $k^s_\lambda \propto \frac{1}{\lambda^4}$. Red light has $\lambda = 0.7\mu$m while blue light has $\lambda = 0.4\mu$m, indicating an order of magnitude increase in scattering at blue wavelengths.

Contribution of Rayleigh scatter to planetary albedo
Rayleigh scattering's contribution to albedo depends on the solar zenith angle. *Q: why?*. The solar zenith angle determines the pathlength of the radiation. When the sun is overhead Rayleigh scattering contributes 0.037 to the albedo, while the figure is 0.13 for a solar zenith angle of 80°. The global average value is about 0.06, thus 0.06/0.30= 20% of the planetary albedo is due to Rayleigh scatter

6.7 Radiation budget of clouds

Scattering and absorption by clouds
In clouds Rayleigh scattering approximation no longer holds and $2\pi r/\lambda \approx 100$, and the full (complicated) Mie theory is required.

We saw in Fig. 106 that in this case there was a strong "forward lobe" where the forward scatter was much stronger than the backwards scatter. For liquid water droplets the forward scattering lobe can be many orders of magnitudes greater than the back-scattered radiation. This leads to an apparent paradox as clouds reflect up to 70% of the incident solar radiation back to space. *Q: how can this occur?* The solution is that we have so far considered only single scattering events. In optically thin clouds photons may undergo only a single scattering events and thus the vast majority pass through unimpeded. In optically thick clouds though multiple scattering may occur (*draw sketch*). Thus the possibility of light reemerging at the cloud top is much higher. *This is why thick clouds appear dark when viewed from the surface.* Cloud albedo asymptotes to around 0.8 for thick clouds. We recall that ω tells us according to (163) what proportion of the direct beam extinction is due to scatter or absorption. For solar radiation $\omega > 0.9$ meaning most of the radiation is scattered and indeed for visible wavelengths $\omega > 0.999$; the *conservative scattering* regime.

However, in the thermal infra-red generally $\omega < 0.5$ implying that there is little chance of a photon at these wavelength being multiply scattered and escaping from the cloud. Thus *clouds are essentially black bodies in the infra-red.*

We can see from the above that clouds will have large effect on the earth's radiation budget depending on their height and optical depth.

Low clouds

- SW: Low clouds will sufficient optical depth will reflect sunlight back to space efficiently, thereby reducing the amount of solar radiation absorbed at the surface.

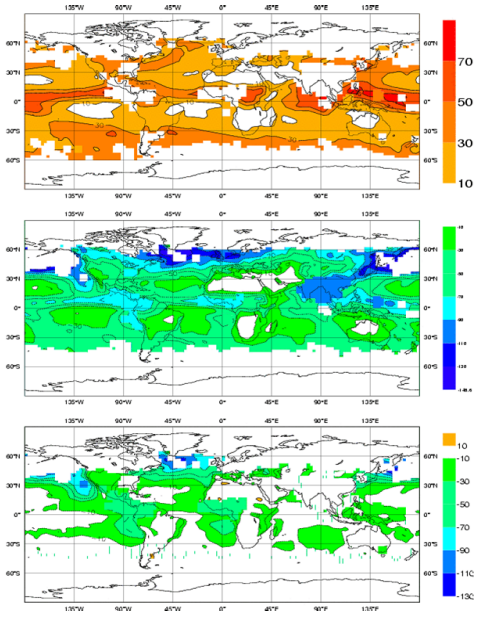

Figure 108: Cloud radiative forcing calculated from ERBE in the (top) LW (middle) SW and lower net (LW+SW)

- LW: In the long wave infra red, cloud absorb the surface emitted radiation efficiently as they are effectively black bodies. They emit infrared radiation back to earth at the approximate temperature of the cloud lower surface, and to space the cloud top temperature. *Q: Do low clouds have a strong impact in the IR therefore?* The answer is no, since the cloud top temperature will be similar to the surface.

Combining these two effects implies that low clouds cool the earth's surface.

High clouds

High clouds of both reflect light back to space, but they can also have a strong IR signature since they are very cold (temperatures close to that of the tropopause). The balance can be in favour of warming or cooling depending on the crystal type[11] and the optical depth. An intriguing result in the tropics is that on the average it appears that cloud radiative forcing is almost exactly zero, i.e. the solar and the infra-red effects balance each other.

This may be a coincidence of the present climate and not hold in past or future climates, but some authors have suggested that this result is no accident, and have put forward mechanisms involved negative feedbacks between radiation and convection that maintain this balance (see Hartmann et al., 2001). These effects of clouds can be seen in Fig. 108 which shows the cloud radiative forcing in the SW, IR and net (SW+IR). These are calculated at each location by comparing the mean TOA outgoing radiative flux *at all times* with the mean averaged for only those times *when clouds are present*. The difference between these two values gives a measure of the cloud radiative forcing. The effect of the low cloud (stratocumulus) regimes off the West coasts of the major continents in clear in the SW but they are not visible in LW. In contrast the deep convective clouds in the tropics have a marked and opposing signal in both the IR and SW.

Calculating heating rates

To calculate the atmospheric heating rate a range of models are used that divide the spectrum up into a number of bands, with the spectrum resolution depending on available computing time.

- *Line by Line*: The most complicated models will divide the spectrum of 0-2500cm^{-1} into well over 100,000 spectral intervals. These models are very expensive to run but provide the benchmarks by which to test the cheaper models below.

[11] Remember that these are ice clouds with complex crystal geometries affecting scattering properties. See Macke et al. (1996) for a seminal analysis of ice crystal scattering.

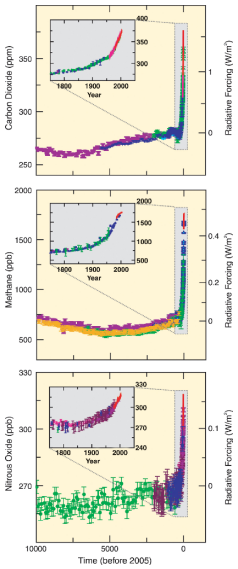

Figure 109: Greenhouse gas emissions and their equivalent top of atmosphere (TOA) radiative forcing (source IPCC AR4)

- *Narrow Band*: These models will divide the infra-red spectrum into ~ 250 spectral intervals, but these models are still too expensive to use in weather prediction or climate models.
- *Broad Band*: These may employ 5 to 20 spectral intervals, although numerical tricks can be used to improve representation of gas absorption bands.

The actual heating rate will depend on the amount of the gas absorber present and the strengths of the absorption by the gas. The calculation is relatively easy for solar heating rate, despite the occurrence of scattering, since the atmosphere does not emit at $\lambda < 4\mu$m. If we calculate how much the radiative flux at the boundaries is reduced by the presence of absorbers δE, in other words the rate that energy is deposited in the layer, then the the change in temperature will be related to the energy divided by the heat capacity of the layer $c_p \rho \Delta z$:

$$\frac{dT}{dt} = \frac{\Delta E}{c_p \rho \Delta z}. \tag{172}$$

with the units of the RHS being K s^{-1} as expected. We recall that the main absorbers in the solar spectrum are O_3 and H_2O, with ozone absorbing mainly in the stratosphere resulting in a heating rate of 10K day^{-1} at a height of 50km, and water vapour mainly active in the troposphere (*Q: why?*) with a heating rate of approximately 1 K day^{-1}. In the thermal infra-red calculation the situation is more complicated due to the emission in each layer.

Infrared radiation tends to cool the atmosphere, with the dominant coolers being H_2O in the troposphere and CO_2 in the stratosphere. Typical cooling rates are 2 to 3 K day^{-1}

Anthropogenic global warming

From the above discussion it is clear that increasing the concentrations of radiatively active gases that absorb in the infra-red will tend to warm the surface. Thus burning fossil fuels increases concentrations of CO_2 which to date are estimated to have had an equivalent TOA radiative forcing of around 1.5 W m^{-2} (Fig. 109).

Likewise, humans can have other climate impacts such as changing surface albedo through land-use changes or changing atmospheric albedo through the emission of aerosols that reflect sunlight (Fig. 110). Indeed it is the later effect that is now thought to be partly the cause of the cooling in northern latitudes during the 1950s and 1960s. The calculation of the projected man-induced warming in future is greatly complicated by the existence of natural feedbacks, that may *amplify* or *reduce* the eventual warming. Two of the major positive feedbacks are:

- *Ice Albedo Feedback*: Increased temperatures $\rightarrow$ ice melting at poles $\rightarrow$ lower albedo $\rightarrow$ increased solar absorption $\rightarrow$ increased temperatures

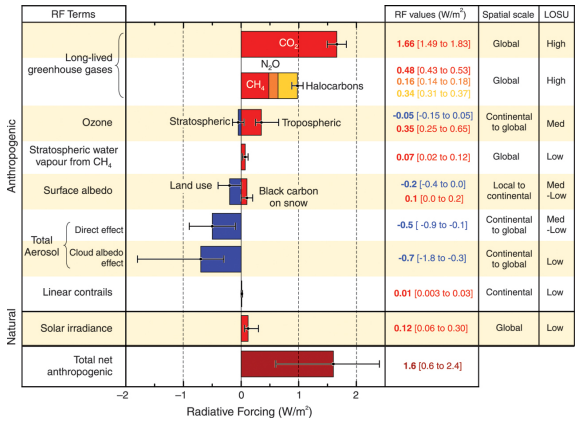

Figure 110: Human impacts and their assessed radiative forcing equivalent. (source IPCC AR4)

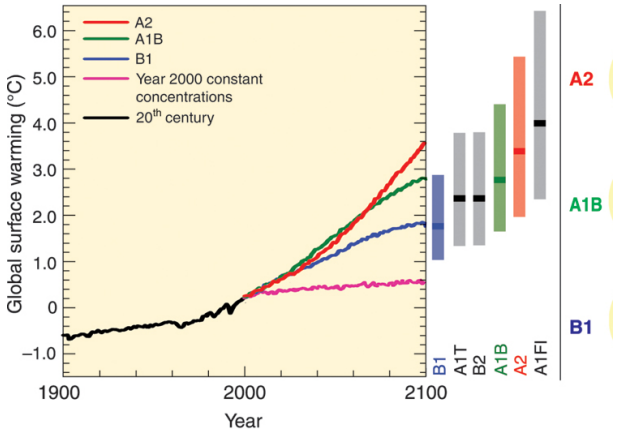

Figure 111: Future projected warming from many different climate models under different emission scenarios (source IPCC AR4, see this report for further details).

- *Water Vapour Feedback*: Increased temperatures → more water vapour → enhanced greenhouse effect → increased temperatures

One of the major uncertainties though is the future role played by clouds. This is complicated as clouds could get thicker, thinner, higher, change phases, change radiative properties, etc. Global climate models do not agree on the role of clouds and many models show clouds amplifying the future warming, while other show clouds offsetting future possible warming. Note: Just because clouds tend to *cool* the present-day climate does not imply that they will *offset* future warming. It is interesting to note that the uncertainty due to clouds has not reduced with increasing knowledge of cloud physics over the past three decades! Despite these uncertainties, estimates of future warming are made and must also take into account uncertainties in emission scenarios. Projections from IPCC AR4 are shown in Fig. 111.

The end!

Gas constant for dry air	R_d	287.06	J kg^{-1} K^{-1}
Gas constant for vapour	R_v	461.5	J kg^{-1} K^{-1}
Density of liquid water	ρ_l	1000	kg m^{-3}
Universal Gas Constant	R	8.314	J K^{-1} mol^{-1}
Stefan Boltzmann constant	σ	5.67×10^{-8}	Wm^{-2} K^{-4}
radius of the earth	r_e	6340	km
radius of the sun	r_s	0.7×10^6	km
distance between earth and sun	r_d	149.6×10^6	km
Solar Constant	S_0	1370	W m^{-2}
Planck Constant	h	6.625×10^{-34}	J s
Constant c_1 in Planck's Law	c_1	3.74×10^{-16}	W m^{-2}
Constant c_2 in Planck's Law	c_2	1.45×10^{-2}	m K

Table 6: Constants

Readings
The following reading assignments are to be presented in week 5 of the course.

Each student will make a 20 minute presentation and then will field questions for 10 minutes from the other students and myself. The reading will contribute 30% to the final mark.

1. *Buoyancy sorting model of convection* Explain this method of representing the convective process: (Paluch, 1979; Raymond and Blyth, 1986)

2. *Mass flux convection schemes* Explain this method of representing the convective process as presented by Tiedtke (1989)

3. *Adjustment convection schemes* Explain this method of representing the convective process as presented by betts (1986); Betts and Miller (1986)

4. *Thermodynamic control of tropical rainfall* Explain the ideas of Raymond (2000)

5. *Convective equilibrium in the tropics* Explain the boundary layer equilibrium ideas of Raymond (1995)

6. *Squall Lines* What is a squall line and how does it propagate according to (Rotunno et al., 1988)?

7. *CAPE/CIN* Explain the concept of CAPE and CIN and the findings of Parker (2002) concerning CAPE and CIN variations

8. *Saturation point analysis* Explain the core points of the Betts (1982) saturation point analysis.

9. *Convective boundary layer* Explain the model of convective equilibrium of Betts and Ridgway (1989)

References

Berry, E. X., 1967: Cloud droplet growth by collection. *J. Atmos. Sci.*, **24 (6)**, 688–701.

Berry, E. X. and R. L. Reinhardt, 1974: An analysis of cloud drop growth by collection Part II. Single initial distributions. *J. Atmos. Sci.*, **31 (7)**, 1825–1831.

Betts, A., 1982: Saturation point analysis of moist convective overturning. *J. Atmos. Sci.*, **39 (7)**, 1484–1505.

betts, A. K., 1986: A new convective adjustment scheme. part 1: Observation and theoretical basis. *Q. J. R. Meteorol. Soc.*, **112 (473)**, 677–691.

Betts, A. K. and M. J. Miller, 1986: A new convective adjustment scheme. Part 2: Single column tests using GATE WAVE, BOMEX, ATEX and arctic air-mass data sets. *Q. J. R. Meteorol. Soc.*, **112**, 693–709.

Betts, A. K. and W. Ridgway, 1989: Climatic Equilibrium of the Atmospheric Convective Boundary Layer over a Tropical Ocean. *J. Atmos. Sci.*, **46 (17)**, 2621–2641.

Byers, H. R. and R. R. Braham Jr., 1948: Thunderstorm structure and circulation. *J. Meteorology*, **5**, 71–86.

Demott, P. J., D. J. Cziczo, A. J. Prenni, D. M. Murphy, S. M. Kreidenweis, and D. S. Thomson, 2003: Measurements of the concentrations and composition of nuclei for cirrus formation. *Proc. Nat. Acad. Sci.*, **100**, 14 655–14 660.

Emanuel, K. A., 1994: *Atmospheric Convection*. Oxford University Press, 580 pp.

Fischer, E. M., S. I. Seneviratne, P. L. Vidale, D. Lüthi, and C. Schär, 2007: Soil Moisture–Atmosphere Interactions during the 2003 European Summer Heat Wave. *J. Climate*, **20 (20)**, 5081–5099.

Fleishauer, R. P., V. E. Larson, and T. H. Vonder Haar, 2002: Observed microphysical structure of midlevel, mixed-phase clouds. *J. Atmos. Sci.*, **59 (11)**, 1779–1804.

Fowler, L. D., D. A. Randall, and S. A. Rutledge, 1996: Liquid and ice cloud microphysics in the CSU general circulation model. Part I: Model description and simulated cloud microphysical processes. *J. Climate*, **9**, 489–529.

Gierens, K., 2003: On the transition between heterogeneous and homogeneous freezing. *Atmos. Chem. Phys.*, **3**, 437–446.

Gierens, K., U. Schumann, M. Helten, H. Smit, and A. Marenco, 1999: A distribution law for relative humidity in the upper troposphere and lower stratosphere derived from three years of MOZAIC measurements. *Ann. Geophysicae*, **17**, 1218–1226.

Gunn, K. L. S. and J. S. Marshall, 1958: The distribution with size of aggregate snowflakes. *J. Atmos. Sci.*, **15 (5)**, 452–461.

Hartmann, D., L. Moy, and Q. Fu, 2001: Tropical Convection and the Energy Balance at the Top of the Atmosphere. *J. Climate*, **14 (24)**, 4495–4511.

Klett, J. D. and M. H. Davis, 1973: Theoretical collision efficiencies of cloud droplets at small reynolds numbers. *J. Atmos. Sci.*, **30 (1)**, 107–117.

Koop, T., B. P. Luo, A. Tsias, and T. Peter, 2000: Water activity as the determinant for homogeneous ice nucleation in aqueous solutions. *Nature*, **406**, 611–614.

Macke, A., J. Mueller, and E. Raschke, 1996: Single scattering properties of atmospheric ice crystals. *J. Atmos. Sci.*, **53**, 2813–2825.

Manabe, S. and R. F. Strickler, 1964: Thermal equilibrium of the atmosphere with a convective adjustment. *J. Atmos. Sci.*, **21 (4)**, 361–385.

Marshall, J. S. and W. M. K. Palmer, 1948: The distribution of raindrops with size. *J. Atmos. Sci.*, **5 (4)**, 165–166.

Mason, B. J., 1978: Physics of a raindrop. *Physics Education*, **13 (7)**, 414–419.

Paluch, I. R., 1979: The Entrainment Mechanism in Colorado Cumuli. *J. Atmos. Sci.*, **36 (12)**, 2467–2478.

Parker, D. J., 2002: The response of CAPE and CIN to tropospheric thermal variations. *Q. J. R. Meteorol. Soc.*, **128**, 119–130.

Pruppacher, H. R. and J. D. Klett, 1997: *The Microphysics of Clouds and Precipitation*. Kluwer Academic Publishers, pp. 954.

Raymond, D. J., 1995: Regulation of moist convection over the west Pacific warm pool. *J. Atmos. Sci.*, **52**, 3945–3959.

Raymond, D. J., 2000: The thermodynamic control of tropical rainfall. *Q. J. R. Meteorol. Soc.*, **126**, 889–898.

Raymond, D. J. and A. M. Blyth, 1986: A stochastic mixing model for nonprecipitating cumulus clouds. *J. Atmos. Sci.*, **43**, 2708–2718.

Ren, C. and A. R. Mackenzie, 2005: Cirrus parametrization and the role of ice nuclei. *Q. J. R. Meteorol. Soc.*, **131**, 1585–1605.

Rogers, R. R. and M. K. Yau, 1989: *A short course in cloud physics*. Pergamon Press, 290pp pp.

Rotunno, R., J. B. Klemp, and M. L. Weisman, 1988: A theory for long-lived squall lines. *J. Atmos. Sci.*, **45**, 463–485.

Spichtinger, P., K. Gierens, and W. Read, 2003: The global distribution of ice-supersaturated regions as seen by the Microwave Limb Sounder. *Q. J. R. Meteorol. Soc.*, **129**, 3391–3410.

Taylor, C. M., F. Said, and T. Lebel, 1997: Interactions between the land surface and mesoscale rainfall variability during HAPEX-Sahel. *Mon. Wea. Rev.*, **125**, 2211–2227.

Telford, J. W. and J. Warner, 1962: On the measurement from an aircraft of buoyancy and vertical air velocity in cloud. *J. Atmos. Sci.*, **19 (5)**, 415–423.

Tiedtke, M., 1989: A comprehensive mass flux scheme for cumulus parameterization in large-scale models. *Mon. Wea. Rev.*, **117**, 1779–1800.

Tompkins, A. M., K. Gierens, and G. Rädel, 2007: Ice supersaturation in the ECMWF integrated forcast system. *Q. J. R. Meteorol. Soc.*, **133**, 53–63.

Warner, J., 1955: The water content of cumuliform cloud. *Tellus*, **7**, 449–457.

WARNER, J. and T. D. Newnham, 1952: new method of measurement of cloud water content. *Q. J. R. Meteorol. Soc.*, **78 (335)**, 46–52.

Willis, P. T., 1984: Functional fits to some observed drop size distributions and parameterization of rain. *J. Atmos. Sci.*, **41 (9)**, 1648–1661.